JULY, 2017

Ph.D in Civil Engineering

ASEEL MADALLAH MOHAMMED

GAZIANTEP UNIVERSITY

GRADUATE SCHOOL OF

NATURAL & APPLIED SCIENCES

MECHANICAL BEHAVIOR OF UHPC HAVING VARIOUS BINDER COMPOSITIONS AND INFLUENCE OF SUCH INFILLED CONCRETE ON THE STRUCTURAL RESPONSE OF CFST COLUMNS

Ph. D. THESIS
IN
CIVIL ENGINEERING

BY

ASEEL MADALLAH MOHAMMED

JULY 2017

Mechanical Behavior of UHPC Having Various Binder Compositions and Influence of Such Infilled Concrete On the Structural Response of CFST Columns

Ph. D. Thesis
in
Civil Engineering

University of Gaziantep

Supervisor
Assoc. Prof. Dr. Esra Mete Güneyisi

by

Aseel Madallah MOHAMMED

July 2017

REPUBLIC OF TURKEY
UNIVERSITY OF GAZİANTEP
GRADUATE SCHOOL OF NATURAL & APPLIED SCIENCES
CIVIL ENGINEERING DEPARTMENT

Name of the thesis: Mechanical Behavior of HPC Having Various Binder Compositions and Influence of Such Infilled Concrete on the Structural Response of CFST Columns.

Name of the student: Aseel Madallah MOHAMMED

Exam date: 31/07/2017

Approval of the Graduate School of Natural and Applied Sciences

Prof. Dr. A. Necmeddin YAZICI
Director

I certify that this thesis satisfies all the requirements as a thesis for the degree of Philosophy of Doctorate.

Prof. Dr. Abdulkadir ÇEVİK
Head of Department

This is to certify that we have read this thesis and that in our consensus/majority opinion it is fully adequate, in scope and quality, as a thesis for the degree of Doctor of Philosophy.

Assoc. Prof. Dr. Esra METE GÜNEYİSİ
Supervisor

Examining Committee Members:	Signature
Prof. Dr. Hanifi ÇANAKCI	....
Assoc. Prof. Dr. Ali Fırat ÇABALAR	....
Assoc. Prof. Dr. Esra METE GÜNEYİSİ	....
Assist. Prof. Dr. Hatice Öznur ÖZ	....
Assist. Prof. Dr. Hasan Erhan YÜCEL	....

I hereby declare that all information in this document has been obtained and presented in accordance with academic rules and ethical conduct. I also declare that, as required by these rules and conduct, I have fully cited and referenced all material and results that are not original to this work.

Aseel Madallah MOHAMMED

ABSTRACT

MECHANICAL BEHAVIOR OF UHPC HAVING VARIOUS BINDER COMPOSITIONS AND INFLUENCE OF SUCH INFILLED CONCRETE ON THE STRUCTURAL RESPONSE OF CFST COLUMNS

MOHAMMED, Aseel Madallah
Ph.D. in Civil Engineering
Supervisor: Assoc. Prof. Dr. Esra METE GÜNEYİSİ
July 2017
134 Pages

To enhance the sustainability of a structure, three pillars of the sustainability, namely, environmental, social, and economical factors are needed to be considered in the design. On this issue, the development of new structural composite systems with high performance plays a critical role. This study contained two parts: Firstly, the experimental results on the mechanical behavior of ultra-high performance concrete (UHPC) mixed with various binder types and volumes were given. Whereas, the second part provided the numerical results on the structural behavior of steel tube column infilled with such UHPC. For this, single, binary, ternary and quarternary binder systems up to 75% replacement levels were used to develop 26 different UHPC mixtures with low cement content. All designed mixtures were tested for identifying the properties of core concrete. Moreover, three diameter to wall thickness D/t ratios (35, 65, and 95) matched by 300, 450, and 600 MPa of yield strength (f_y) of the steel tube were used to calculate and examine the axial load capacity of circular concrete filled steel tube (CFST) with UHPCs through design equations given by Eurocode 4 (EC4), American Concrete Institute (ACI) and Chinese (DL/T) codes. The results of experimental and numerical study were given and discussed accordingly.

Keywords: Concrete filled steel tube column, Column capacity, Fracture properties; Mechanical properties, Ultra high performance concrete.

ÖZET

FARKLI BAĞLAYICI KOMPOZİSYONUNA SAHİP UYPB′ LARIN MEKANİK DAVRANIŞI VE BUNLARIN BETON DOLGULU ÇELİK TÜP KOLONLARIN YAPISAL TEPKİSİNE ETKİSİ

MOHAMMED, Aseel Madallah
Doktora Tezi, İnşaat Mühendisliği Bölümü
Tez Yöneticisi: Doç. Dr. Esra METE GÜNEYİSİ
Temmuz 2017
134 Sayfa

Bir yapının sürdürülebilirliğini artırmak için, tasarımda sürdürülebilirliğin üç temel unsuru, yani çevresel, sosyal ve ekonomik faktörler dikkate alınmalıdır. Bu konuda, yüksek performanslı yeni yapısal kompozit sistemlerin geliştirilmesi kritik bir rol oynamaktadır. Bu çalışma iki bölümden oluşmaktadır: Birincisinde, çeşitli bağlayıcı türleri ve hacimleri ile tasarlanmış ultra yüksek performanslı betonun (UYPB) mekanik davranışı üzerine deney sonuçları verilmiştir. İkincisinde, UYPB ile doldurulmuş çelik tüp kolonların yapısal davranışı üzerine sayısal sonuçlar verilmiştir. Bunun için, düşük çimento içeriğine sahip 26 farklı UYPB karışımı %75'e kadar değiştirme seviyelerinde tekli, ikili, üçlü ve dörtlü bağlayıcı sistemler kullanılarak tasarlanmıştır. Bütün karışımlar çekirdek betonun özelliklerini belirlemek için test edilmiştir. Ayrıca, çelik tüpün akma dayanımı (fy) 300, 450 ve 600 MPa ile eşleşen üç farklı çap-et kalınlığı D/t oranı (35, 65 ve 95) kullanılarak dairesel kompozit kolonun eksenel yük kapasitesi Avrupa (EC4), Amerikan (ACI) ve Çin (DL/T) kodları ile hesaplanmıştır. Deneysel ve nümerik çalışma sonuçları karşılaştırmalı olarak tartışılmıştır.

Anahtar Kelimeler: Beton dolgulu çelik tüp kolon; Kolon kapasitesi, Kırılma özellikleri; Mekanik özellikler; Ultra yüksek performanslı beton.

TO MY GIRL RAWAN

TO MY PARENTS

TO SOUL OF MY HUSBAND

ACKNOWLEDGEMENTS

First, I would like to give my sincere thanks to my GOD ALLAH who helped me to complete this research.

I would like to give my sincere thanks to my supervisor Assoc. Prof. Dr. Esra METE Güneyisi for her constant guidance and encouragement.

Thanks for my parents and my sweet daughter Rawan Alaa and to everyone who took part in completion of this thesis.

TABLE OF CONTENTS

Page

LIST OF TABLES

LIST OF FIGURES

LIST OF SYMBOLS/ ABBREVIATIONS

Ac	Cross-sectional area of concrete
ACI	American Concrete Institute
AISC	American Institute of Steel Construction
As	Cross-sectional area of steel tube
Asc	Area of composite section
CFST	Concrete Filled Steel Tube
CSH	Calcium silicate hydrate
CO_2	Carbone dioxide
$Ca(OH)_2$	Calcium hydroxide
DL/T	Chinese Design Code for Composite Structures
Ec	Modulus of elasticity of concrete
EC4	Eurocode 4
$(EI)_{eff1}$	Effective stiffness of composite section
$(EI)_{eff2}$	Effective flexural stiffness
Es	Modulus of elasticity of steel
FA	Fly ash
fc $_{fcu}$	Mean cube compressive strength
fc	Compressive strength
f_{ck}	nominal strengths of the concrete
f_{flex}	Net flexural strength
f_{st}	Splitting tensile strength
f_{scy}	Nominal yielding strength of the composite section

fy	Yield stress of steel
FRC	Fiber reinforced concrete
GF	Fracture energy
GGBFS	Ground granulated blast furnace slag
UHPC	Ultra High performance concrete
HCFST	High strength concrete-filled square steel tube
ITZ	Interfacial Transition zone
Ic	Moment of inertia of concrete core
Is	Moment of inertia of steel tube
Ke	Correction factor
L_{ch}	Characteristics length
LVDT	Linear variable displacement transducer
LM	Limestone micro filer
L/D	Aspect ratio
MK	Metakaolin
OPC	Ordinary Portland cement
P_u	Ultimate axial load carrying capacity
P_{max}	The ultimate load
RPC	Reactive powder concrete
S	Slag
SF	Silica fume
SP	Superplasticizers
SCM	Supplementary cementitious materials
SM	Silicon microfiber
UHPFRC	ultra high performance concrete fiber-reinforced concrete
Wo	Area under load-deflection curve
w/b	Water/binder ratio

w/c	Water/cement ratio
δs	The specified deflection of the beam
ξ, η	Confinement factor
ηa, ηao	Factors related to the confinement of steel tube
ηc, ηco	Factors related to the confinement of concrete
$\bar{\lambda}$	Relative slenderness

CHAPTER 1

INTRODUCTION

1.1 General

For a particular structure, the selection of steel, concrete and composite construction depends on several factors. In this regard, construction is an essential part of any country particular reference to infrastructure and industrial development. Concrete is a key structural material in the construction industry and is the second most consumed substance on earth after water. The development of modern concrete industry also introduces many environmental problems such as pollution, waste dumping, emission of dangerous gases, and depletion of natural resources. The concrete construction industry is not sustainable because it consumes huge quantities of virgin materials [1].

In the mid 60's, the structural concrete with strength ranging from 40 to 80 Mpa, named high-strength concrete (HSC). It is first used in significant quantities in the main structures in Chicago, USA. As the development has continued, the definition of HSC has changed. In the 1950s, concrete with a compressive strength of 34 Mpa was considered a high strength. In the 1960s, concretes with 41 and 52 MP, a compressive strength was used commercially, and in the early 1970s, 62 Mpa concrete was being produced and introduced in many applications such as high-rise buildings and long-span prestressed concrete bridges [2].

More recently, compressive strengths of concrete over 120 Mpa have been known as ultra-high performance concrete (UHPC) which improves the advantages of HSC and presents a great interest in casting concrete industry by using this new product. So, it is possible to produce lighter structural members with thinner sections and open up new possibilities for bridge and high-rise building and offer economic advantages through savings in reinforcing steel and cross-sectional dimensions, this leads to lower dead weight, thus allowing large spans [2].

UHPC is one of the latest advances in concrete technology, and it addresses the shortcomings of many concretes today [3]. UHPC is advanced cement-based material, which originally developed in the early 1990s by the technical division of Bouygues, France [4].

UHPC is a composite product which incorporates standard cement, sand and different additives like silica fume, fly ash, quartz powder, slag, and metakaolin. The workability of RPC is enhanced by utilizing superplasticizers. Indeed, even with the expansion of steel fibers into the solid UHPC produces a momentous flexural quality of more than 50 Mpa [5].

The first commercial applications of a very high-strength product started around 1980, in Denmark [6]. It was primarily used for special applications in the security industry– like vaults, strong rooms, and protective defense constructions. The UHPC was first applied to the Sherbrook pedestrian-bikeway bridge in Canada on 1997 and later on for the expansion of the Cattenom nuclear power plant in France, two 20.50 and 22.50 m long road bridges used by cars and trucks at Bourg-lès-Valence in France built in 2001 [7]. Other footbridges with decks and/or other load bearing components made of fine-grained, fiber-reinforced UHPC was produced in Seoul and in Japan [8]. A spectacular architectural example that takes advantage of the special benefits of UHPC is the toll-gate of the Millau Viaduct in France. For these projects, the UHPC was reinforced with about 2.5 to 3 vol.% of steel fibers of a different shape. Inspired by first applications in Canada, Asia, and Europe and by intensive research and development efforts at various universities and by the construction industry, in 2002 the first recommendations on High Performance Fiber-Reinforced Concrete (HPFRC) were proposed by the French Association of Civil Engineering (AFGC). These recommendations were intended to constitute a reference document that would serve as a basis for the use of this new material in civil engineering applications. In other European countries, UHPC was gaining increasing interest as well. In Germany, extensive research projects have been developed to use regionally available raw materials for fine or coarse-grained UHPC and to reduce the cement content depending on the requirements given by individual design and construction [9].

1.2 Composite Columns

Composite columns are categorized under structural members that directed to end moments and axial forces in the compression state. The most popular composite column named as concrete-filled steel tubular (CFST), which steel and concrete compositely act together against applied load. These columns due to unnecessary formwork and eliminating to longitudinal steel bars have widely spread with different cross sections, as shown in Figure 1.1. The CFST columns can be designed to be an economy by making plates thinner and resisting more axial force. For this, UHPC or

UHPC was proposed as infilled materials that resulted in developing buckling capacity. In addition, the infilled material enhanced against unwanted concrete properties like shrinkage and creep [10]. CFST columns have been widely used in modern structural systems [11]. The major aim of the using CFST members in construction can be expressed as concrete is perfect in compression and steel is very good in tension, and by joining the two materials together structurally, these strengths can capitalize to result in a light weight and very highly efficient design. Moreover, they exhibit a higher level of performance compared when the two materials functioned separately [12].

In spite of above-mentioned advantages, the application of CFST columns has been limited due to unsufficient design requirements and complexity specify connections. Subsequently, for choosing appropriate joint, the whole strength and stiffness properties of CFST columns have to be addressed for construction purposes [13].

Due to their super properties of compressive and tensile strengths, toughness, durability, high durability, and flowable, UHPC is suitable for various structural purposes. These large performances of this type of concrete motivate to use with CFST material as infilled [14-16]. Actually, a study revealed that composite column of CFST five times more economical than building with conventional steel columns. In multistory construction structures, the dead load plays an adverse role specifically at ground levels that required to withstand a major axial load because of a collection of above stories dead loads. For instance, the ground floor column diameter for 20-30 stories building is about three meter when the conventional concrete has been used. Therefore, it is a great requirement to implement UHPC with high story buildings. UHPC combined with structural steel to form CFST may be utilized in beams, slabs, foundations, and columns [14].

Evirgen et al. [17] studied the compressive strength of CFST column used different cross-sectional forms such as rectangular, circular, square and hexagonal. The study was implemented via different grades of concrete and width to thickness (B/t) ratio then the results were compared with ABAQUS software. They also illustrated that the ductility of the circular is more effective than hexagonal, rectangular and square sections, respectively.

Previous researchers analyzed the behavior of circular CFST columns under axial compression and eccentric loading [18, 19]. At initial stages of loading, concrete and steel tube have little interaction due to differences in Poisson's ratio of the two materials [20, 21]. As axial load increases, concrete softens and begins to dilate. Concrete forms a radial lateral pressure on the steel tube. The steel tube protects concrete from spalling by confinement. On the other hand, the concrete core prevents inward buckling of steel. Thus strength and ductility are improved in CFST composite elements, allowing for smaller column dimensions and applications in seismic regions [22].

Stiffness typically increases with concrete compressive strength. However, due to the presence of steel fibers, UHPC can achieve to improve the ductility. Benefits of this type of UHPC are expected to improve the performance of filled tube columns under axial compression [16].

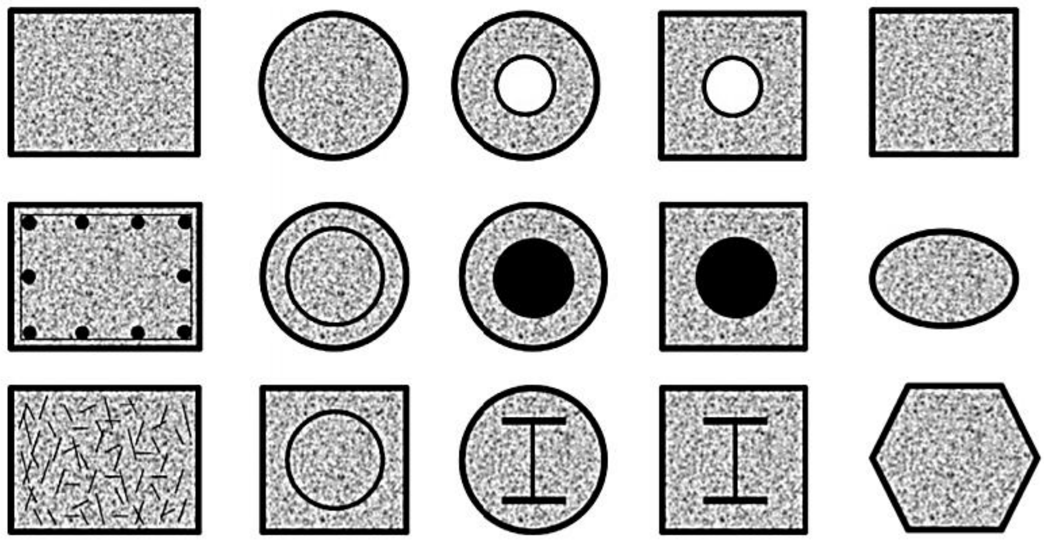

Figure1.1. Typical cross section of CFST columns [23]

1.3 Objective of Study

UHPC continue to develop from on-going research to improve material strength, ductility, lightness, and ecological soundness. Based on the recent research by the authors and reviews of the literature, it seems beneficial and possible to produce a homogeneous and dense skeleton of UHPC with a low binder content. Subsequently, depended on this idea, the objective of this study is to investigate firstly the mechanical performance of UHPC containing different binders. Then after, in the second stage, the load carrying capacity of steel tubular columns filled with UHPC having different systems is studied comparatively. To examine the capacity of composite column, three different design codes, namely, American (ACI), European (EC4), and Chinese (DL/T) codes were utilized.

1.4 Outline of the Thesis

In this Ph. D. thesis, the whole work is demonstrated via seven chapters;

Chapter 1 is a general introduction and the significance of the thesis.

Chapter 2 gives the review of the literature and background of the compounds as well as properties and structural applications of UHPCs. The description of CSFT composite columns and the use of UHPCs in steel tube are explained.

Chapter 3 covers the highlights of the experimental and numerical analysis carried out in this study. The properties of the materials used, mixture design, the preparation of samples and testing procedures are mentioned. The properties of the composite column and design codes (ACI 318-05, Eurocode 4 and Chinese codes) are given.

Chapter 4 consists of the experimental results and discussion.

Chapter 5 presents the numerical results and discussion.

Chapter 6 is a key to the main conclusions drawn.

CHAPTER 2

LITERATURE REVIEW AND BACKGROUND

2.1 Ultra High-Performance Concrete (UHPC)

Ultra high performance concrete (UHPC) is a very dense structured fine or coarse aggregate concrete with a low water-cement ratio (w/c) smaller than 0.30, high cement content and mineral admixtures which are selected to increase the bond between the aggregates and the cement past. The optimization of the granular mix for UHPC leads to minimize the number of defects such as micro cracks and pore spaces that allow achieving a greater percentage of the potential ultimate load carrying capacity defined by its components and providing enhanced durability properties. Because of the high compressive strength, this type of concrete is named high strength concrete [2].

The key factor for the mixture design of UHPC is using fine aggregates like quartz powder and eliminating coarse aggregate to improve homogeneity, which plays a major role in reducing the maximum paste thickness [24].

2.1.1 UHPC– Generation and Mix Proportions

Richard and Cheyrezy [16] studied UHPC by eliminating the coarse aggregate from concrete to enhance the homogeneity and used post-set heat treatment to improve the microstructure. Furthermore, they added high-tensile microfibers to new-generation concrete to advance the tensile strength and ductility of concrete. Two kinds of concretes were designed and developed as UHPC 200 and 800. The novelty concrete was implicated in industrial and nuclear waste storage solids.

Dattatreya. et al. [25] improved UHPC through studying many models of particle packing. They focused on developing durability and mechanical properties by ingredient granular packing optimization. The optimization results included most important constituents of UHPC like cement, SF, standard sand, quartz powder then compared to theoretical packing models.

Plawsky et al. [26] revealed a novel way for dispersing cement in the sand to generate dry mix design with higher properties of physical and mechanical. The main issue in mixing dry constituents and water dispersion were addressed. Additionally, the more knowledge of mixing procedure chiefs to design denser mortar via a new-generation equipment.

Staquet and Espion [27] investigated the mechanical performance of UHPC that produced by existing constituents in their country. They produced 180 Mpa compressive strength by using CEM I 52.5 instead of CEM I 42.5 with no contribution of steam curing (water curing). During the production of UHPC, they also concluded that the white and light gray had better workability than white and black SF manufactured from the same industry.

Blais and Couture [28] found that UHPC reinforced steel fibers of 0.2 mm diameter, and 25mm length is equal to normal concrete strengthened by 1000mm length and 0.2 mm diameter of steel bars. They improved the tensile strength of UHPC via reducing interfacial transition zone (ITZ) by removing coarse aggregate [29, 30]. Mineral admixture like SF was used to produce low permeability and denser mixture. An effort has been made on using nanosize particles for producing and application of UHPC [31].

Dattatreya et al. [25] investigated a number of particle packing models to improve a mix design of UHPC. The granular packing of materials consists of cement, standard sand, quartz powder, and SF. The optimized of granular packing of the constituents was a significant factor for obtaining enhanced durability and mechanical properties, and the investigational results were matched with the theoretical packing models.

2.1.2 UHPC-Design Considerations

Almansour and Lounis [32] advanced UHPC with lower permeability and higher strength to apply for the production of bridges of longer life. The novel UHPC designed according to the Canadian Highway Bridge Design Code led to a significant reduction of the volume of the bridge by a volume of 50-65%.

Hoang et al. [33] reported the mechanical properties of UHPC incorporated with two fiber types, individually and binary. Mixing fibers gave better results of flexural, compressive strength, and more flowable concrete than their effective alone. While the individual effect of micro steel was more than corresponded hooked fibers in addition to the recommendation of adding higher fiber volume than 1% to UHPC. The SF and other filler powders should be in the range of 20-25% of the total of the binder with a w/b ratio of not exceed of 0.2.

Orgass and Klug [34] studied the specific mechanical properties like size effect and ductility of UHPCs containing a type and/or cocktail of short and longer fibers with length ranging between 0.8 to 5.0 mm and dosage ranging of 1 to 2%. There was an enhancement of flexural and crack manner with any increase in fiber volume. The ductility post behavior was noted with the mixtures contained the maximum volume of fibers more than the others.

Jungwith and Muttoni [35] tested the tensile strength behavior of the laboratory structural members of UHPC incorporated with different volume of steel fibers. They observed good stiffness, great tensile value, and very high bond of structural concrete members. They endorsed using fibered UHPC for pre-stressing to tolerate most tensile stresses.

Rossi and Parant [36] studied optimization of the strength of UHPC through adding the continually multi-scale of fibers. The generated concrete behaved as elastoplastic then reached to tension strain hardening. They concluded an increment about 25% during the flexural strength test by controlling rate of loading.

In the study of Bonneau et al. [37], they produced the two-mix type of UHPC in Sherbrooke University at a precast plant; one was a ready-mix UHPC, and the other was used in the precast plant. In the ready mix, the samples were prepared both with and without steel fibers. The concrete specimens were tested for compressive, elastic modulus, freezing, and thawing, scaling deicing salts resistant and chloride ion penetration. The results show that the mixes were resistance to freeze-thaw and under scaling test, the mass loss was very low, chloride ion penetration was under 10 coulombs for UHPC with steel fiber.

Rong et al. [38] used Hopkinson bars to find spalling strength of UHPC. Prepared samples were exposed to the impact of the projectile at the free end of different volume of steel fibers incorporated with UHPC. Reflected tensile waves and the compressive waves were recorded. Moreover, a finite-element analysis was implemented by simulating using the material model.

2.1.3 UHPC–Mechanical Properties

Habel et al. [39] studied the improved performance of high performance fiber-reinforced (HPFRC) concretes with fiber cocktail. This study revealed that the small fibers were contributing the strain hardening resulting in the bridging of micro cracks and long fibers were responsible for transferring of forces in localized cracks and govern the softening part. So the improved HPFRC resulted in higher stiffness and higher resistance to cracking with a hardening modulus of more than 45 Gpa preventing softening behavior.

Redaelli [40] studied the mechanical behavior of real scale HPFRC ties with reinforced steel bars. It is proved that fibers improved the ductility of concrete when the volume of fiber is more than 1.5%. However, at the ultimate limit state, even a large amount of additional ordinary reinforcement cannot avoid strain localization and a brittle failure. This study revealed that HPFRC tensile members could not be made fully ductile by introducing ordinary reinforcement and an alternative definition of the amount of minimum reinforcement to avoid brittle failure or HPFRC tensile members had been proposed.

Jungwirth et al. [41] tested structural members of UHPC reinforced with steel bars. To represent actual structures, they carried out large scales in the laboratory simulating the same condition. For this, the beam dimensions of 160 x 160 x 1500 mm reinforced with three volume ratios of ribbed steels with yield strengths of 556 Mpa were tested. Because of the existence of fibers and their influence, the performance in tension in UHPC displayed a severe variance as matched to that of normal concrete.

Reineck and Greiner [42] implemented mechanical property tests for UHPC reinforced with 2% of steel fibers. They obtained UHPC with a compressive and tensile strength values of about 180 and 10 Mpa, respectively, with a commercially existing formation. These results were matched with the other works that published by authors.

Teutsch et al. [43] produced a ductile UHPC with the contribution of short steel fibers. A significant difference was observed when discontinuous fibers added to be concrete compared to that of plain UHPC. For example, more improvements of tensile strength and higher load carrying capacity were achieved due to crack controlling behavior of fibers.

Dubey et al. [44] studied on the mechanical energy required to pull out fibers across the crack. They revealed brittleness behavior of UHPC due to the addition of pozzolanic materials like SF. Increasing of loads resulted of crushing and splitting of specimens of the plain UHPC that controlled by adding fibers due to the ability to transfer stressed. The toughness of UHPC was enhanced using high reactivity metakaolin that consecutively in turn to higher durability.

Lee and Chisholm [45] reported the behavior of the mechanical of properties of UHPC due to adding fibers. They observed incorporating 2% steel fibers with an aspect ratio of 65 led to enhancement of low tensile strength value of plain UHPC. on the other hand, the compressive strength of UHPC was also significantly improved via adding steel fibers.

Yaakoub [46] studied the properties and structural behavior of UHPC containing, straight micro steel fiber (diameter 0.2 mm, length 13 mm) with maximum volume fraction 2% , the maximum content of SF of 15% as a replacement by weight of cement. The main aim of this research is to study the mechanical properties of UHPC containing different volume fraction (1, 2, and 3%) of hooked macro steel fiber (diameter 0.5 mm, length 30 mm), the different content of SF (10, 15, 20, 25, and 30%).

Plank and Schroefl [47] improved the flowability of fresh UHPC using a new generation of superplasticizers named as Polycarboxylate (PCE). They measured the consistency of PCE with cement and SF. The latter one due to the larger surface area than the former had a character of absorbing PCE charging negatively. Hence, UHPC contained SF had highly flowable fresh concrete than that with only contain cement.

Collepardi et al. [48] compared the ordinary UHPC that contained superplasticizer, SF, natural sand, and steel fibers with modified UHPC which natural aggregates were graded. The both types of concrete were cured using room temperature, steam curing at 90^{o}C, and steam curing under pressure at 160 ^{o}C. The test results illustrated that the results of compressive strength were not changed with different UHPC types. The strength, dry shrinkages, and creep strain results showed curing under pressure better than steam, and room curing, respectively.

Rougeau and Borys [49] completed a study on several ultrafine used to produce UHPC. The ultrafine powders as supplementary cementitious material (SCM) used were metakaolin (MK), fly ash (FA), limestone microfiber (LM), siliceous microfiber

(SM) and micronized phonolith (PH). The UHPC with LM and PH lead to a good fluidity. The UHPC with MK, FA and SM required more SP and water to achieve the same workability. Despite a significantly higher dosage of SP in comparison of those with SF, the UHPC with MK shows poor workability with a slump of 17 cm. The fluidity of metakaolin blended cement become poorer than that of Portland cement at the same dosage of SP and the same water-cement ratio. The UHPC with FA required significantly higher water content. All the compressive strengths of UHPC were above 150 Mpa at the age of 28 except for those with FA. The higher performances are obtained with SF. Much higher strengths at periods ranging from 28 to 90 days have been noted using SF.

Yazici [50] studied UHPC incorporated by 20, 40, 60 and 80% of FA and S using water, steam, and autoclave curing of the specimens. The author produced a mixture of 185 Mpa compressive strength with 340 kg/m^3 of cement per total binder content. from the total constant amount of binder. The same UHPC mixture cured with steam and autoclaving had superior to standard curing.

Li and Ding [51] studied physical and mechanical properties of concrete contained the individual and binary effect of pozzolanic materials like MK and S. In addition to improving compressive strength, the fluidity of fresh concrete also enhanced.

Thomas et al. [52] preferred a ternary blending of cementitious materials than binary effect and individual effect of only cement, respectively. They found that the mechanical property results of concrete contained cement+ SF+FA higher than corresponded cement+ SF, cement+ FA, and cement.

Popovics [53] considered the cement+ SF+ FA (ternary) systems in UHPC. They observed many advantageous effects due to mixing pozzolanic reaction of SF and FA such as workability, sonic pulse velocity, and strength results.

Lam et al. [54] reported mechanical properties of UHPC with different mineral admixture percentages. The experimental results indicated favorable effect of SF and FA on improving fracture property and compressive strength of UHPC.

Gonen and Yazicioglu [55] studied the influence of the pozzolanic effect of SF and FA on short and long term properties of UHPC. They found that SF significantly effects on both terms, but FA had the role adversely in the short-term and positively on long-term reactions. The binary effect of SF+FA had the desirable effect of the transport properties more than strength improvement.

Qian and Li [56] investigated many properties of UHPC incorporating 5, 10, and 15% of MK. They concluded favorable effect of MK on significant improving tensile strength and peak load with infant enhancement of modulus of elasticity. The contribution of MK was optimized with 10% when results of flexural and compressive strength showed maximum enhancement.

Schachinger et al. [57] used steam at 90ºC from the age of 24 to 48 for curing of UHPC contained mineral admixtures. It was observed that curing by steam accelerated pozzolanic reaction of SF. Due to reaction SF with $Ca(OH)_2$, C-S-H gel formed and resulted in improving strengths of UHPC.

Khadiranaikar and Muranal [58] investigated the compressive strength variation of UHPC due to various parameters like w/c ratio, SF, quartz sand, and curing condition. In experiment shows the average compressive strength to the w/c ratio graph and it shows 0.2 gets a maximum strength for 28 days and the effect of the influence of SF on compressive strength, and maximum doses of SF is 15% at 0.2 w/c ratio. Another study shows the effect of the addition of quartz sand on compressive strength, and it indicates that increase the strength up to 20% at accelerated curing condition and the influence of curing regime on compressive strength by normal curing at 27 ºC. and hot water curing at 90 ºC for 48 hours and results shows the increment up to 10% in strength at 90 ºC.

Lin et al. [59] carried out an experimental program to evaluate the mechanical properties of UHPC. Test variables included w/c ratio, the dosage of SF and volume fraction of steel fiber. Compressive strength test, direct tensile strength test, splitting tensile strength test, abrasion resistance test and drop weight test were performed, and the results were analyzed statistically. It was found that the composites containing 10% SF demonstrate better compressive strength, splitting tensile strength, direct tensile strength and abrasion resistance, and worse impact resistance than composites containing 5% SF. The 10% SF specimens with w/c ratios of 0.35 and 0.65 have 18 and 15% higher compressive strength, 3 and 8% higher direct tensile strength, 40 and 38% higher toughness, 32 and 42% lower abrasion coefficient and 83 and 62% lower impact toughness than the control specimen, respectively. The addition of steel fiber to SF composites at w/b ratios of 0.35 and 0.65 achieves 10 and 9% increase in compressive strength, 68 and 59% increase in splitting tensile strength, 31 and 15% increase in direct tensile strength, 23 and 28% increase in toughness, 18 and 8%

reduction in abrasion coefficient, and 4118 and 296% increase in impact toughness, respectively.

Liu and Huang [60] proposed a UHPC with flow value of 200% for repair and habitation. Series of tests like slant shear, rebar pull-out, tensile tests were performed, and the results were compared with the cylinders repaired with epoxy resins. The strength of cylinders with mortar was higher while the slant shear strength is almost equal to that of epoxy resin.

Uzawa et al. [61] applicate reinforced UHPC with micro steel fibers. In spite of using water curing, a superior UHPC with 200 Mpa compressive strength, and high toughness has been produced. The mixture design generally consists of SF, cement, new generation of superplasticizer, and high-strength steel fibers of 15 mm length and 0.2 mm diameter. In addition to superior mechanical properties of high toughness and strength, UHPC during the fresh state had great fluidity, and self-compaction performance has been observed.

Lee et al. [62] studied the usage of UHPC as repair material and evaluated its bond and durability properties. The compressive strength, bond strength, steel pull out strength, and relative dynamic modulus of elasticity tests was carried out. The test result proved the superiority of UHPC with respect to other concretes. The mechanical properties are 200% more when compared to the normal strength concrete.

Lee [45] reported on UHPC produced in the laboratory to study the effect of w/b ratio, the dosage of SP, curing regime and the effect of SF and quartz powder on the compressive and tensile behavior of concrete. The UHPC tested had a maximum compressive strength of 200 Mpa and flexural strength of 15-20 Mpa. The mechanical properties examined were directly correlated to the particle packing of the fine reactive powders added to the concrete.

Ma et al. [63] in their study investigated UHPC with and without coarse aggregate for autogenous shrinkage and other mechanical properties. The autogenous shrinkage of UHPC with coarse aggregate is about 60% of UHPC. In addition, the compressive strength showed no difference for UHPC with and without coarse aggregate.

2.1.4 UHPC- Structural Applications

Donnaes and Phillippenes [64] also developed UHPC in a research laboratory at Bouygues, France. This concrete is composed of extremely fine powders of sand, cement, quartz, and SF. A new pedestrian walkway bridge was constructed in Sherbrooke, Quebec on November 27, 1997. This prefabricated 197ft walkway was built using prefabricated UHPC structural elements. An innovation introduced in the assemblages which allowed in each cable a single strand and Anchorage head was simplified by elimination of support plates since UHPC can directly take the compressive stress developed during prestressing. Also a 2,150 sq.ft., façade for a Paris school was constructed using UHPC. The façade demonstrated the materials aesthetic qualities creating plates with an untreated surface similar to polished concrete.

Grabeal [65] studied the strength and durability characteristics of UHPC that make it suitable for the use of highway bridge structures. Prestressed highway bridge girders were cast from this material and tested under flexure and shear loadings. The testing of these AASHTO Type II girders containing no mild steel reinforcement indicated that UHPC, with its internal passive fiber reinforcement. Based on this research, a basic structural design philosophy for bridge girder design is proposed.

Voo et al. [66] studied the effect of large-scale girders failing in shear. The girders were cast using 150-170 Mpa steel fiber reinforced UHPC to carry shear stresses in thin webbed prestressed beams without shear reinforcement. Comparisons were made for crack patterns for the specimens with respect to quantity and types of concrete mix and types of fibers in the concrete mix. Also, the shear beams were modeled using finite elements with a good correlation observed for the non-linear numerical model against the experimental data.

Figure 2.1 demonstrated the pedestrian cable-stayed bridge that built in the Republic of Korea. Normal concrete and UHPC was used for constructing rear and front girders, respectively. First, the bridge was designed theoretically using the serious 3D software. The designed bridges analyzed then constructed to study the structural performance of applicable UHPC. The bridge constructed and designed attending the following limitations [67]:

- Thickness of girder is less than 0.75 m

- Hybrid structures of UHPC and normal concrete were implemented.

- The old and new buildings were connected.

- The self-weight of the bridge didn't transfer to the old building.

Figure 2.1. UHPC pedestrian girder cable-stayed bridge [67]

Utilization of UHPC in the U.S. has been limited, but its international roots have led to many different applications in Canada, Europe, Asia, and Australia. While many of the applications have been related to the transportation industry, more and more uses for this innovative material are being discovered to reap not only the benefits of its strength, but also UHPC's durability. Only a brief overview of UHPC functions in the world are presented here. However, more detailed investigations of these uses can be found in other sources [68-70].

Development of UHPC began in the early 1990's, and in 1997 the first structure made of UHPC, the Sherbrooke pedestrian bridge, was constructed in Quebec, Canada. The 197-foot-long structure is a post tension open space truss (Figure 2.2). Six match cast segments compose the main span. Among many other benefits, the enhanced mechanical properties of UHPC allowed for the use of a deck top of only 1.2 in. thick [71]. To develop an understanding of how UHPC works in actual applications, a long-term monitoring program was also implemented on the bridge to monitor deflections and forces in the prestressing tendons.

Figure 2.2. UHPC example: Sherbrooke footbridge [72]

In 1997, UHPC's durability received a test when it was used to replace steel beams in the cooling towers of the Cattenom power plant, in France. The environment is extremely corrosive, and UHPC was chosen because of its durability properties with the expectation of reduced or eliminated maintenance. Three years later an AFGC-SETRA working group visited the site, and under a normal layer of sediment, no deterioration of the UHPC was noted [72].

Other transit applications include footbridges constructed in South Korea, Japan, France, and Germany. The Footbridge of Peace in Seoul, South Korea (Figure 2.3a and b), is an arch bridge with a span of 394 ft, the arch height of only 49 ft , and a deck thickness varying anywhere between 1.2 in. and 4 in. [73]. In Japan, the Sakata-Mirai footbridge (Figure 2.3c) was completed in 2002 and demonstrated how perforated webs in a UHPC superstructure could both reduce weight and be aesthetically pleasing [69]. France utilized UHPC's fire resistant capabilities and high load carrying properties to construct an aesthetically pleasing yet, highly fire resistant footbridge (Figure 2.3 d) at a Chryso Plant in Rhodia [69]. Most recently, the Gärtnerplatz Bridge was completed in Kassel, Germany (Figure 2.3e) [68].

a)

b)

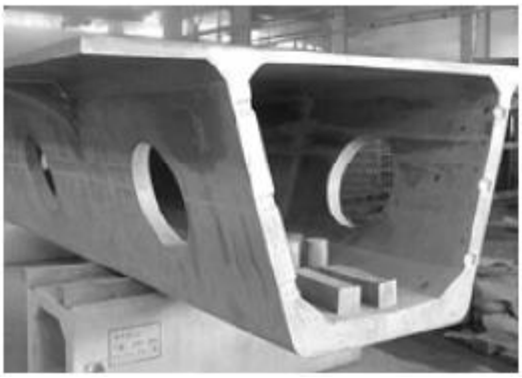

c)

d)

e)

Figure 2.3. UHPC applications: (a) Footbridge of Peace in Seoul, South Korea at night [69]; (b) and during the day [74]; (c) perforated hollow UHPC bridge girder [74]; (d) fire resistant UHPC footbridge in Rhodia, France; (e) Gärtnerplatz Bridge - Kassel, Germany

In 2001, the Bourg Les Valence Bridge in France was the 1st vehicle bridge constructed using UHPC. It spans approximately 145 feet with two equal spans consisting of 5 π-shaped prestressed elements. The π-shaped elements were connected by casting UHPC in situ [72]. Additionally, the Shepards Creek Bridge in New South Wales, Australia used UHPC to carry four lanes of traffic over a skewed (16°) single span of 49 ft. while reducing the dead weight by over half [75].

UHPC made the transition to the United States in 2001 with the construction of the roof of a clinker silo (Figure 2.4a) in Joppa, Illinois [74]. The 24 wedge-shaped precast panels with a thickness of 0.5 in. covered the 58 ft. diameter silo. Utilizing UHPC saved time and labor as the roof was constructed faster and with fewer workers than the two companion metal roofed silos. Continuing in the cement industry, UHPC has since been used to create columns with a smaller cross section in a cement terminal in Detroit, Michigan (Figure 2.4b) which allows for five more feet of truck width clearance for the three loading bays [74].

a) b)

Figure 2.4. UHPC construction examples: (a) UHPC panels on Joppa clinker silo and; (b) 54 ft UHPC columns in Detroit [69]

2.2 Concrete Filled Steel Tubular Columns (CFST)

Gardner and Jacobson [18], and Knowles and Park [76] are the primary authors directed to concentric compression of CSFT column. They revealed that concrete controlled by improving compressive strength while with the developing of stresses the yield strength of steel faced reduction. Then after, many other theoretical and experimental researched implemented (i.e. Knowles and Park [77]; Shea and Bridge [78]).

Tomii et al. [79] investigated that the ultimate load of CSFT is significantly bigger than the nominal load that consists of the summation of two-factor strengths. They returned to the developing of strain hardening of composite steel and restricted concrete. The authors tested about 270 stub columns then they draw the relation between axial load and strain. Accordingly, they declared the parameters of CSFT depended on the D/t, cross section area of column, and strength of concrete and steel.

tests on approximately 270 stub columns calculated showed that axial load versus longitudinal strain relationships in a classification based on test parameters including cross-section shape, diameter to wall thickness ratio (D/T) and concrete and steel strength.

Zhang and Shahrooz [80] used the test data from the past studies and three additional specimens test. The test specimens include short and slender CFSTs made with normal and high strength steel tubes filled with normal and high strength concrete. The comparison was made with ACI and AISC codes for calculating the capacity of

CFST columns. It was found that the capabilities from ACI and AISC codes varied significantly. However, the results from ACI method are generally closer, and the both codes were reasonable for slender CFST made with normal strength steel tubes. Neither ACI nor AISC method is applicable for the case in which high strength tubes are used.

Several researchers have studied the behavior of CFST columns with circular, square, rectangular sectional shapes in the past forty years [18, 81, 82]. Under axial compression, the steel tube was found to increase the axial strength of CFST columns. This increase in column axial strength is due to concrete confinement, and limited extension of internal concrete cracking [11, 83]. Effects of concrete confinement are typically not considered at initial stages of axial loading. This is because Poisson's ratios of the two materials differ so that steel has higher deformations compared with concrete [84]. Thus, concrete and steel lack interaction under small loads. When concrete begins to soften under greater load, the deformation properties change. The concrete dilates outward, applying lateral pressure on the steel tube. The steel tube is said to be mobilized at this point, as transverse hoop stresses develop to confine concrete. Therefore, the concrete falls under triaxial confinement, while the steel tube experiences biaxial stresses. This confinement effect causes the filled tube column to withstand load greater than the sum of individual steel and concrete axial strengths [85]. Concrete also delays inward steel buckling, which is typically characteristic of hollow structural sections (HSS). Local buckling does not occur if bond strength between concrete and steel is strong enough [86].

Sakino et al. [82] classified CFST columns based on loading conditions. Type A columns refer to load applied to steel and concrete portions simultaneously. Type B columns relate to load applied on the concrete core only. The degree of confinement in Type B columns was more significant compared to that of Type A columns. However, Type A loading conditions may arise in practical applications. Furthermore, the design of CFST columns based on Type A loading may provide beneficial conservatism for safety considerations.

A wide range of factors affects confinement and axial strength of CFST columns under axial compression. Concrete confinement has been found to be more effective for circular CFST with low slenderness ratio, resulting in higher axial strength in these columns [20, 87, 88]. Hossain [89] performed experimental investigations on thin-walled composite columns of varying slenderness to find that strength reduction increased dramatically due to increasing slenderness ratio (until slenderness of 24 was reached). The difference in slenderness resulted in different failure modes of CFST columns. Concrete crushing and steel yielding occurred in shorter columns, and longer columns failed by global instability. Failure modes of conventional concrete filled columns given the slenderness ratio are common in the literature. Nonetheless, failure modes of filled steel tube columns are expected to be dependent on the strength, ductility, and material properties of concrete in-fill. Softer concretes may lead to greater axial stress on the steel tube, resulting in buckling failure. Conversely, stiffer concretes may cause shear failure. Therefore, resulting in behavior due to slenderness ratio should vary with concrete type.

Furthermore, concrete confinement also increases as diameter-to-thickness ratio decreases. In addition, CFST columns were found to exhibit more local buckling and crushing of concrete for higher diameter-to-thickness ratio [86, 90].

The axial capacity of CFST columns increases with steel and concrete material strength, as expected [20, 88]. Although it was determined that axial strength of CFST columns increased linearly with steel yield strength [82], this is not necessarily the case with concrete compressive strength. Whether or not the relationship between the axial capacity of CFST columns and concrete compressive strength follows linearity is yet to be confirmed.

Due to requirements from certain code provisions which state that bar reinforcements are mandatory in concrete columns, a new challenge emerged in quantifying the axial capacity of CFST columns in-filled with bar-reinforced concrete. Hoop reinforcements also provide additional concrete confinement and axial capacity of CFST column increases due to contributions from longitudinal bars. However, few studies have been completed on CFST columns with bar reinforcements, especially using different types of concrete in-fill [78].

Tube and hoop reinforcement confinement in filled tube columns have been analyzed and quantified by researchers in the past based studies on normal concrete. However, concrete behavior under compression was also found to relate to Poisson's ratio and elastic modulus. Moreover, the relationship between elastic modulus and compressive strength is not necessarily the same for normal concrete compared with concrete reinforced with various types of fibers [91].

2.2.1 CFST-Normal and High Strength Concrete

Investigations on high-strength concrete [92] concluded that not only does concrete compressive resistance have an effect on axial column capacity, in-fill material also changes deformation characteristics and behavior. Deformation capacity was reduced with the use of high-strength concrete in normal-strength steel tubes but is expected to improve by increasing steel strength or tube thickness. Furthermore, publications on the effects of compaction on filled tube column ultimate strength show that even the same core materials within the steel tube can yield different results based on homogeneity of concrete [83, 93, 94]. However, limited experimentation has been done comparing the effects of different in-fill material on steel tube columns, especially for recently developed high-performance concretes.

Experimentation was done in the past on CFST under axial compression [95]. Prior to Yu et al. [95], the performance of self-compacting concrete (SCC) filled columns was analyzed for compressive strengths ranging from 50 to 90 Mpa [91, 94]. To further extend the range of SCC compressive strengths tested in CFST, Yu et al. [95] performed experiments on circular and square thin-walled columns in-filled with concrete of up to 121 Mpa cube compressive strength. In addition to water, cement, sand, slag, and high range water reducing admixture, the mix design included coarse aggregates. The resulting slump flow was 600 mm. Thin-walled sections were fabricated by cutting and tack welding steel sheets in the desired configurations. Column slenderness ranged from 12 to 120, tube thickness was constant at 1.6 mm, and load eccentricity ratios differed from 0.0 to 0.6. As the load was applied at intervals across both concrete and steel (rather than continuous loading), columns are classified as Type A. Square columns filled with high-strength concrete failed in a similar manner as those tested with normal-strength concrete by other researchers [93, 96]. However, circular columns filled with high-strength concrete failed in shear. In addition, the post-peak behavior of load-displacement responses was found to be steeper in square columns compared with circular CFST columns. Thus, circular columns showed more efficient concrete confinement, even with high-strength concrete as in-fill. Yu et al. [95] concluded that CFST columns in-filled with self-consolidating high-strength concrete under axial compression showed lower ductility compared to those with normal strength concrete.

However, the ductile behavior of CFST columns is expected to improve with the presence of steel fiber reinforcement [97]. Steel fibers are anticipated to improve brittle behavior in normal strength concrete by creating a bridge between cracks to hold materials together rather than allowing portions to spall off under load. Researchers in the past had studied mechanical properties and durability of self-consolidating steel fiber-reinforced incorporating various materials such as FA and S [98-101]. Khaloo et al. [97] presented experimental results on standard 150 x 300 mm short column specimens and 100 x 140 x 1200 mm beam specimens made of concrete with steel fiber volume fractions ranging from 0.5 to 2 percent. Two concrete mix designs were used with compressive strength from 40 to 60 Mpa. In addition to steel fibers, concrete materials included cement, SF (included in 60 Mpa concrete but not in 40 Mpa concrete), water, fine aggregates, coarse aggregates, filler, and admixtures. Slump flow diameter of structural concrete decreased with the increased presence of steel fiber reinforcements, but less so for those with higher compressive strength due in part to the inclusion of SF content. Although slump flow diameter of 60 Mpa concrete decreased from 800 to about 720 mm with the increase in steel fiber content, the mixture for the test specimens can still be considered workable, capable of self-consolidation, and is acceptable based on EFNARC [102] standards. These results indicate how the increased steel fiber content in higher strength for the test specimens with SF can improve its ductile characteristics while maintaining workability.

2.2.2 CFST- High Performance Concrete

The use of concrete-filled composite columns may be dated back to the 1960s [103]. The state of art review on steel–concrete composite columns by Shanmugam and Lakshmi [104] highlighted the significant research into this field. Most of the researchers focused on concrete-filled tubular columns with conventional concrete [84].

With the development of the economy and the depletion of resources, the concrete-filled steel column should get higher performance. So, being higher with the specific strength and lower the consumption of natural resource and the cost in their life cycle, reactive powder concrete as the representative of green super high strength concrete is a promising application and has become the focus of research and implementation to the modern concrete. However, the structural behavior of concrete-filled tube columns is affected by many factors, such as member material properties, column slenderness and the geometry of steel section. Simultaneously, domestic and foreign researches done on super high-strength concrete composite members are rare. This necessitates the search for the compressive behavior of the super high strength concrete used in stone-chip steel tube columns. To enable a better understanding of the compressive behavior of the high strength concrete-filled steel tubular columns, the constitutive relation of the super high strength and high-performance concrete was studied [84].

Yang et al. [105] tested two concrete-filled steel tube column specimens in order to investigate the axial compressive behavior of short concrete-filled steel tube columns with different concrete grades. Of the 2 tests, two specimens were compositely loaded with the concrete core and hollow section steel tube to investigate the effect of concrete strength on the axial compressive behavior of short composite columns. As seen in Table 2.1, the compressive strength of high performance concrete of 130 and 137 Mpa was used for the columns. The parameters of the test specimens are also given in Table 2.2.

The numerical modeling method presented will mainly be focusing on the axial compressive behavior of short concrete-filled composite columns compositely loaded and will not take into account the concrete shrinkage effect. The axial compressive load versus the average axial strain relationship. Based on the experimental studies of 2 short steel tubular columns filled with super high strength concrete used stone-chip , it is found that within the factor scope of these tests, both the confinement index and the concrete strength of the specimens have significant influence on their features of specimen subjected to the axial load experiment results show that the load and average strain curves of the specimens might be divided into four stages: elastic deformation process, elastic-plastic deformation process, the descent process and the recovery process of its carrying capacity, and also that specimens with the lower confinement index exhibit a rapid softening process in the post-peak region with a towering peak and a shorter incremental portion plus the weak recovery in the four stage, while specimens with the higher confinement index exhibit a gradual softening process in the post-peak region with a chubby curve and a longer incremental portion plus the strong momentum of recovery in the fourth The experimental phenomena indicate that all specimens are typical of the higher residual load capacity and excellent ductility, as shown in Figure 2.5 [105].

Table 2.1. Mix of extra-high strength concrete mixed with stone-chip for the columns [105]

Mix type	Mix							w/b ratio	Cement content	f_{cu}
	Cement	SF	MK	FA	Rock ballast	Macadam	Water Reducer		Kg. m^{-3}	Mpa
A3	1	0.167	0.167	0.333	2.028	3.056	0.0694	0.22	350	137.3
A5	1	0.175	0.175	0.338	1.75	2.575	0.0625	0.22	380	130.1

Where f_{cu}= compressive strength

Table 2.2. Parameters of column test specimens [105]

Specimen number	D x t mm	D/t	L mm	L/D	f_y Mpa	Mix type	f_{cu} Mpa	ɵ
G106	121x5.0	24.2	370	3.1	295	A3	137.3	0.57796
G132	121x5.0	24.2	370	3.1	295	A5	130.1	0.60994

Where, D= outer diameter of steel tube, the t= thickness of the steel pipe, the f_y=yield strength of steel tube, θ= generalized ferrule indicators, the L= length of steel tube.

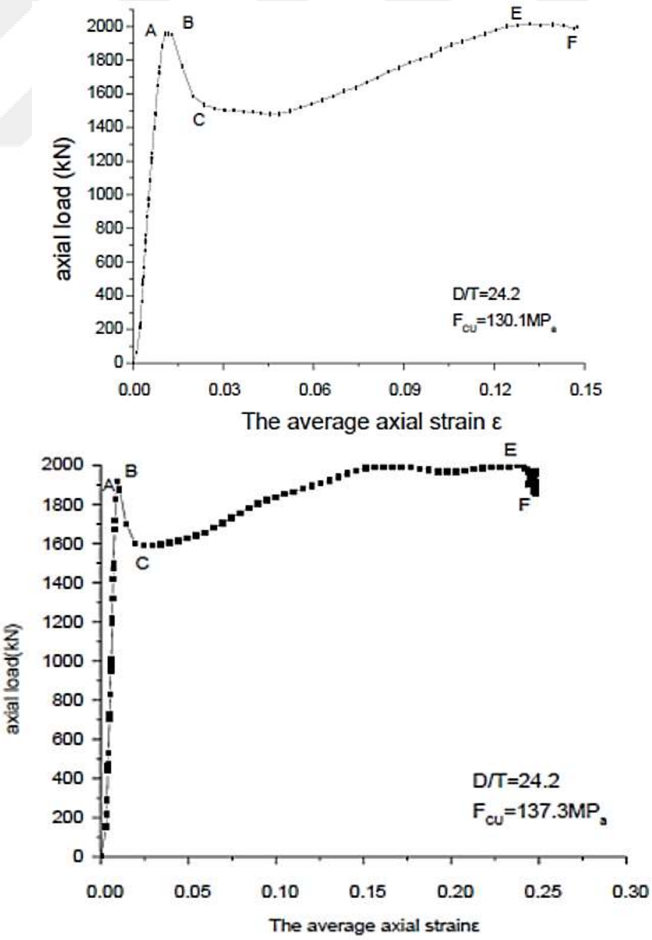

Figure 2.5. Load-steel tube average strain curve [105]

In the study of Yang [105], the simulation in developing a numerical model through the ABAQUS/Standard solver was also used to investigate the axial compressive behavior of high strength concrete filled circular steel stub columns. The feasibility and accuracy of the numerical method and the proposed stress–strain model were verified by comparing the predicted results with the experimental observations, and the following conclusions are made: The FE numerical method developed via the ABAQUS/ Standard solver could be used to predict the main structural behavior of strength concrete-filled steel tube columns under axial compressive loads.

Xiang et al. [106] investigate the flexural performance of CFST members. One would doubt the meaning to study the flexural behavior of the CFST members as, in reality, the CFST members are seldom subject to pure bending. This may be true for building structures, where CFSTs are mainly used as column members. However, CFSTs are also widely used for bridge construction and in pole structures where they are subject to predominately flexural action. Besides, when designing CFST columns under combined axial force and bending moments in high-rise structures, one may have to determine the bending resistance according to the moment-axial force (M-N) interaction curves as shown in Figure 2.6.

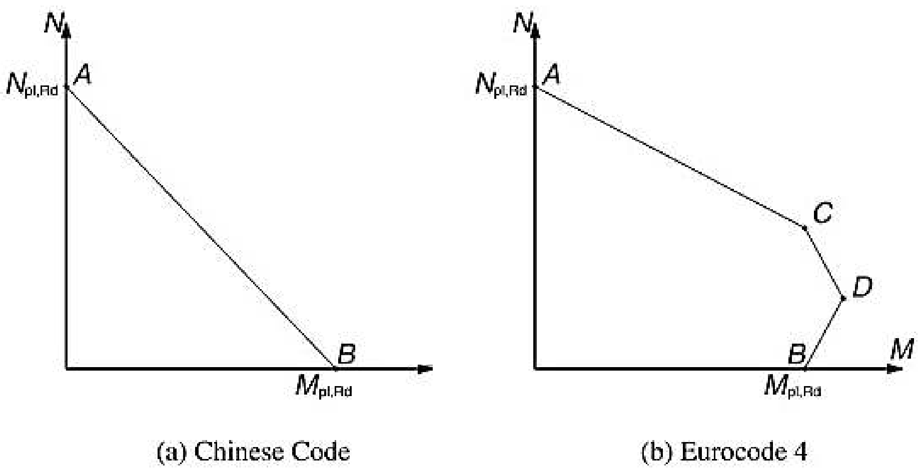

Figure 2.6. M-N interaction curves for CFST members [106]

He presented the experimental work on 8 CFST specimens subject to flexural loads. Test results, including maximum moment resistance, elastic flexural stiffness, load-displacement curves and load-strain curves, were presented. Eurocode 4 method was adopted to predict the flexural resistance of CFST members with high strength steel and high strength concrete, and its accuracy is discussed by comparing with the test results and additional data from the literature. The aim is to extend the current guides to design CFST members with high tensile steel and high strength concrete. High tensile steel with yield strength up to 780 Mpa and high strength concrete with compressive cylinder strength up to 180 Mpa were used. The test results seek to clarify if the cross-section plastic moment resistance can be achieved if high tensile steel and high strength concrete are used in CFST members. The maximum moment resistance from tests was compared with the analytical results predicted by Eurocode 4 method. Then design recommendations were provided so that Eurocode 4 method could be safely extended to determine the flexural resistance of CFST members with high tensile steel and high strength concrete [106].

Li et al. [107] studied the performance of square steel tube columns composite with high strength concrete. Six square steel tube filled with high strength concrete samples were constructed and tested directed to bi-axial eccentric loading. The details of tested samples demonstrated in Table 2.3. The primary test factors were the steel ratios, eccentricity, and slenderness ratios. The behavior of strength and concrete filled square steel columns were illustrated due to the effect of factors mentioned above. The experimental results show that steel ratio plays a major factor affecting the specimen bearing capacity. As what shows in the experimentation, the steel ratio is a significant factor which affects the bearing capacity of the samples, and the stable bearing capacity of the specimens reduced rapidly with the increasing the ratio of slenderness. Roper material constitutive models for HCFST columns are verified by ABAQUS software versus experimental data. A good agreement showed a comparison of experimental failure loads against the expected failure loads taken method mentioned in the reference. The analysis of the results is summarized in Figures 2.7-2.10 and Table 2.4.

Table 2.3. Specimens in details [107]

Specimen Number	B (mm)	L (mm)	t (mm)	t^{-} (mm)	f_y (MPa)	f_u (MPa)	E_s (Gpa)
ES4-4-71	200	800	4	3.5	306	430	200
ES4-6-71	200	800	6	5.8	340	440	206
ES6-4-71	200	1200	4	3.5	306	430	200
ES6-6-71	200	1200	6	5.8	340	440	206
ES8-4-71	200	1600	4	3.5	306	430	200
ES8-6-71	200	1600	6	5.8	340	440	206

Table 2.4. Comparison of test results and calculation results [107]

Specimen number	t (mm)	f_y (MPa)	φ_{xy}	N_e (kN)	N_{c1} (kN)	N_{c2} (kN)	N_{c1}/N_e	N_{c2}/N_e
ES4-4-71	3.5	306	0.957	1524	1636.9	1501.2	1.074	0.985
ES4-6-71	5.8	340	0.958	1895.6	1899.4	1827.7	1.002	0.964
ES6-4-71	3.5	306	0.909	1548.4	1546.3	1406.1	0.999	0.908
ES6-6-71	5.8	340	0.913	1844.9	1818.2	1722.7	0.986	0.934
ES8-4-71	3.5	306	0.863	1516.5	1455.4	1314.4	0.96	0.867
ES8-6-71	5.8	340	0.869	1717.3	1738.4	1619.2	1.012	0.943

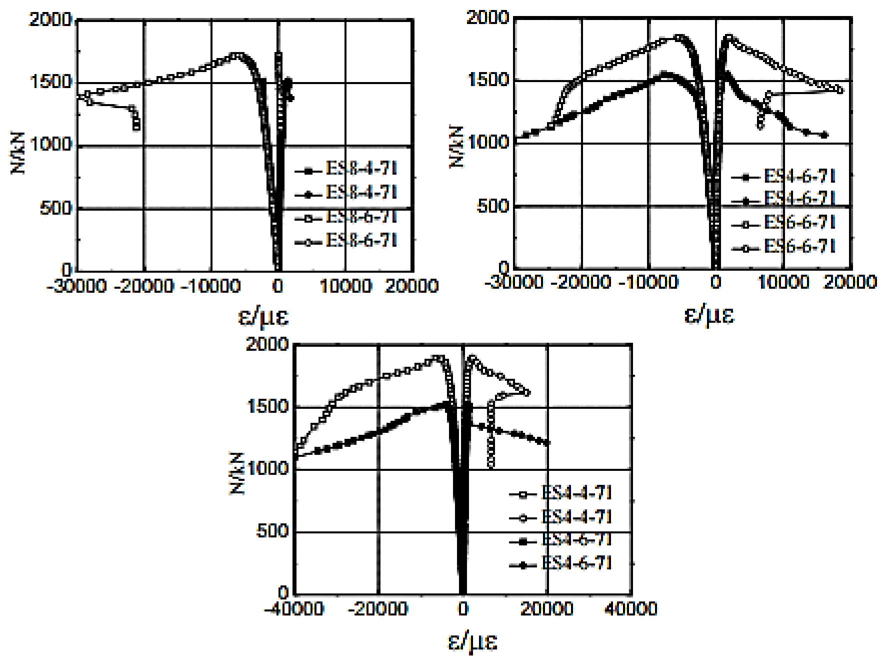

Figure 2.7. Load (N) vs. axial strain (ε) relations [107]

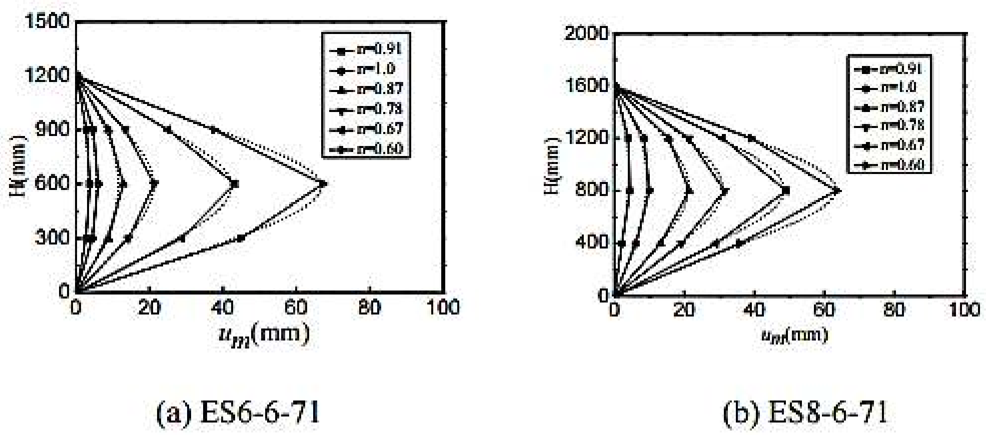

Figure 2.8. Deflections curves of CFST specimens [107]

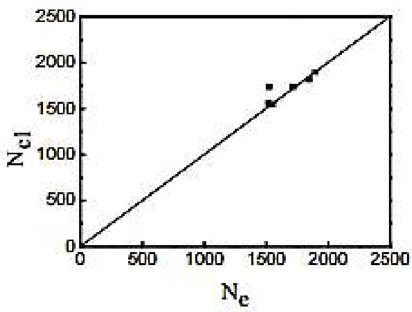

a)

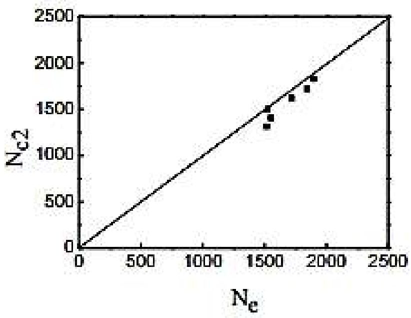

b)

Figure 2.9. a) Comparisons of finite element results Vs. test results and b) comparison of results of the simplified method and test results [107]

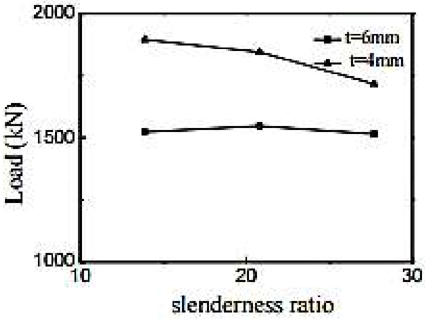

a)

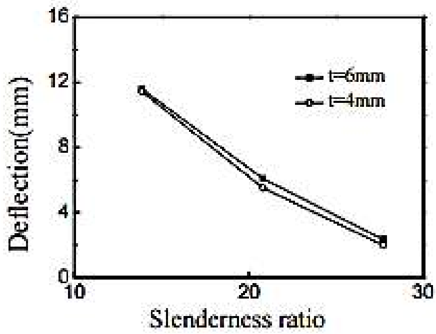

b)

Figure 2.10. a) Relationship between load and slenderness ratios and b) the slenderness ratio and deflection interaction curves [107]

2.2.3 CFST–Structural Applications

Recently, CFST method developed to replace the classical methods in vogue [90]. CFST is a steel column that designed by filling it with concrete. Because of their superior properties, CFST column applicant in bridges, offshore structures, buildings, etc. [108]. Composite steel column infilled with concrete improve both ductility and strength properties with the same section size. Authors revealed multiple advantages of CFST columns such as higher stiffness, strength, ductility and greater seismic resistance that categorized from unilateral of concrete reinforcement or ordinary steel. As concrete internally protected steel from buckling, the steel at outside confined concrete [109].

There are about 200 of such bridges have been built or under construction in China, in which 23 of them have a span more than 200 m. The Qunyi Bridge, located in Fuan City, Fujian Province, China, is a half-through CFT arch bridge with a clear span of

46.00m and a rise of 15.333m, giving a rise-to-span ratio of 1/3. General views of this bridge are shown in Figures. 2.11 and 2. 12. Generally, for CFST arch bridges with a small span, the single tube is used as the rib. The arch rib in Qunyi Bridge is a single steel tube of φ800mmX14mm, filled with C30 concrete. The parallel arch ribs are braced by two lateral steel tubes near the crown and two reinforced concrete cross-beams near the abutments with diagonal steel tube struts [109].

The reinforced concrete deck system carries 12 m wide roadway and two 1.5 m wide sidewalks. It consists of cast-in-place continuous reinforced concrete slabs of 200 mm thickness, supported by cross beams and two small longitudinal beams. It is hung from the arch ribs by 109.5mm high-strength steel strands hangers underneath the ribs and supported by reinforced concrete spandrel columns over the arch ribs. The bridge was constructed from 1996 to 1998 and opened to traffic in July 1998 [109].

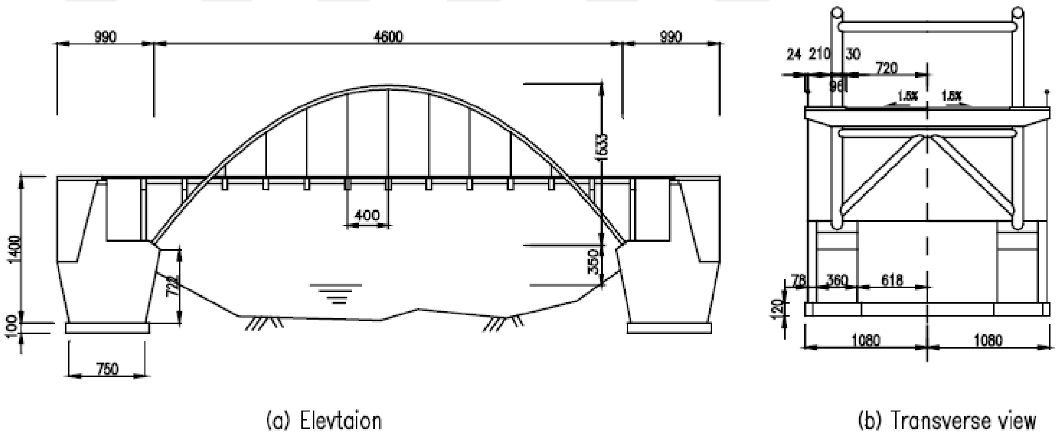

Figure 2.11. Elevation of Qunyi Bridge (unit: cm) [109]

Figure 2.12. Completed Qunyi Bridge [109]

To date, as shown in Figures 2.13- 2.16, most of the CFST used in Washington State are below ground in pile and shaft foundations where the structural loads are the highest. But there is also a strong potential to use CFST as bridge columns in high seismic zones. CFST columns are very tough elements with an ability to withstand large deformations. And further research will demonstrate that they can be used to resist major earthquake events by absorbing seismic energy reliably. In order to expand the use of CFST, more research is also planned to validate and optimize structural connections between CFST and adjacent beams and footings. Also, connections to prefabricated elements have been studied, which is an important step into incorporating CFST into the growing practice of “Accelerated Bridge Construction” In the meantime, CFST will be used in structures where they provide unique advantages such as tall structures, structures on soft soils, ferry terminal structures, and structures in zones of high seismic activity [110].

a) CFST pile groups supporting the main span of the Nooksack River Bridge

b) Completed Nooksack River Bridge

Figure 2.13. The Nooksack River Bridge is having steel truss span and supporting on groups of 3.5 ft. and 2 ft. diameter driven CFST piles [110]

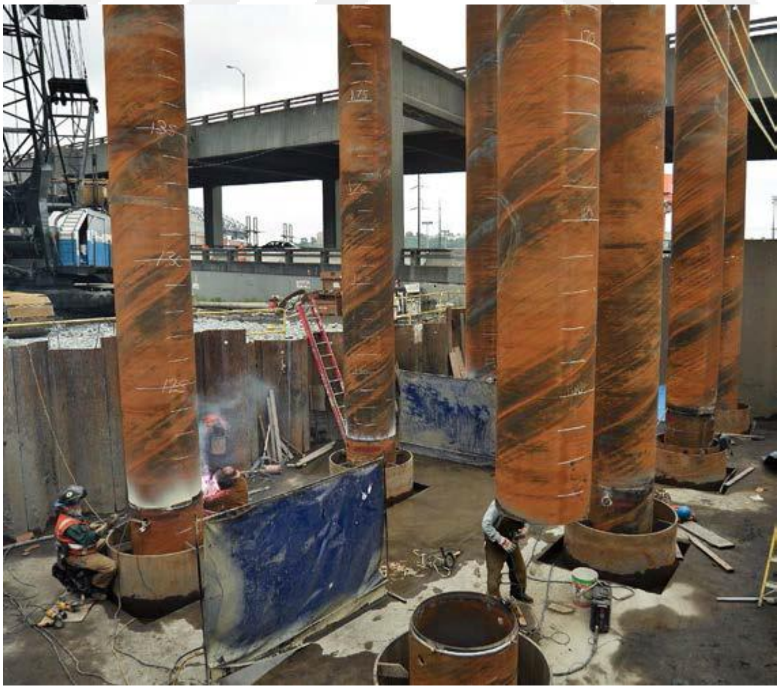

a) Pile driving on the Alaskan Way Viaduct Replacement

b) Alaskan Way Viaduct Replacement site

Figure 2.14. Alaskan Way Viaduct Replacement has 3 and 5ft. diameter driven CFST piles located in high seismic activity [110]

a) Pile driving on the Ebey Slough Bridge

b) Completed Ebey Slough Bridge

Figure 2.15. Ebey Slough Bridge supported on 5 ft. diameter driven CFST piles [110]

a) Shaft installation on the Puyallup River Bridge

b) Completed Puyallup River Bridge

Figure 2.16. Puyallup River Bridge supported on 10 ft. diameter CFST shaft [110]

Eurocode 4 [111] would be extended to cater for higher strength concrete, and steel since composite columns exhibit better stiffness and ductility and higher buckling resistance compared with individual steel or reinforced concrete columns. Considering this idea, at Techno Station, Tokyo, Japan, CFST used (steel: 780MPa, concrete: 160MPa) for the main columns; column size reduced from 800 mm (based normal strength materials) to 500 mm as shown in figure.2.17. high strength fire-reinforced mortar (170MPa) is used for indoor bridges. The depth of the bridge is kept to 335 mm [112].

a) Reduce column size

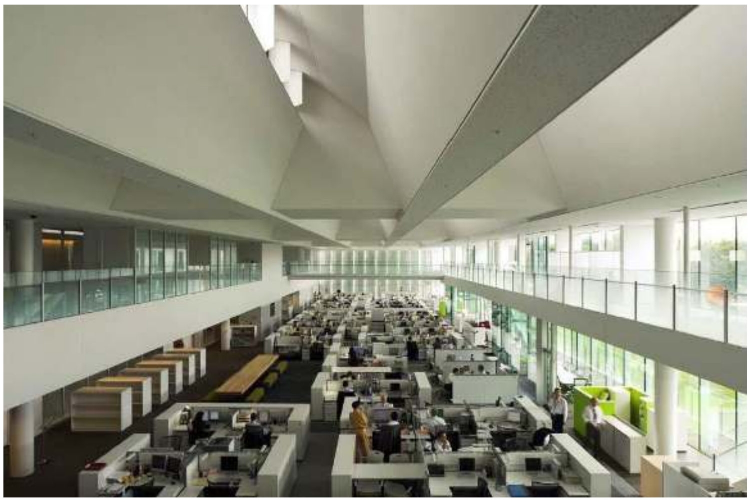

b) Large span workspace

Figure 2.17. Composite construction used CFST with high strength concrete [112]

The project of Raffless city in China incorporates retail, offices, housing, and hotel facilities. The project is composed of two 250 m tall twisting towers with a form of vibrant waves, along with a commercial podium and three stories of basement car parking.it reaches almost 400,000 square meters, as shown in figure.2.18. A composite moment frame plus concrete core structural system was adopted for the tower structures. CFST columns together with steel reinforced concrete beams form the outer moment frame of tower structures. The internal slabs and floor beams are of reinforced concrete [113].

(a) Artistic image

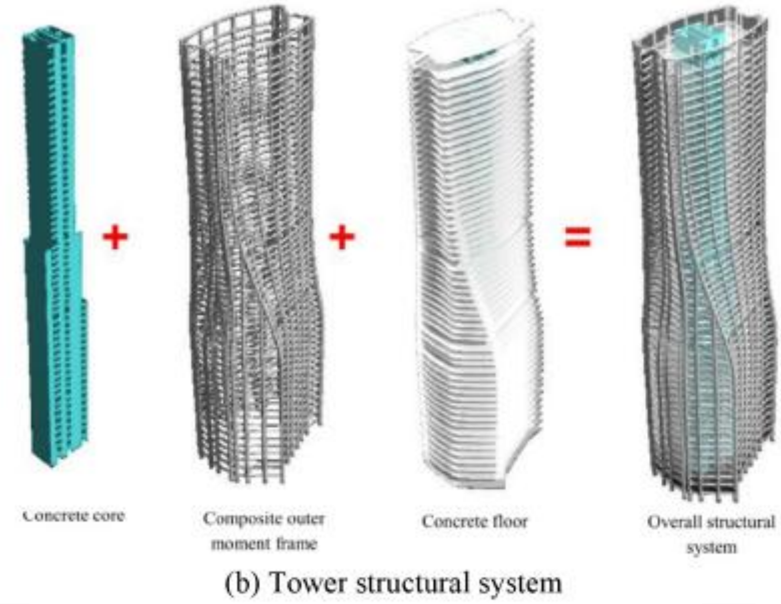

Figure 2.18. Raffles City Hangzhou, China [113]

CHAPTER 3

RESEARCH METHODOLOGY

3.1 Introduction

In this thesis, the experimental and numerical studies were considered. In the first part of the study, the experimental program was carried out in this study involved the mix design of UHPC with SCM like Flyash (FA), Slag (S), Silica Fume (SF), and Metakaolin (MK) at 15, 25, 50 and 75% replacement levels. Strength and fracture properties of UHPC were investigated experimentally.

The second part of the study encompasses the numerical study to show the possible use of SCM blended UHPC concrete in the composite columns and it′s effect on the axial capacity of such columns. For this, three widely used design codes, namely American Concrete Institute (ACI), Eurocode 4 (EC 4) and Chinese Design Code for Steel-Concrete Composite Structures (DL/T) were taken into account.

3.2 Experimental Study

3.2.1 Raw Materials

The cement used during this study is ordinary Portland cement (CEM I 42.5 R) conforming to the TS EN 197 (2002) (mainly based on the European EN 197-1). FA, S, SF, and MK were used as SCM in the production of UHPC. The materials are presented in Table 3.1. The particle size distribution of the cement and SCM is given in Figure 3.1. A new-generation superplasticizer (SP) of polycarboxylate-based type F was used to provide the target workability. As a particular, according to Table 3.4, it was evident that the 15% of SF demands lesser SP then followed by 15% of SF+MK, 15%MK, and subsequently control mixture, respectively. On the other hand, 25% FA and 25% S requested SP little less than control concrete, but when the amount of SF increased to 50%, the demand of SP increased because of increasing the surface area. Furthermore, any increased amount of S and FA resulted in decreasing workability with any form of mixture even binary, ternary, etc. Table 3.2 provides the properties of the SP. A commercial quartz sand with a specific gravity of 2.65 was used as fine aggregate. Three fractions of Quartz aggregate were utilized, namely 1.2-2.5, 0.6-1.2, and 0-0.4 mm. Figure 3.2 shows the three sizes of the aggregate used. The particle size distribution of Quartz 0-0.4 mm is also illustrated in figure 3.1.

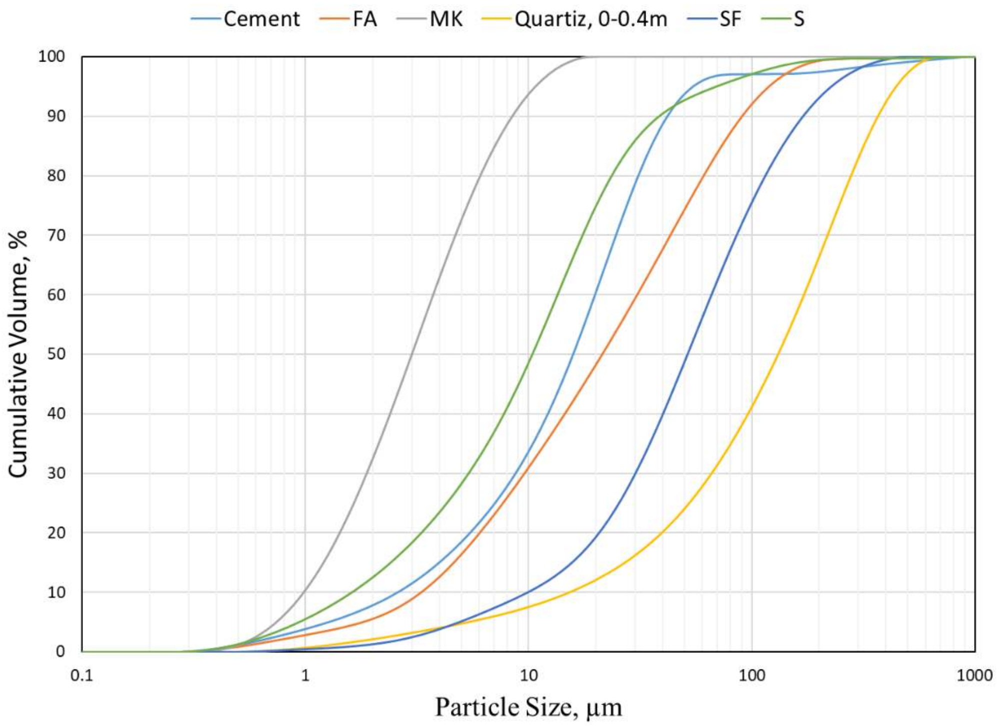

Figure 3.1. Particle size distribution of the material used

Figure 3.2. Sizes of Quartz aggregates

Table 3.1. Properties of materials

Constituent (%)	Cement	FA	S	SF	MK
CaO	57.87	4.24	34.12	0.45	0.78
SiO_2	17.99	56.2	36.41	90.36	52.68
Al_2O_3	3.88	20.17	10.39	0.71	36.34
Fe_2O_3	3.36	6.69	0.69	1.31	2.14
MgO	1.49	1.92	10.26	-	0.16
SO_3	2.47	0.49	-	0.41	-
K_2O	-	1.89	0.97	1.52	0.62
Na_2O	-	0.58	0.35	0.45	0.26
Cl	0.005	-	-	-	-
Loss on ignition	3.37	1.78	1.64	3.11	0.98
Insoluble residue	0.34	-	-	-	-
Free CaO	2.18	-	-	-	-
C_3S (%)	56.9	-	-	-	-
C_2S (%)	13.8	-	-	-	-
C_4AF (%)	8.8	-	-	-	-
Specific surface (m^2/kg)	394[a]	287[b]	418[b]	21080[b]	12000[b]
Specific gravity	3.15	2.25	2.79	2.2	2.5

[a] Blaine specific surface area.
[b] BET specific surface area.

Table 3.2. Properties of SP

Properties	Results
Appearance	Light brown to yellow liquid
Specific gravity at 20°C	1.08 ± 0.02
PH- value	7 ± 1
Alkali content (%)	≤ 1
Chloride content (%)	≤ 0.1

Brass-coated steel fibers with a length of 6 mm and a diameter of 0.16 mm were used to supply fiber reinforcement as (see Figure 3.3). As shown in Table 3.3, the manufacturer reported that the aspect ratio; specific gravity and tensile strength of the fibers were 37.5, 7.17 and 2250 Mpa, respectively.

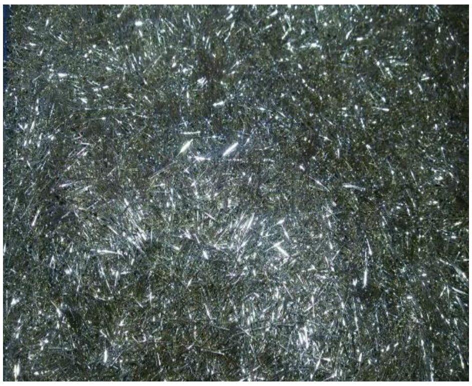

Figure 3.3. Micro steel fiber used in this study

Table 3.3. Physical, mechanical properties and aspect ratios of micro steel fibers

Name of Fiber	Length (L) (mm)	Diameter (d) (mm)	Aspect ratio (L/d)	Density (g/cm^3)	Tensile strength (N/mm^2)
Micro steel Brass coated	6	0.16	37.5	7.17	2250

3.2.2 Mixture Design, Sampling, and Curing

The details of mix design are given in Table 3.4. Group 1, 2, 3 and 4 in mix design codes show 15, 25, 50 and 75% SCM replacement, respectively. The enough workability for the mixtures was obtained by using varying amounts of SP. The mixtures in Table 3.4 were designated according to SCM replacement level. The two mixtures 75% FA and mixtures of 75 FA+S have been canceled because they did not harden well and they dissolved in the curing water as shown in Figure 3.4 a, b and c.

As shown in Figure 3.5, a Hobart mixer was used for mixing UHPCs; the mixtures were prepared by a special designed, vertical axis, high-speed mixer, which has been mixing speed of as high as 470 rpm. Dry binder and quartz aggregates were mixed for about 3 min with a speed of 100 rpm. The mixture was remixed for about five minutes after a half of water added to the speed of 100 rpm. Finally, SP and remaining water were added to premix material, and mixing was resumed at 470 rpm for about five minutes. After that the micro steel fibers added to premix material for 2 minutes. Fresh concretes were then poured into the molds and compacted by using a vibrating table.

a) After removing from the mold

b) After 6 hr in the curing water

c) After 1 day in the curing water

Figure 3.4. Failure of 75% FA and mixture of 75 FA+S

Figure 3.5. Mixing of UHPC: (a) dry mix, (b) water addition, (c) SP addition with low speed, and (d) SP addition with high speed

Table 3.4. Design of UHPC (kg/m^3)

Group	Mix	Cement	FA	S	SF	MK	SP	Quartz
1 (15%)	FA0S0SF0MK0	1150	0	0	0	0	48.3	1024.3
	FA0S0SF15MK0	977.5	0	0	172.5	0	26.5	1015.7
	FA0S0SF0MK15	977.5	0	0	0	86.25	36.8	1006.3
	FA0S0SF7.5MK7.5	977.5	0	0	86.25	86.25	36.8	1006.3
2 (25%)	FA25S0SF0MK0	862.5	287.5	0	0	0	47.4	929.7
	FA0S25SF0MK0	862.5	0	287.5	0	0	43.7	1005.2
	FA12.5S12.5SF0MK0	862.5	143.75	143.75	0	0	48.3	961.1
3 (50%)	FA50S0SF0MK0	575	575	0	0	0	53.5	819.7
	FA0S50SF0MK0	575	0	575	0	0	24.6	977.5
	FA25S25SF0MK0	575	287.5	287.5	0	0	59.2	871.1
	FA35S0SF15MK0	575	402.5	0	172.5	0	19.6	918.3
	FA35S0SF0MK15	575	402.5	0	0	172.5	48.3	859.7
	FA0S35SF15MK0	575	0	402.5	172.5	0	22.4	982.9
	FA0S35SF0MK15	575	0	402.5	0	172.5	44.9	960
	FA35S0SF7.5MK7.5	575	402.5	0	86.25	86.25	21.9	908.7
	FA0S35SF7.5MK7.5	575	0	402.5	86.25	86.25	27.6	986.3
	FA17.5S17.5SF7.5MK7.5	575	201.25	201.25	86.25	86.25	23.0	951.7
4 (75%)	FA0S75SF0MK0	287.5	0	862.5	0	0	41.4	950
	FA37.5S37.5SF0MK0	287.5	431.25	431.25	0	0	52.9	823.5
	FA60S0SF15MK0	287.5	690	0	172.5	0	12.7	819.2
	FA60S0SF0MK15	287.5	690	0	0	172.5	32.2	803.2
	FA0S60SF15MK0	287.5	0	690	172.5	0	16.1	968
	FA0S60SF0MK15	287.5	0	690	0	172.5	50.6	915.4
	FA60S0SF7.5MK7.5	287.5	690	0	86.25	86.25	16.1	826.8
	FA0S60SF7.5MK7.5	287.5	0	690	86.25	86.25	25.3	961.5
	FA30S30SF7.5MK7.5	287.5	345	345	86.25	86.25	17.3	902.5

3.2.3 Testing Procedures

3.2.3.1 Mini Slump Test

The slump test of UHPC was measured using the mini-slump test recommended by EFNARC (2002) as illustrated in Figure 3.6. After pouring fresh UHPC to the mini cone, the cone was lifted straight upwards to allow fresh UHPCs on the plate. The flow value of the designed UHPC was calculated as the average of two measured diameters of the mixture, i.e. D1 and D2. The UHPC mixtures had slump values that controlled by using an adequate amount of SP.

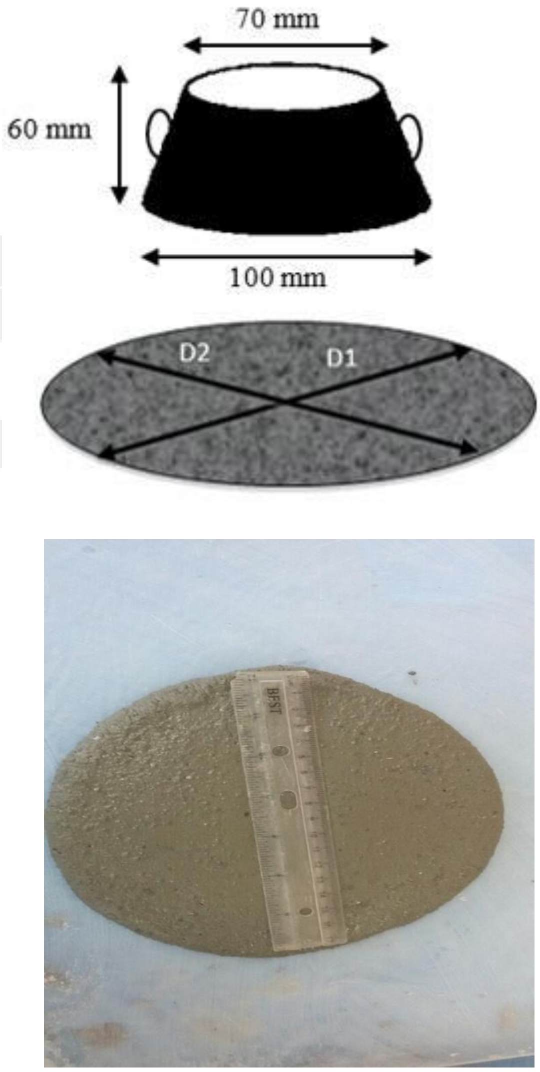

Figure 3.6. Mini-slump test

3.2.3.2 Mechanical Tests

Compression test was conducted on 50 mm cubes at 7, 28 and 90 days, with respect to ASTM C39 (2003), at a rating load of 0.9 kN/s using a digital testing machine of 3000 kN capacity. Splitting test of UHPCs has performed on 70 mm cubical samples at a rating load of 0.2 kN/s in accordance with ASTM C496 at 90 days.

Static modulus of elasticity was determined on 150 cubes at 90 days in accordance with BS EN 1352 (1997). For this, the cube specimens were loaded and unloaded three times up to 40% of the ultimate load determined from the compression test. The first set of readings from each cube was discarded, and the elastic modulus was reported as the average of the other two sets of readings. Each test represented in this study is the average of three samples.

3.2.3.3 Fracture Energy Test

Fracture energy, termed as a work of fracture, is an indirect surface energy measure of cementitious materials (Hillerborg, 1983). The test for determining the fracture energy was performed in accordance with the recommendation of RILEM 50-FMC/198 Technical Committee (1985). The displacement was measured simultaneously by using a linear variable displacement transducer (LVDT) at mid-span. As shown in Figure 3.6a, Instron 5500R closed-loop testing machine with a maximum capacity of 250 kN was used to apply the load. Figure 3.7 b shows the prepared beam for the fracture energy tests. The opening notch was achieved through reducing the effective cross-section to 42x70 mm via a diamond saw to accommodate large aggregates in more abundance. Thus, the notch to depth ratios (a/W) of specimens was 0.4. According to RILEM (RILEM 50-FMC, 1985) , the fracture energy, GF, of a single edge notched beam can be calculated under three points bending as:

$$G_F = \frac{W_o + mg\delta_s \frac{S}{U}}{B(W-a)} \tag{3.1}$$

Where Wo is the area under the load - deflection curve; m is the mass of the beam; g is the acceleration due to gravity; δs is the specified deflection of the beam, while S, U, B, W, and a are span length, width, depth, and notch depth of the beam, respectively. For each mixture, at least three specimens were tested at the age of 90 days. All the beams were loaded at a constant rate of 0.02 mm/min.

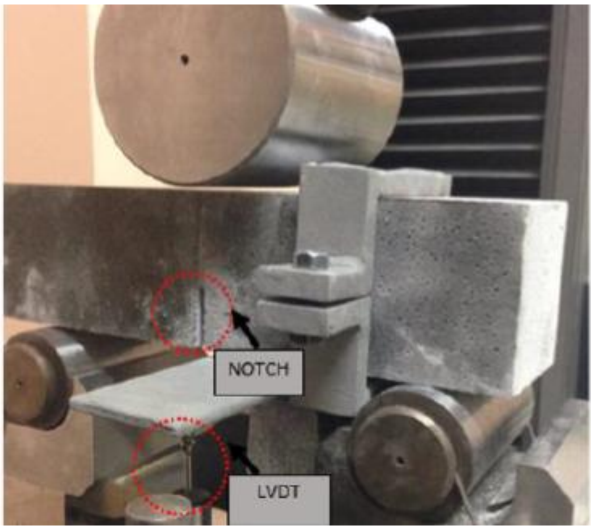

a)

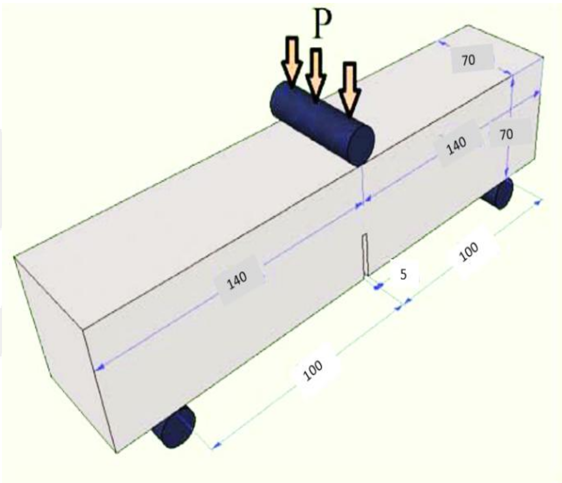

b) (all dimensions are in mm)

Figure 3.7. View of beam specimen under the flexural test

In accordance with the literature, the net flexural strength, f_{flex}, was calculated via Eqn (3.2) by assuming no notch sensitivity [114, 115].

$$f_{flex} = \frac{3P_{max}S}{2B(W-a)^2} \tag{3.2}$$

Where P_{max}, S, B, W, and a are ultimate load span, length, width, depth, and a notch depth of the beam, respectively.

Characteristic length (l_{ch}) as a measure of ductility was computed using Eq. (3.3) as a function of the modulus of elasticity (E), fracture energy (GF), and splitting tensile strength (f_{st}).

$$l_{ch} = \frac{EG_F}{f_{st}^2} \tag{3.3}$$

3.3 Numerical Study

3.3.1 Axial Capacity of CFST Columns

In this part, the structural behavior of the composite columns, namely concrete filled steel tube (CFST) columns having UHPC was studied under the effect of axial compression. Benefiting from a set of experimental data, a total of 675 axial load carrying capacity (Pu) test results of the composite columns were calculated via 3 different yield strengths of steel tube (300, 450, 600 Mpa) and five different D/t ratios (35, 65, 90). Basically, the test of ultimate axial load considered several important geometric and material properties taken as predictive parameters such as D/t ratio, the length of columns (L), the nominal strengths of the concrete (f_{ck}) and steel tube (f_y). The compression test of circular CFST columns is schematically depicted in Figure 3.7 in which the steel tube was loaded simultaneously with the concrete core. For each investigated code, the test specimens had 2.5 mm in thickness of circular steel tube and length to diameter ratio (L/D) of 3. The parameters of CFST columns applied in design codes are listed in Table 3.5 below.

Table 3.5. Parameters of CFST columns applied in design codes

Diameter of steel tube (mm)	Diameter of concrete (mm)	Length of CFST (mm)	D/t	Area of concrete (Ac) (mm^2)	Area of steel (As) (mm^2)	Concrete moment of inertia (Ic)(mm^4)	Steel moment of inertia (Is) (mm^4)
87.5	82.5	262.5	35	5346	667	2273975	603437
162.5	157.5	487.5	65	19483	1256	30205924	4022221
237.5	232.5	712.5	95	42456	1845	143437176	12742441

The details of mix proportion as well as the compressive strength of concrete were imported from Table 3.4; in which totally 25 ultra high performance concrete (UHPC) mixtures were manufactured and the concrete specimens were 50 mm cubic. The concretes were produced by utilizing FA , S , SF, and MK at specific proportions and the concrete properties were enhanced by these SCM. In this regard, the concretes were mixed with water/binder ratios (w/b); 0.15. The effect of above mentioned parameters on the Pu results would be observed, compared and discussed in detail.

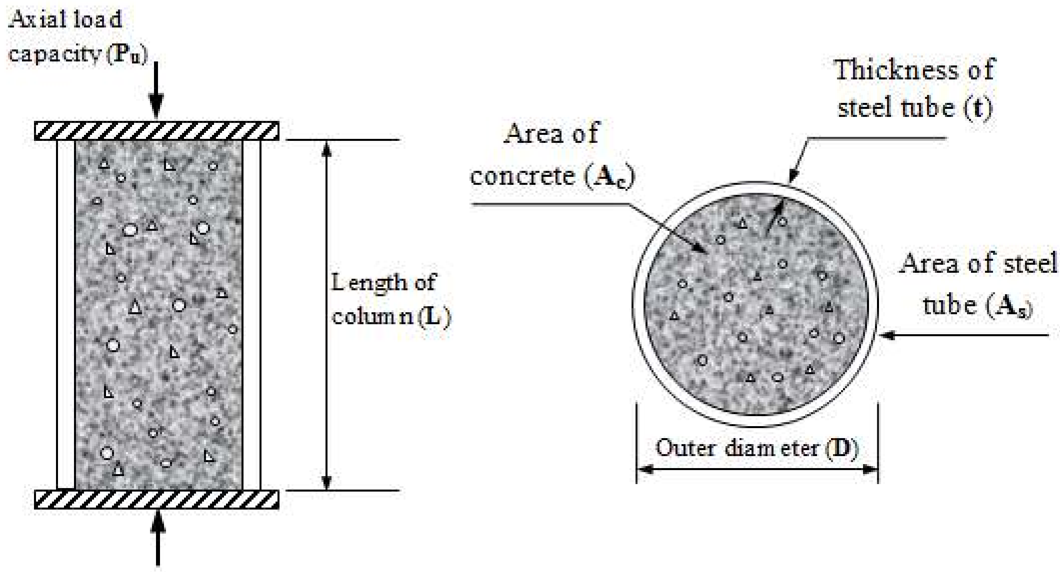

Figure 3.8. Test representation of load applied to cross section of circular CFST columns

In order to achieve a good comparison of the database of circular CFST columns with various codes, the compressive strength of tested concrete (fc') used in codes was generally measured for 150X200 mm cylindrical specimens. However, the results of compressive strength of UHPC were obtained through 50 mm cube test; thus, significant effects on the predicted results would occur. For this, conversion factors proposed by Kazemi [116] and Skazlic et al. [117] were yielded to convert these results. It is worth mentioning that kazemi [116] specifies the conversion factors to convert the 50 mm cube of UHPC to cylinder of 100 mm by dividing the compressive strength value of 50mm cube on 1.14 then the obtained value has been multiplied by 0.9 in order to convert it to cylinder 150*200 according to Skazlic et al. [117]. The details, as well as the conversion factor, applied in design codes for 7, 28 and 90 days of water curing are listed in Tables 3.6, 3.7 and 3.8 below.

Table 3.6. Compressive strength of concrete applied in design codes for 7 days

Mix code	Strength of 50 mm cubes (fc') (MPa)	Strength of 100mm cylinder(fc') (MPa)	Strength of (150*300)mm cylinder (fc') (MPa)
control	105.9	92.9	83.6
25F	94.7	83.1	74.7
50 F	62.5	54.8	49.3
25 S	92.8	81.4	73.3
50 S	81.2	71.2	64.1
75 S	61.5	53.9	48.5
15SF	136.6	119.9	107.9
15 MK	126.2	110.7	99.7
25 F+S	105.6	92.6	83.3
50 F+S	58.3	51.2	46.0
50 F+SF	129.7	113.8	102.4
75 F+SF	96.0	84.2	75.8
50 F+MK	52.0	45.6	41.1
75 F+MK	78.6	68.9	62.1
50 S+SF	147.5	129.4	116.5
75 S+SF	129.0	113.2	101.9
50 S+MK	125.0	109.7	98.7
75 S+MK	101.8	89.3	80.4
15SF+MK	144.8	127.0	114.3
15SF+MK+50 F+SF+MK	141.1	123.8	111.4
75F+SF+MK	112.9	99.0	89.1
50S+SF+MK	141.1	123.8	111.4
75S+SF+MK	118.9	104.3	93.9
50F+S+SF+MK	114.4	100.3	90.3
75F+S+SF+MK	103.3	90.6	81.6

Table 3.7. Compressive strength of UHPC applied in design codes for 28 days

Mix code	Strength of 50 mm cubes (fc') (MPa)	Strength of 100mm cylinder (fc') (MPa)	Strength of (150 *300)mm cylinder (fc') (MPa)
control	118.4	103.9	93.5
25F	113.1	99.2	89.3
50F	101.0	88.6	79.8
25 S	124.9	109.6	98.6
50 S	121.8	106.8	96.2
75 S	104.9	92.0	82.8
15SF	138.5	121.5	109.4
15 MK	132.8	116.5	104.9
25 F+S	124.3	109.1	98.1
50 F+S	97.2	85.3	76.8
50 F+SF	142.8	125.2	112.7
75 F+SF	111.1	97.5	87.7
50 F+MK	94.3	82.7	74.5
75 F+MK	84.9	74.5	67.0
50 S+SF	154.6	135.6	122.0
75 S+SF	144.5	126.7	114.1
50 S+MK	131.4	115.3	103.8
75 S+MK	111.2	97.6	87.8
15SF+MK	152.7	133.9	120.5
15SF+MK+50 F+SF+MK	150.6	132.1	118.9
75 F+SF+MK	128.2	112.5	101.2
50 S+SF+MK	150.6	132.1	118.9
75 S+SF+MK	134.3	117.8	106.0
50F+S+SF+MK	139.1	122	109.8
75 F+S+SF+MK	118.8	104.2	93.8

Table 3.8. Compressive strength of concrete applied in design codes for 90 days

Mix code	Strength of 50 mm cubes (fc') (MPa)	Strength of 100mm cylinder (fc') (MPa)	Strength of (150 *300)mm cylinder (fc') (MPa)
control	123.4	108.3	97.5
25F	130.6	114.5	103.1
50 F	108.5	95.2	85.6
25 S	136.8	120.0	108.0
50 S	136.7	119.9	107.9
75 S	108.2	94.9	85.4
15SF	156.4	137.2	123.5
15 MK	143.0	125.4	112.9
25 F+S	134.9	118.3	106.5
50 F+S	102.7	90.1	81.1
50 F+SF	155.2	136.1	122.5
75 F+SF	121.8	106.8	96.1
50 F+MK	103.6	90.8	81.8
75 F+MK	86.1	75.5	68.0
50 S+SF	165.5	145.2	130.7
75 S+SF	152.7	133.9	120.5
50 S+MK	134	117.5	105.8
75 S+MK	120.0	105.3	94.8
15SF+MK	159.3	139.7	125.7
15SF+MK+50 F+SF+MK	155.8	136.7	123.0
75 F+SF+MK	130.5	114.5	103.0
50 S+SF+MK	163.8	143.7	129.3
75 S+SF+MK	135	118.4	106.6
50F+S+SF+MK	145.2	127.3	114.6
75 F+S+SF+MK	122.0	107.1	96.3

3.3.2. Calculation of Axial Capacity of Circular CFST Columns According to Design Codes

In order to evaluate the axial load carrying capacity (Pu) results and make a good comparison, a brief review of related standards would be given. The details of relations would also be presented for each design codes. In different codes, several limitations such as yield strength of steel tube (fy), fc', D/t, steel ratio and confining coefficient (î) are prescribed. Moreover, multiple approaches and design philosophies have been adopted in these design codes.

3.3.2.1. ACI-318R

Unlike similar codes, American Concrete Institute (ACI-318R, 2005) underestimated the effectiveness of concrete confinement and the interaction between the concrete core and steel tube. For this, the predictive results of axial load capacity are expected to be smaller than corresponding codes. The ultimate axial capacity of circular CFST columns can be calculated by

$$\mathrm{N_u} = 0.85 f_C^{-} A_c + f_y A_s \tag{3.3}$$

3.3.2.2. Eurocode 4 (EC4)

In all design codes, there are circular, square, rectangular and circular hollow CFST structure design regulations. In these regulations, the design methods are different. Moreover, the code must be combining the design approach of both reinforced concrete columns and structural steelwork in order to dedicate the composite construction. In the present study, the formula was designated as EC 4. In Eurocode 4, (2004) code, the strength capacity of circular CFST column was calculated by taking in account the contribution of the concrete core and steel tube as well as the confinement effect of steel tube. Indeed, the strength of concrete core increases for circular cross-section CFST columns due to concrete confinement coefficients (ηc) and to the occurrence of a triaxial state of stress condition. Conversely, the yield strength of steel decreases by the confinement coefficients of steel (ηa) since the hoop stresses cause a reduction in the effective yield stress of the steel. Hence, the axial load capacity of circular CFST columns can be calculated by:

$$N_u = \left(1 + n_c \frac{t}{D} \frac{f_y}{f_{c-,150}}\right) f_{c-} + n_a f_y A_s \tag{3.4}$$

In which

$$n_c = 4.9 - 18.5\gamma^{-} + 17\gamma^{-2} \qquad (n_c \geq 0) \tag{3.5a}$$

$$n_a = 0.25(3 + 2\gamma^{-}) \quad (n_a \leq 1.0) \tag{3.5b}$$

$$\lambda^{-} = \sqrt{\frac{N_{pIR}}{N_{cr}}} \tag{3.5c}$$

$$N_{pIR} = f_y A_s + f_{c-} A_c \tag{3.5d}$$

$$N_{cr} = \frac{\pi^2 (EI)_{eff2}}{l^2} \tag{3.5e}$$

$$(EI)_{eff2} = E_s I_s + K_e E_{c2} I_c \tag{3.5f}$$

$$E_{c2} = 22000\ [(f_c + 8)/10]^{0.3} \tag{3.5g}$$

Where, n_a is the coefficient of confinement for the steel tube, n_c is the coefficient of confinement for the concrete, l is buckling length of the CFST column, λ^{-} is relative slenderness, K_e is a correction factor which is equal to 0.6, $(EI)_{eff2}$ is the effective flexural stiffness for calculation of relative slenderness, and E_{c2} is elastic modulus of concrete.

Essentially, when $\lambda^{-} = 0$, the zero length strength (the sectional capacity), N_o can be shortened as:

$$N_o = \left(1 + 4.9\frac{t}{D}\frac{f_y}{f_{c-,150}}\right) f_{c-,150} A_c + 0.75 f_y A_s \tag{3.6}$$

3.3.2.3. DL/T (1999)

The Chinese code (DL/T, 1999) also used either the allowable stresses of the concrete and steel or the working stress method. In effect, DL/T (1999) code assumes that the composite column is made of one material with a total area of composite columns (A_{sc}) and nominal yielding strength (f_{scy}). Moreover, the confinement factor (î) is employed in the standard to describe the superposition composition between steel tube and concrete core. The code introduced the ultimate compressive strength of concrete-filled steel circular hollow section columns by Eq. (5) as shown below:

$$N_u = f_{scy} A_{sc} \tag{3.12}$$

In which

$$A_{sc} = A_s + A_c \tag{3.13a}$$

$$f_{scy} = (1.212 + B\xi + C\xi^2) f_{ck} \tag{3.13b}$$

$$B = 0.1759 \frac{f_y}{235} + 0.974 \tag{3.13c}$$

$$C = -0.1038 \frac{f_{ck}}{20} + 0.0309 \tag{3.13d}$$

$$\xi = \frac{A_s f_y}{A_c f_{ck}} \tag{3.13e}$$

$$f_{ck} = 0.67 f_{cu,150} \tag{3.13f}$$

Where:

ξ the confinement factor; A_{sc} = the area of composite section; f_{scy} = the “nominal yielding strength” of the composite section; and f_{ck} = the characteristic concrete strength.

CHAPTER 4

RESULTS AND DISCUSSION ON EXPERIMENTAL STUDY

4.1 Compressive Strength

Indeed, all mineral admixtures played a positive role in concrete development not only because of utilizing a large volume of disposal materials like FA and S but also for promoting pozzolanic reactions. After a hydration process, which C_3S react with water to produce unwanted calcium hydroxide (CH). The silica inside mineral admixtures reacts with CH to form C-S-H gel (pozzolanic reaction) which is important to improve the strength of UHPC due to filler properties of the generation gel [118]. According to Neville [119], a rise in curing temperature (steam curing) speeds up the hydration process so that the structure of the hydrated cement paste is established earlier then pozzolanic reactions also activated to ensure rapid strength development.

Test results of the compressive strength of the UHPC are shown in Figures 4.1a, b, c, and d. The whole compressive strength ranged from 86.1 (mixture; 60%FA+15%MK WC) to 165.5 (mixture; 35%S+15%SF WC) and from 104.8 (mixture; 60%FA+15%MK SC) to 180 MPa (mixture; 35%S+7.5%SF+7.5%MK SC) for water and steam curing, respectively. The compressive strengths of all concrete mixtures were developed with ages. Nevertheless, on the one hand, the rate increment of the water cured results at 7 to 28 days higher than that from 28 to 90 days for S, MK, and SF but vice versa for FA. This can be returned to retarding of hydration due to the slow reaction of pozzolanic FA [120]. On the other hand, a regular strength enhancement was observed for steam curing from 7 to 28 then 90 days after demonstrating huge results at 7 days comparing to the same age water curing, regardless of mineral admixture types and amounts. These may be due to most chemical reactions were finished at early ages. From figures mentioned above, a marked drop in the compressive strength of UHPC was observed with increasing an amount of FA from 25 to 50% replacement, while S had closer strength values to that of control concrete at 50% replacement. On the other hand, the mixture of SF and/or MK with S had a systematically higher compressive strength than control mixture up to 50% replacement then decreased when the replacements were reached to 75%, as seen in Figure 4.1 d. As a result, at 90 days' age of UHPC, the compressive strength of the mixtures followed an order of; SF+MK> SF> MK> Control, S> FA+S> FA> Control, S+SF> S+SF+MK> FA+SF+MK> FA+SF> FA+S+SF+MK> S> S+MK> Control> FA> FA+MK> FA+S, and S+SF> S+SF+MK> FA+SF+MK> Control> FA+S+SF+MK> FA+SF> S+MK> S for the replacement levels of 15, 25, 50, and 75%, respectively. It can be concluded that mineral admixtures different with each other on effecting on the strength results which the most active is SF then followed respectively by each of MK, S, and FA. The replacement levels undesirable for using mineral admixtures more than 25% for FA, and 50% of S because the results of compressive strength were less than the control mixture. While mixing mineral admixtures in the form of multi-blended systems have decrease an adverse effect of using high volumes. These may relate to different chemical and physical properties of mineral admixtures (see Table 3.1) as together they complete each other to form a complete system of mineral replacement to concrete.

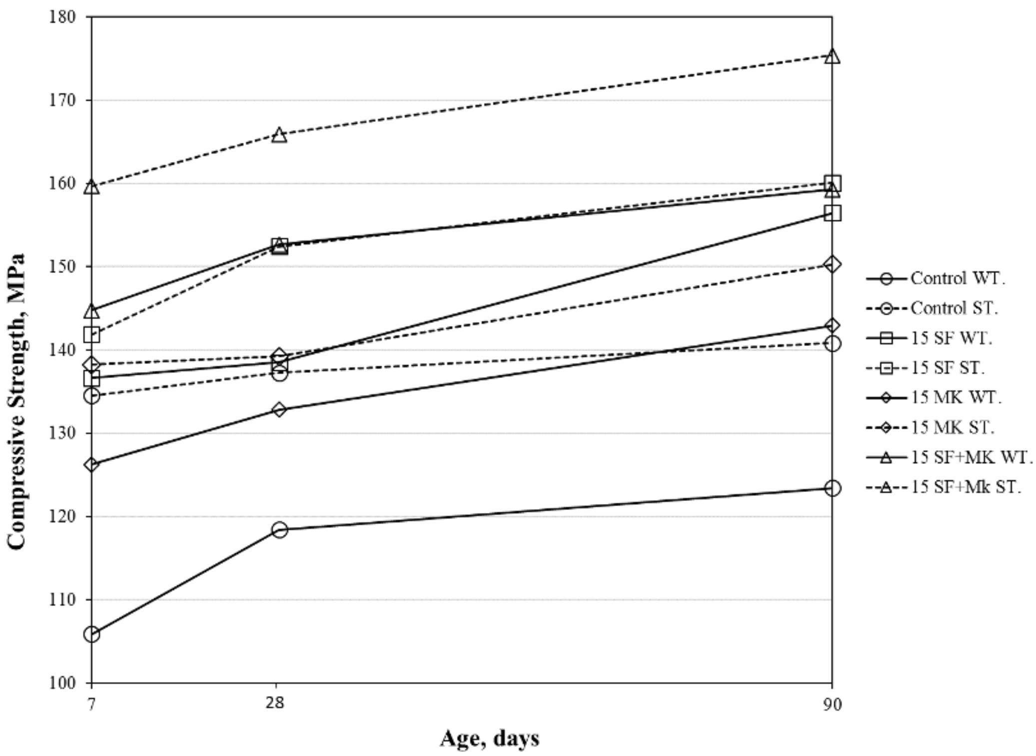

a) 15%

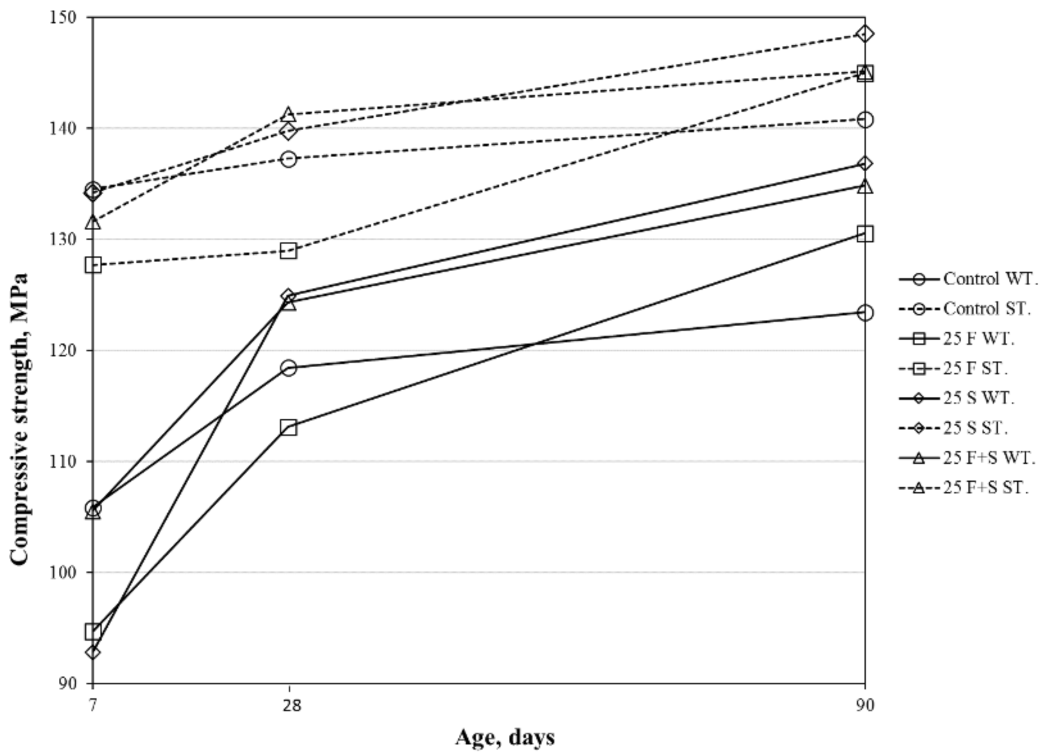

Compressive strength, MPa
Age, days
150
140
130
120
110
100
90
7
28
90
Control WT.
Control ST.
25 F WT.
25 F ST.
25 S WT.
25 S ST.
25 F+S WT.
25 F+S ST.

b) 25%

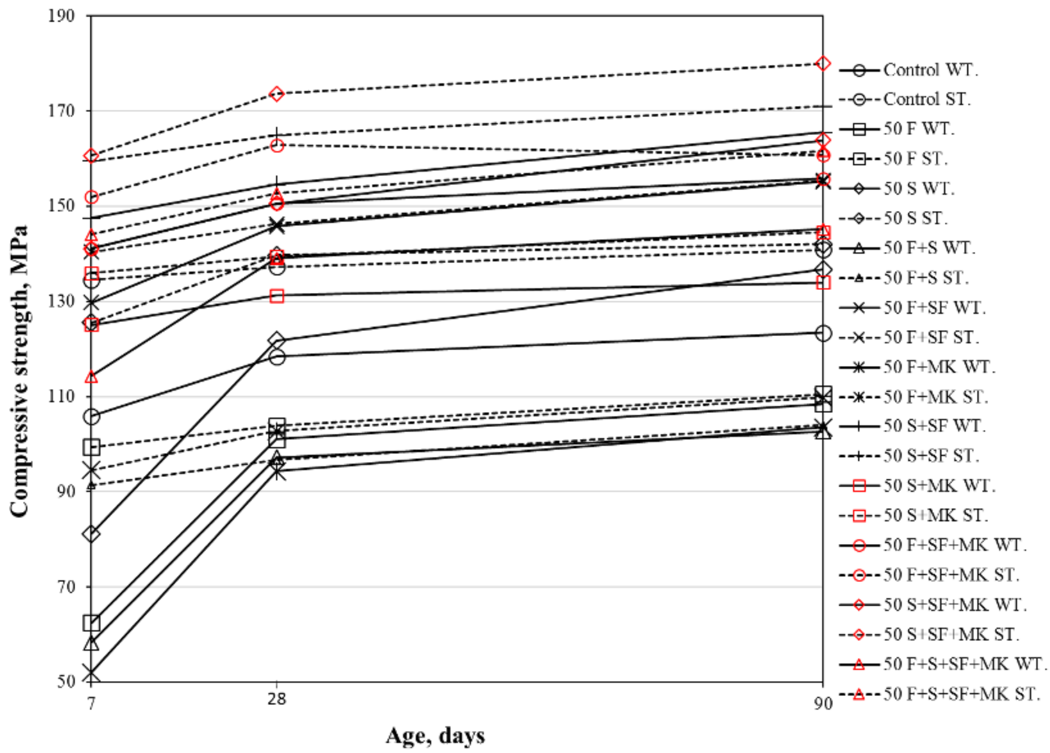

Compressive strength, MPa
Age, days
190
170
150
130
110
90
70
50
7
28
90
Control WT.
Control ST.
50 F WT.
50 F ST.
50 S WT.
50 S ST.
50 F+S WT.
50 F+S ST.
50 F+SF WT.
50 F+SF ST.
50 F+MK WT.
50 F+MK ST.
50 S+SF WT.
50 S+SF ST.
50 S+MK WT.
50 S+MK ST.
50 F+SF+MK WT.
50 F+SF+MK ST.
50 S+SF+MK WT.
50 S+SF+MK ST.
50 F+S+SF+MK WT.
50 F+S+SF+MK ST.

c) 50%

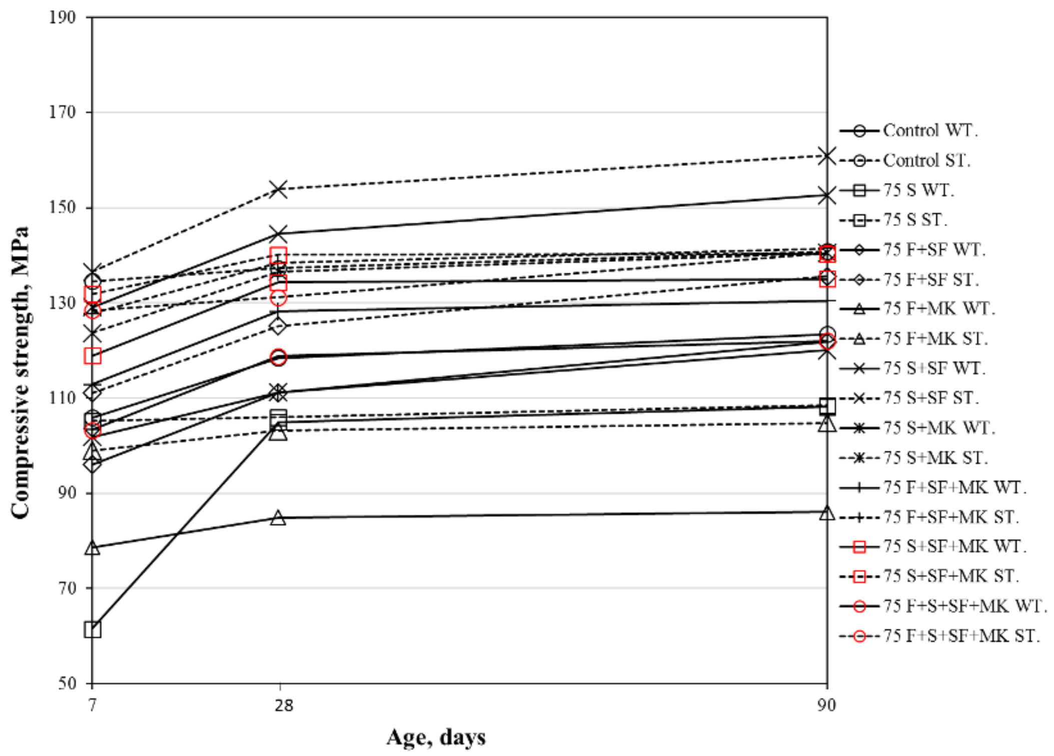

d) 75%

Figure 4.1. Compressive strength of water and steam cured UHPC

4.2 Splitting Tensile Strength

The splitting tensile strengths of mixtures after 90 days of water and steam curing conditions are shown in Figures 4.2a, b, c, and d. For both water and steam curing, the maximum & minimum results were detected to the mixtures of 15% SF& 75% S, 50% S+SF& 75% FA+MK, 50% S+SF+MK& 75% FA+SF+MK, 50% FA+S+SF+MK& 75% FA+S+SF+MK as a binary, ternary, quaternary, and quinary, forms respectively. Moreover, the values of splitting tensile strength were ranged between 4.3-10.2 MPa for water, and 6.4-11.1 MPa for steam cured UHPC. It can be seen from Figures 4.2 c and d that UHPC containing high volumes of FA, S, SF, and MK in the form of multi-blended systems showed satisfactory results. Comparing to the control concrete, there were slightly decreased in the tensile strength results in a contribution of 50% of FA and somewhat higher values for 50% of S replacement. The previous study revealed that FA caused the more tensile strength drop than S, especially over 20% replacement [121]. Furthermore, a binary combination of FA+ S showed better performance than only S or FA replacement. Whereas, the mixtures contain 75% of SF with MK and/or S kept the UHPC general limitations, regardless to lower all results than the control mixture. However, with a small replacement of

SF, the pore structure is densified and the concrete strength growths. Furthermore, SF particles fill micrometer level porosities in a fresh paste that named as filling effect [122]. Those different behaviors of mineral admixtures can be attributed to the nature of dissimilar material properties and compounds (see Table 3.1) that effect on their hydration process and pozzolanic reactions. On the other hand, it is obvious that the results of steam curing were much better than corresponding water curing for all cases of replacing amounts and mixing systems, which also confirmed by Yazici [123]. This behavior can be endorsed that UHPC consists of a high volume of powder with a very low of w/b ratio which may need high temperature for promote hydration and elevated humidity for completing the pozzolanic reactions by compensating a lack of water in fresh concrete. Thus, it is recommended to cure UHPC by steam method nor standard curing. It was evident in Figure 4.3 that the adding fibers to UHPC have the benefit to carrying pieces of tested concrete to connect with each other and to make concrete difficult to split into two parts.

Zhang et al. [124] showed that mineral admixtures significantly lowered the hydration heat extended the arrival time of the maximum temperature. Moreover, when two or three types of mineral admixtures were added, resulted in increasing the strength of concrete. In addition, the 28-day strength in water curing can be matched with 24 hr with high-temperature curing systems.

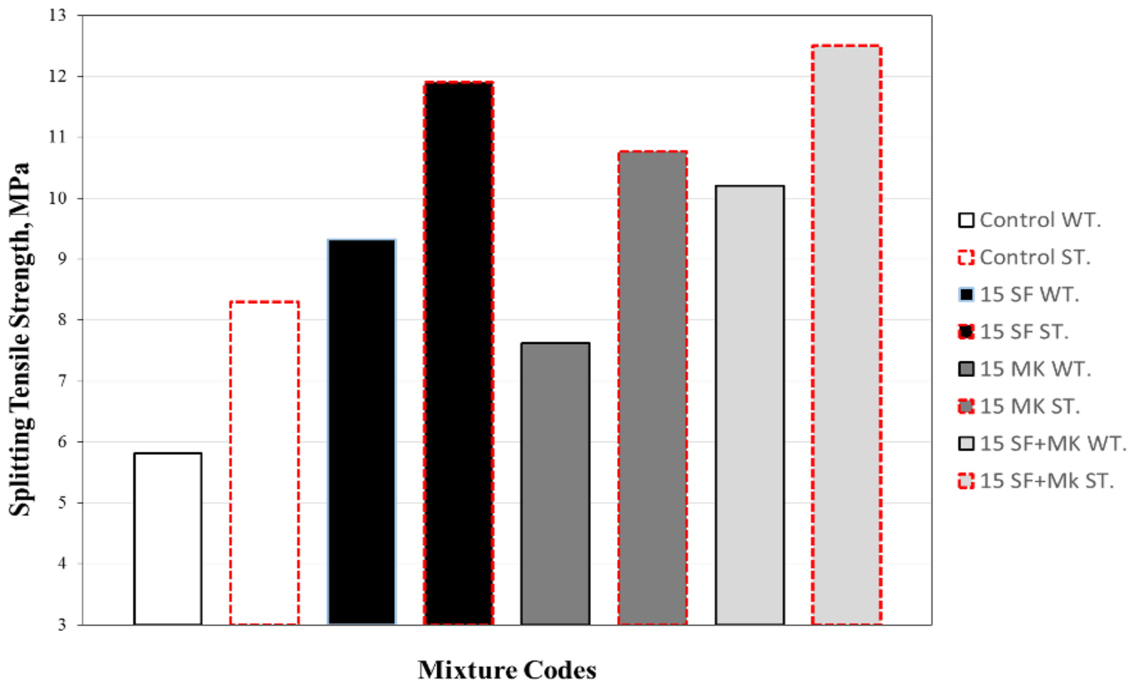

a)

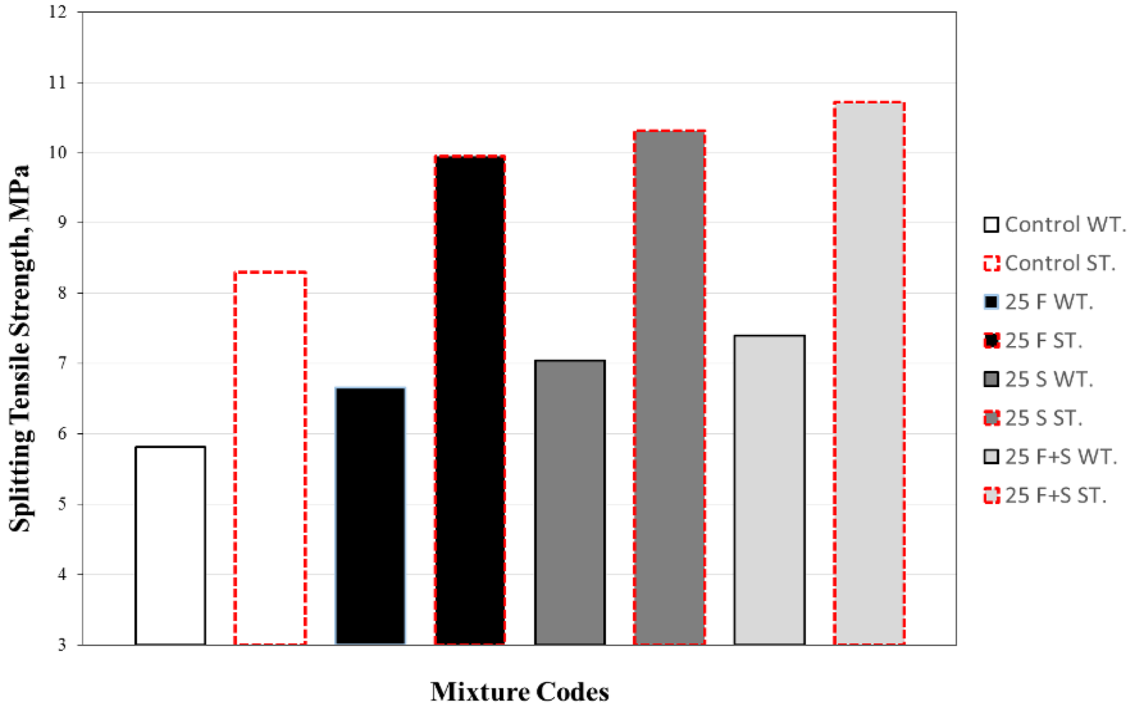

Splitting Tensile Strength, MPa
Mixture Codes
Control WT.
Control ST.
25 F WT.
25 F ST.
25 S WT.
25 S ST.
25 F+S WT.
25 F+S ST.

b)

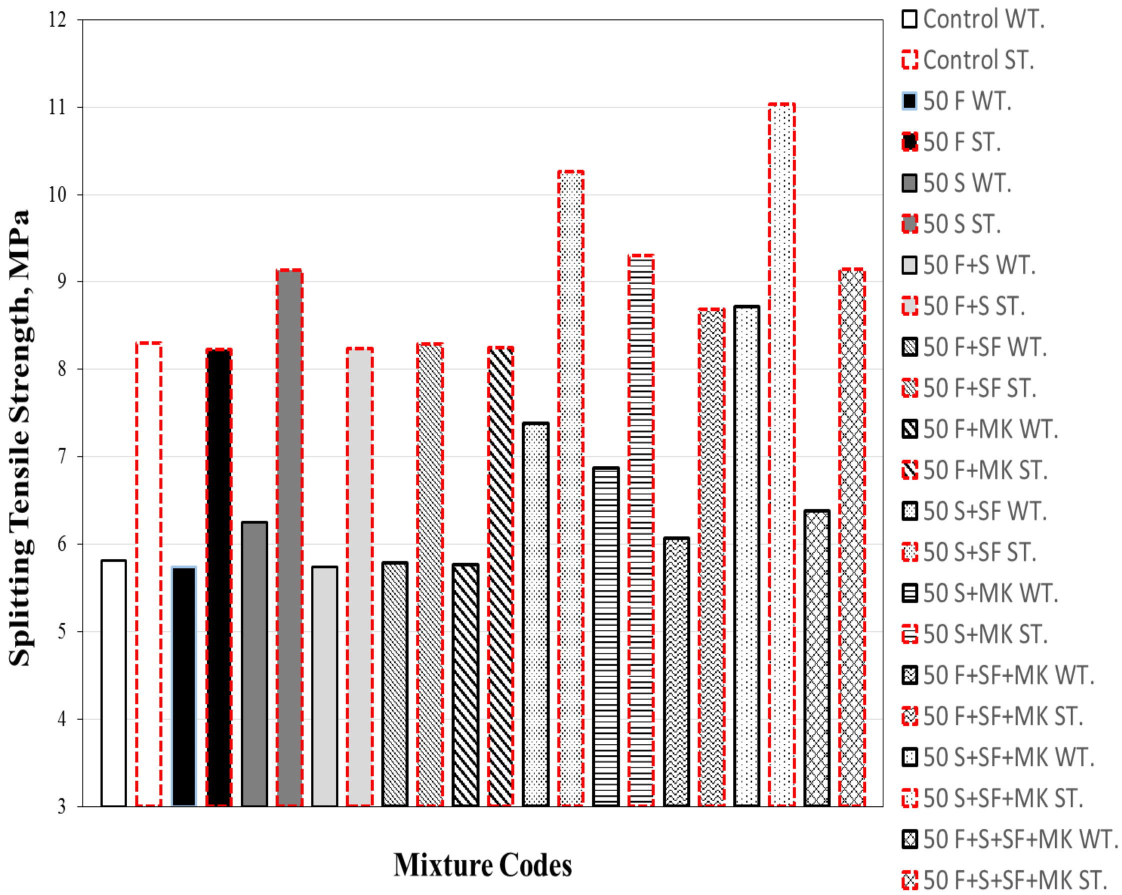

Splitting Tensile Strength, MPa
Mixture Codes
Control WT.
Control ST.
50 F WT.
50 F ST.
50 S WT.
50 S ST.
50 F+S WT.
50 F+S ST.
50 F+SF WT.
50 F+SF ST.
50 F+MK WT.
50 F+MK ST.
50 S+SF WT.
50 S+SF ST.
50 S+MK WT.
50 S+MK ST.
50 F+SF+MK WT.
50 F+SF+MK ST.
50 S+SF+MK WT.
50 S+SF+MK ST.
50 F+S+SF+MK WT.
50 F+S+SF+MK ST.

c)

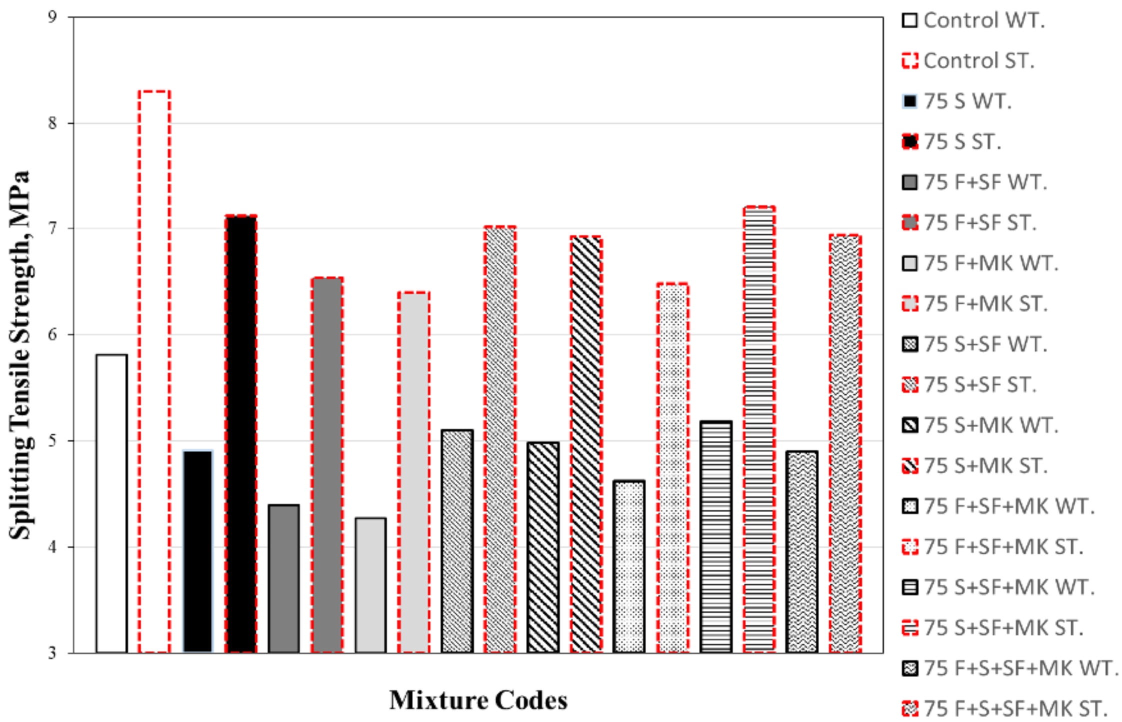

d)

Figure 4.2. Splitting tensile strength of water and steam cured UHPC

c)

Figure 4.3. Failure of test specimens.

4.3 Modulus of Elasticity

The static modulus of elasticity of UHPCs at 90 days' water and steam cured with different mineral admixture types and contents are shown in Figures 4.4 a, b, c, and d. It was observed that the effect of using 15 and 25% of mineral admixtures resulted of increment of the results, comparing to control mixture. While, despite declining the results at 50 % and 70% but the elastic moduli for the mixtures were near or higher than the control mixture for the former and the most mixture results within the range of UHPC limitations for the latter. The maximum & minimum results were assigned to the mixtures of SF+MK& Control (15% replacement), FA+S& Control (25% replacement), S+SF+MK& FA (50% replacement), and Control& FA+MK (75% replacement) with the values of 50.5& 30.4 GPa, 42.5& 30.4 GPa, 35.2& 26.5 GPa, 30.4& 21.6 GPa for the water curing and 57.7& 43.4 GPa, 46.3& 43.4 GPa, 47.5& 37.1 GPa, and 43.4& 31.8 GPa for the steam curing. Thus, the mixture contained 7.5%SF+7.5MK gave the highest elastic modulus, and the lowest results represented by the mixture consisted of 60%FA+15%MK. Accordingly, the test results showed that the mineral admixtures like SF and MK more beneficial than S and then FA on increasing the results. These attributed to in addition to the pozzolanic reactions, SF and MK promoted hydration processes due to higher reactivity of these materials [123]. But using high volumes of the two latter materials (S and FA) served the environmental issues as they listed as disposal materials according to LEED organization [125]. Consequently, it seems like there is a limit demand point for mineral admixtures inside UHPC, after that any other replacement will be on behalf of cement, which has the most cementitious properties. Furthermore, the amount SiO_2 and CaO for mineral admixtures are important to expect the hydration and pozzolanic reactions.

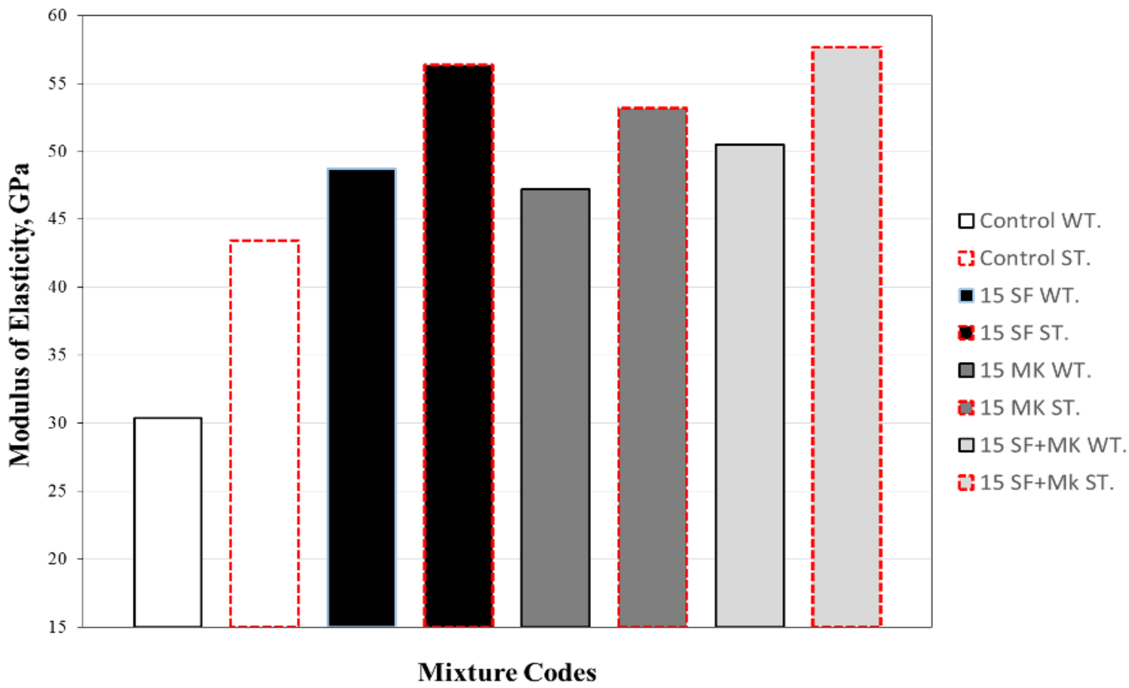

a)

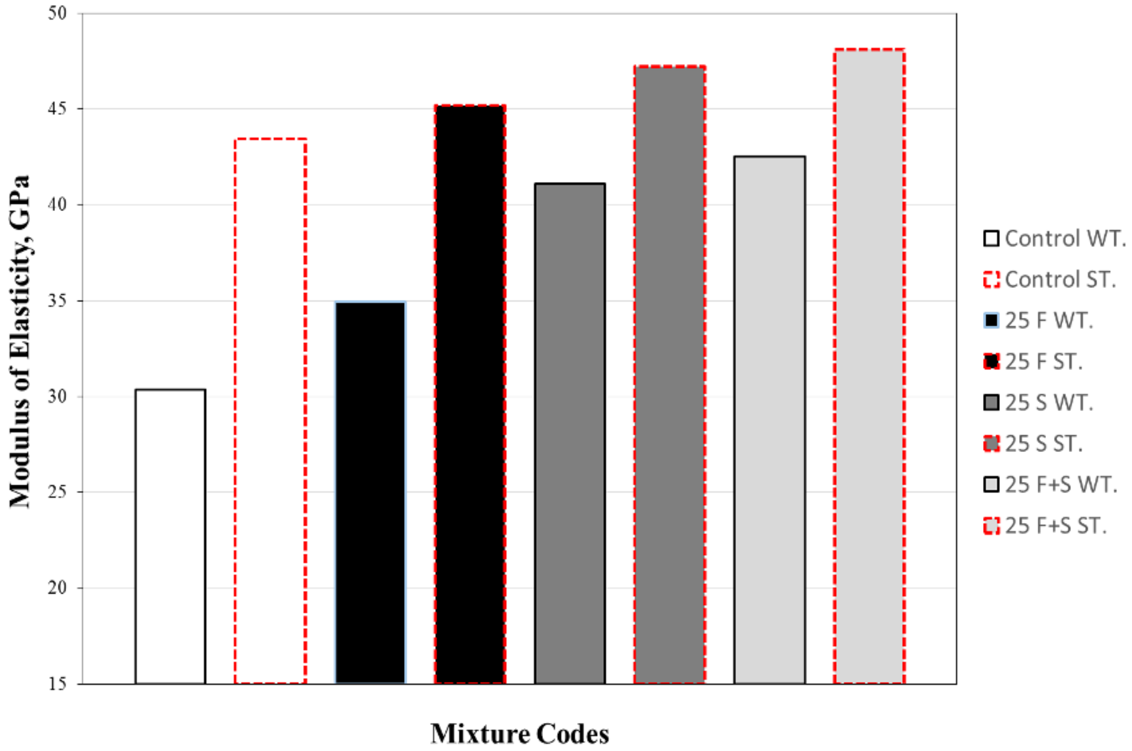

50
45
40
35
30
25
20
15
Modulus of Elasticity, GPa
Mixture Codes
Control WT.
Control ST.
25 F WT.
25 F ST.
25 S WT.
25 S ST.
25 F+S WT.
25 F+S ST.

b)

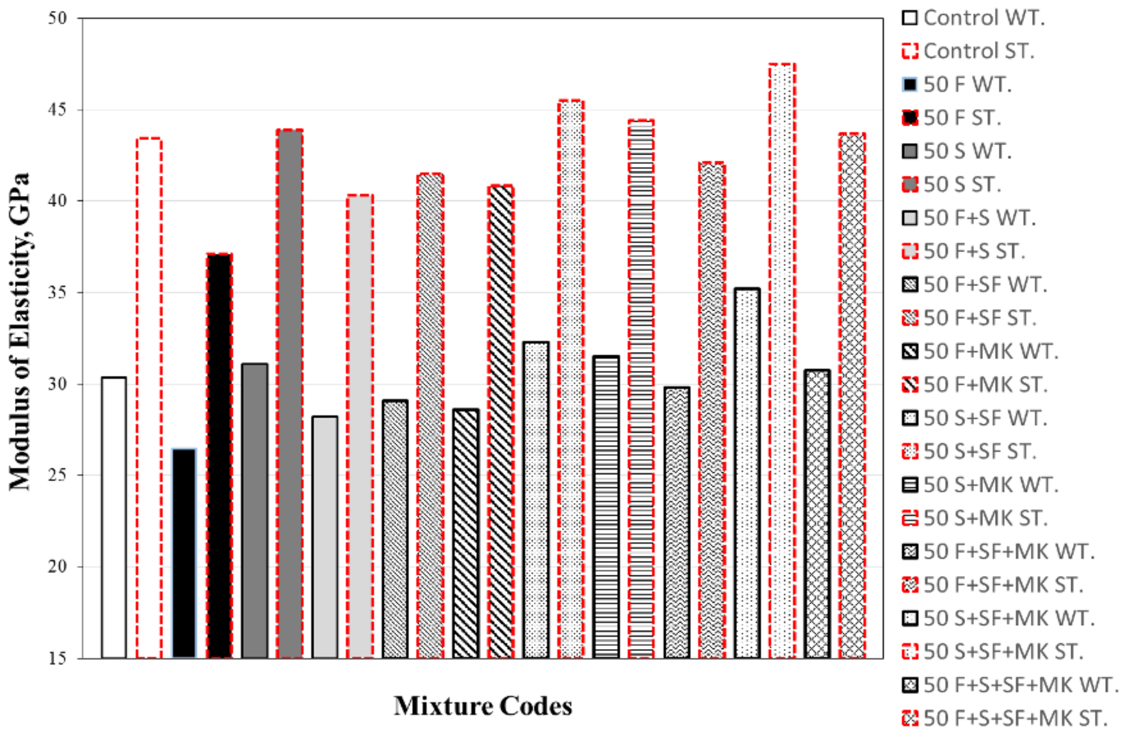

50
45
40
35
30
25
20
15
Modulus of Elasticity, GPa
Mixture Codes
Control WT.
Control ST.
50 F WT.
50 F ST.
50 S WT.
50 S ST.
50 F+S WT.
50 F+S ST.
50 F+SF WT.
50 F+SF ST.
50 F+MK WT.
50 F+MK ST.
50 S+SF WT.
50 S+SF ST.
50 S+MK WT.
50 S+MK ST.
50 F+SF+MK WT.
50 F+SF+MK ST.
50 S+SF+MK WT.
50 S+SF+MK ST.
50 F+S+SF+MK WT.
50 F+S+SF+MK ST.

c)

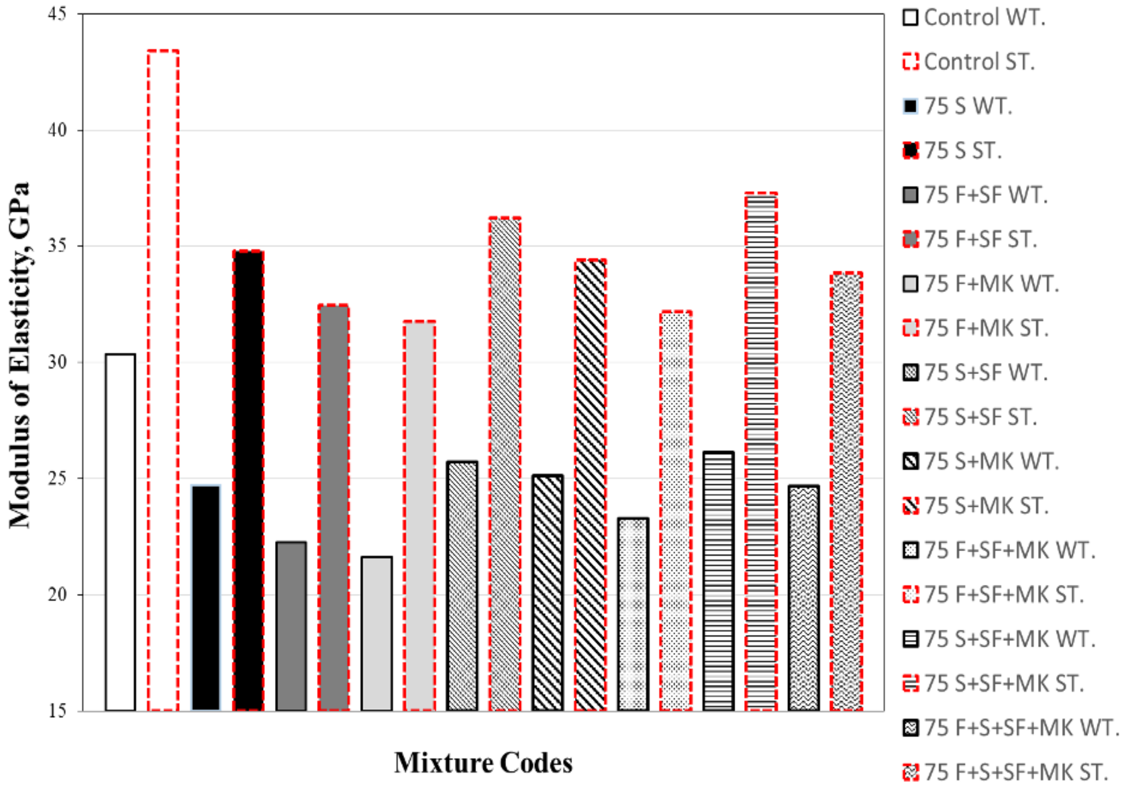

d)

Figure 4.4. Elasticity modulus of water and steam cured UHPC

4.4 Modulus of Rupture

The variation in modulus of rupture with respect to 15, 25, 50, and 75% of different supplementary cementitious materials illustrates in Figures 4.5 a, b, c, and d, respectively. Firstly, when SF, MK, and binary of SF+MK were used with the proportion of 15%, improved the flexural strength by about 14, 9.2, and 26% of water and by 15.7, 12.3, and 28.1% for steam curing, respectively, with regarding their control mixtures. This can be explained by the high pozzolanic reactions of SF and MK particles with CH that released from cement hydration leading to grain size and pore size enhancement processes which reduce the microcracking and strengthen the microstructure. At higher replacement levels of 25, and 50, comparing to their corresponding control mixtures, the maximum enhancements of the flexural strength were belonging to the mixtures of FA+S, and S+SF+MK with 10.7 and 6 % for water curing and 18.3, 7 % for steam curing, correspondingly. On the other hand, related to the 75 % replacements, all mixtures recorded lower results than the control mixtures, but the steam cured mixture of 30%FA+30%S+7.5%SF+7.5%MK had the highest results than the others. This may be attributed to having a critical point between using cement and the other mineral admixtures, and it seems look like using more than 50% of mineral admixtures undesirable. Unless designing mixtures for the aim of solving an environmental issue by utilizing high volumes of disposal materials like FA and S with keeping the limitations of UHPCs is ethical. In addition, at higher replacement levels, flexural strength is reduced, possibly due to the amount of mineral admixtures is in excess to react with CH, i.e. dilution effect [118].

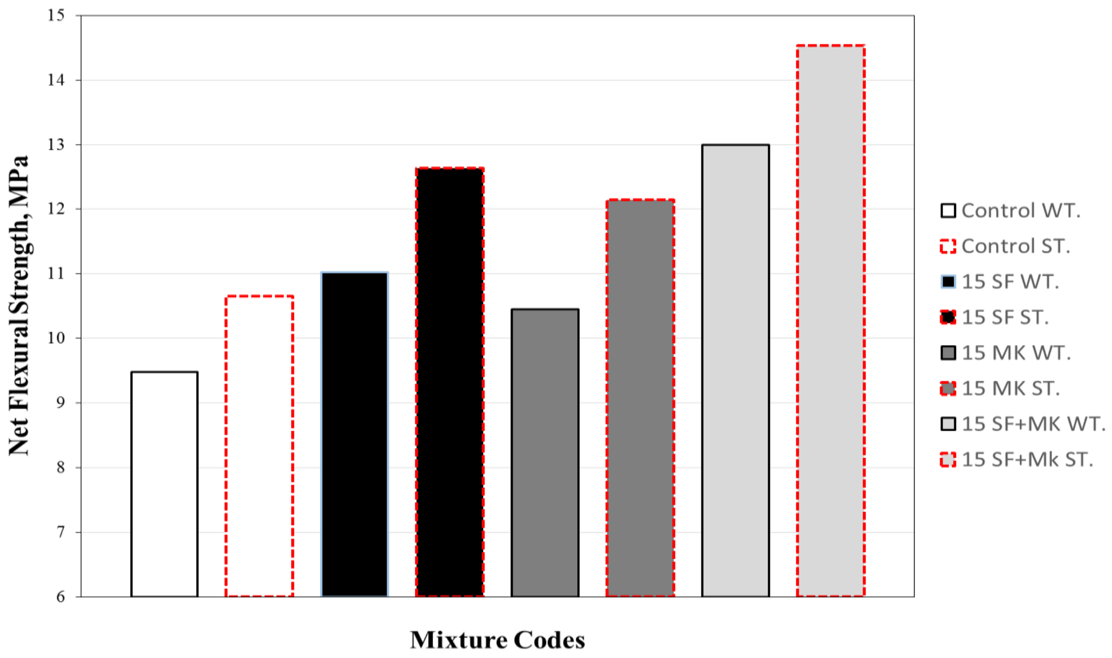

a)

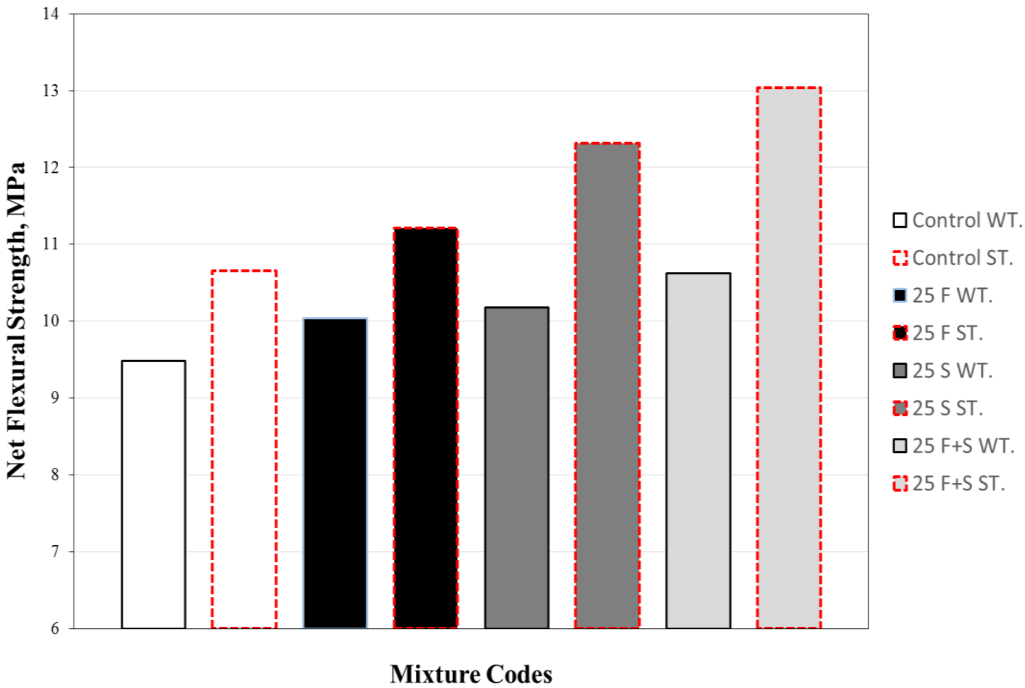

b)

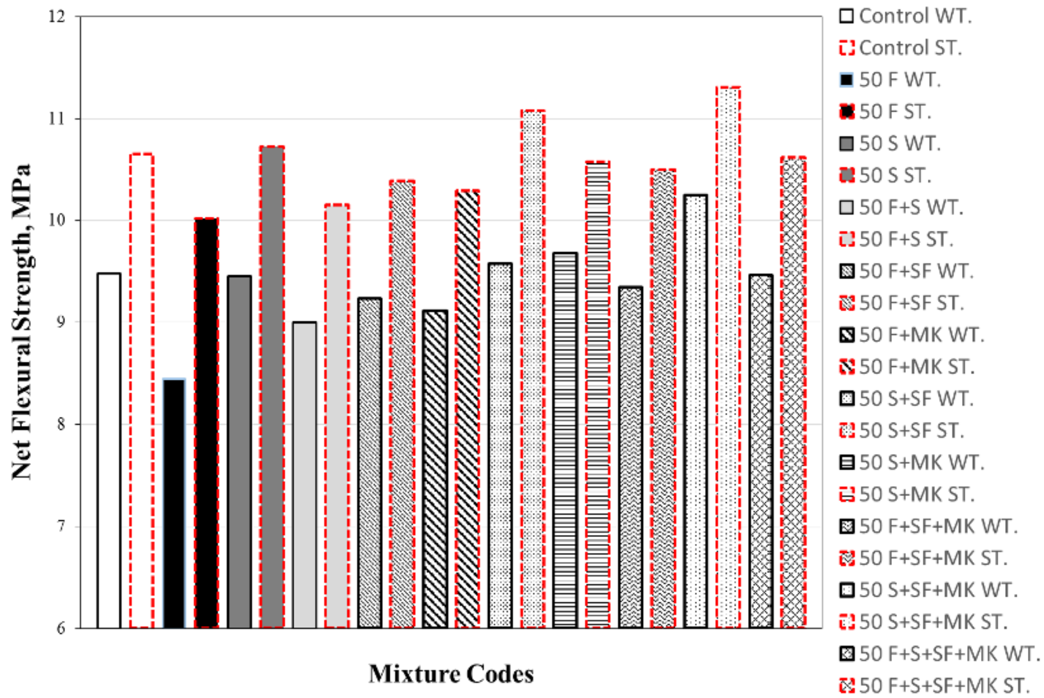

c)

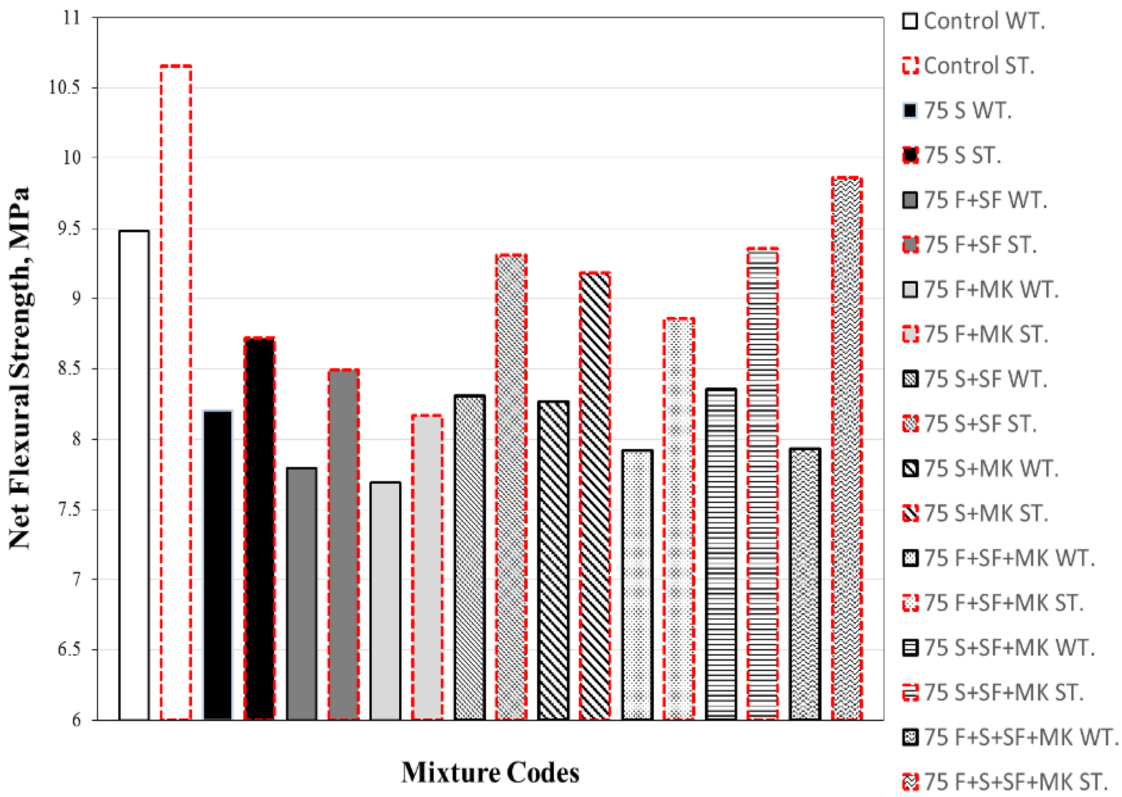

d)

Figure 4.5. Modulus of repture of water and steam cured UHPC

4.5 Load–Displacement Curves

The load versus deflections measured at each loading step by the LVDTs installed at the mid-span of UHPC under two different curing conditions of water and steam curing illustrated in Figures 4.6 a, b, c, d, e, f, g, and h. It can be seen from figures that UHPC cured by hot steam showed a higher performance than curing by water, this probably referred to condensing extremely low water of UHPC by steam then accelerating hydration and pozzolanic reactions of binders by the effect of temperature (90°C). On the other hand, the results also revealed that the binding forces between cement paste, and aggregates were accommodated because of the dense constituents with 50% more than 75%, this can be attributed to the supplementary materials can react to a certain level, after that the mineral admixtures did not participate in the hydration reaction and remain inert in concrete as a weakest point. It is obvious from the figures that the mixing mineral admitures gave stiffer concrete than individual use with cement (binary). The mixture of 50% S had more brittleness than the control mixture, but the mixture contained 35% S+7.5% SF+ 7.5% MK is the stiffest concrete. This is because of bonding developed using of S with SF and MK with these proportions, which is the most significant way to improve the Interface Transition Zone (ITZ). This led to eliminate many of the large pores in ITZ and growths the stiffness of UHPC [126].

It can see also that the peak load that denotes the maximum load, remarkably depends on the quantity and types of mineral admixtures. Moreover, the slope of the pre peak and early post-peak region of the load-displacement curves exposed to some extent or shrink, related to types and mixing binders. The load-displacement curves for the beam incorporating with SF and MK demonstrated a steady drop in load carrying capacity after the peak load, compared to the steeper drop in the mixtures with FA and S. This may be due to increasing of energy required for deboning UHPC components that contained SF and MK. Furthermore, the pre peak and the early post-peak regions in the curves essentially influenced on the microcracks and their expansion, but the declining slope at the end of the softening branch is greatly related to mechanisms causing from the aggregate interlock [127].

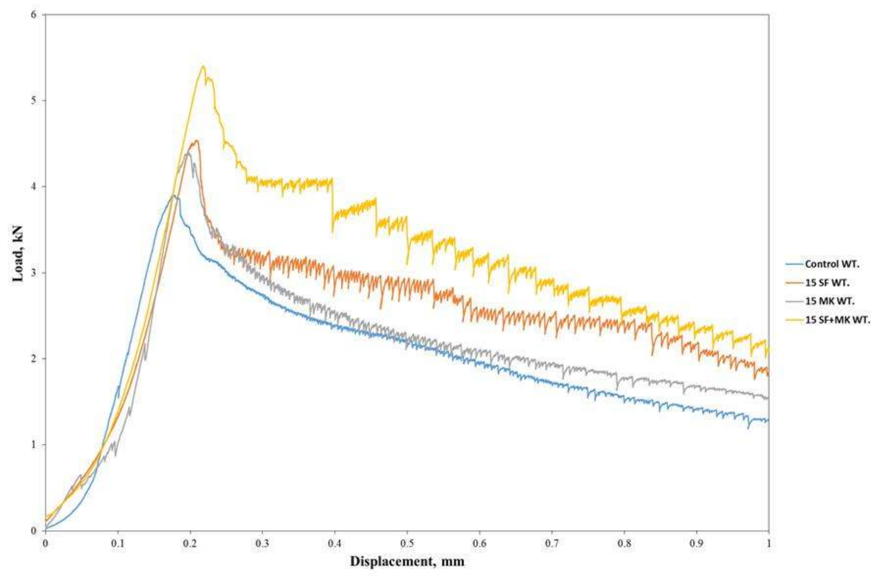
Load, kN
Displacement, mm
Control WT.
15 SF WT.
15 MK WT.
15 SF+MK WT.

a)

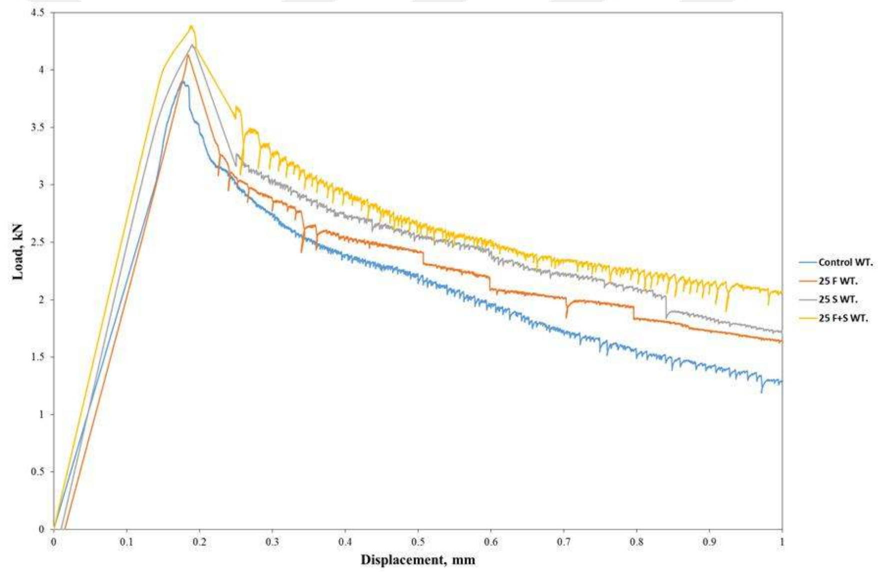
Load, kN
Displacement, mm
Control WT.
25 F WT.
25 S WT.
25 F+S WT.

b)

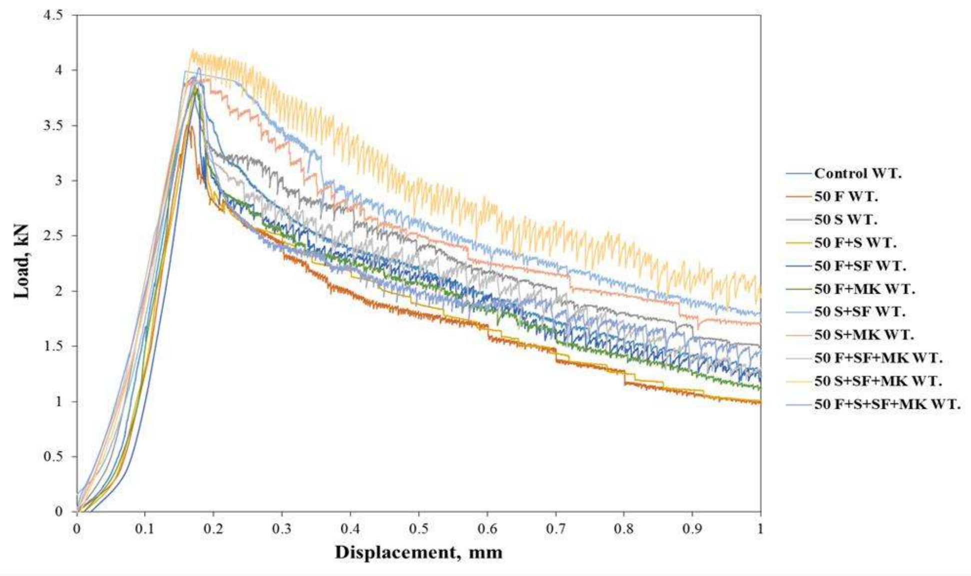
Load, kN
Displacement, mm
Control WT.
50 F WT.
50 S WT.
50 F+S WT.
50 F+SF WT.
50 F+MK WT.
50 S+SF WT.
50 S+MK WT.
50 F+SF+MK WT.
50 S+SF+MK WT.
50 F+S+SF+MK WT.

c)

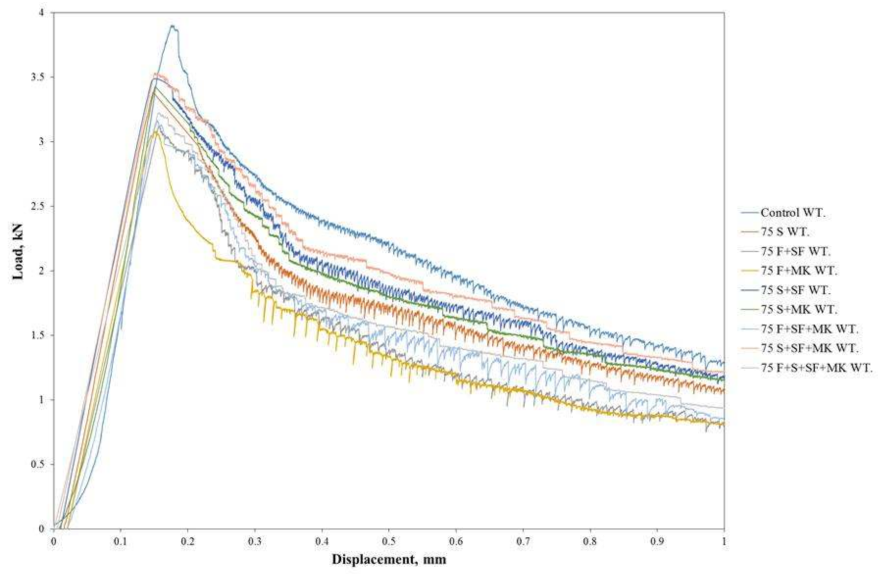
Load, kN
Displacement, mm
Control WT.
75 S WT.
75 F+SF WT.
75 F+MK WT.
75 S+SF WT.
75 S+MK WT.
75 F+SF+MK WT.
75 S+SF+MK WT.
75 F+S+SF+MK WT.

d)

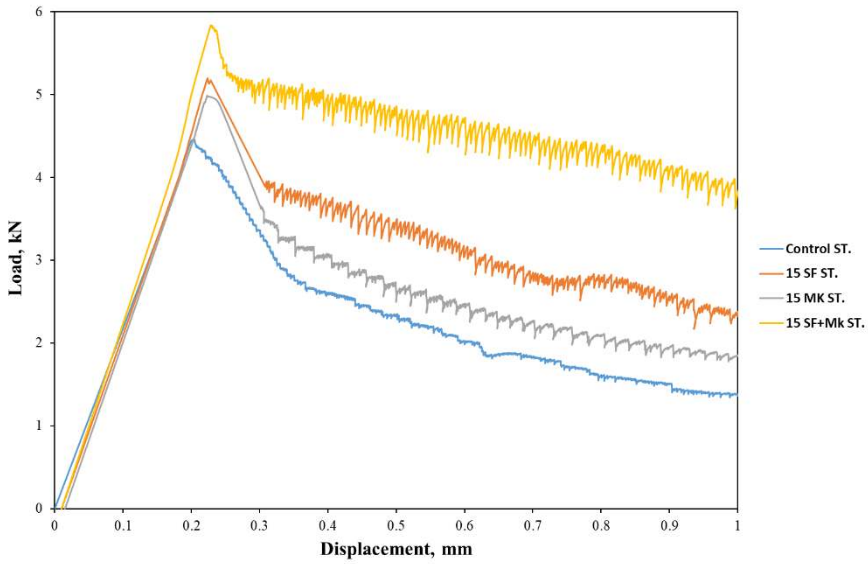
Load, kN
Displacement, mm
Control ST.
15 SF ST.
15 MK ST.
15 SF+Mk ST.

e)

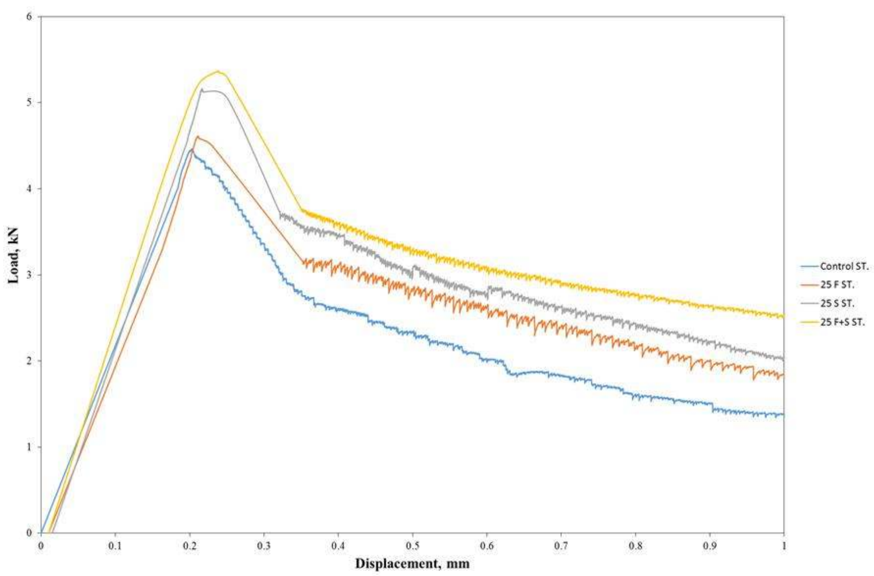
Load, kN
Displacement, mm
Control ST.
25 F ST.
25 S ST.
25 F+S ST.

f)

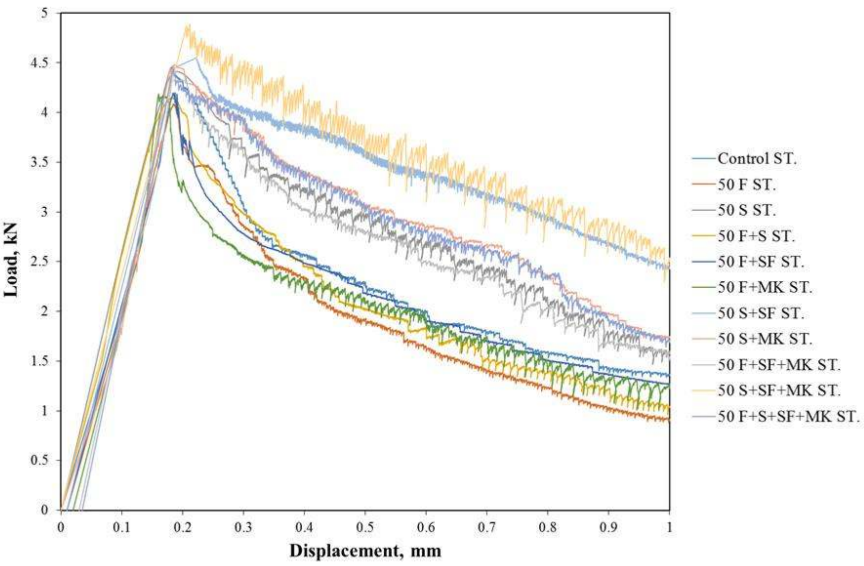

g)

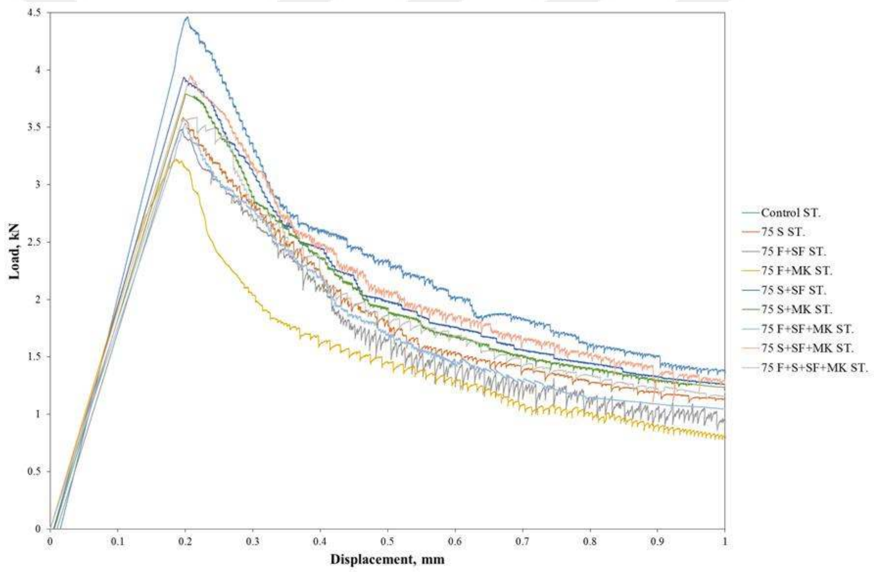

h)

Figure 4.6. Load vs. displacement curves of UHPC with respect to SMC replacement: (a) 15% SMC water curing , (b) 25% SMC water curing,(c)50% SMC water curing ,(d) 75% SMC water curing ,(e) 15% SMC steam curing , (f) 25% SMC steam curing, (g) 50%% SMC steam curing and (h) 75% SMC steam curing

4.6 Fracture Energy

Fracture energy (GF) is the energy dissipated per unit area during the formation of a crack. The region in front of a crack tip where the stress decreases as the crack opens. The area of fracture is the projected area on a plane perpendicular to the direction of stress. In the present study as presented in Figures 4.7 a, b, c, and d, the total fracture energy of UHPC at 90 days depend on two critical considerations, specifically, mineral admixture types and proportion. At binary blender, the UHPC with SF provided the highest fracture energy followed by MK, S, and FA, respectively. Moreover, the mixtures of 15%SF+MK SC, 25% FA+S SC, and 50% S+SF+MK SC that represented the head of their groups on giving the maximum fracture energy with values of 2230.7, 1486.4, and 1542.5 N/m, correspondingly. While the control mixture gave the highest results related to 75% group of replacement subsequently followed by the mixture of 60%S+7.5SF+7.5MK (SC) with the value of 1020.9 N/m. The remarkable superior performance of SF and MK is endorsed to their capacity of reaction with water during hydration process and then completing pozzolanic reactions due to rich in chemical compositions, So, they can increase the energy required to fracture the beams. In addition, this increase may be because the ITZ zone and porosity in the cement paste reduced due to filler characteristics. Consequently, the ITZ zone and cement paste have a high fracture energy. Thus, cracks were more desired to pass across the aggregates than ITZ zone and cement paste. It is also important to notice that the load quickly drops after reaching the peak load in the case of high-volume FA and S replacement. This should be attributed to the fact that FA and S are less effective in stopping the macro-cracks and cannot provide a stable post-peak response then micro-cracks grow and merge into larger macro-cracks.

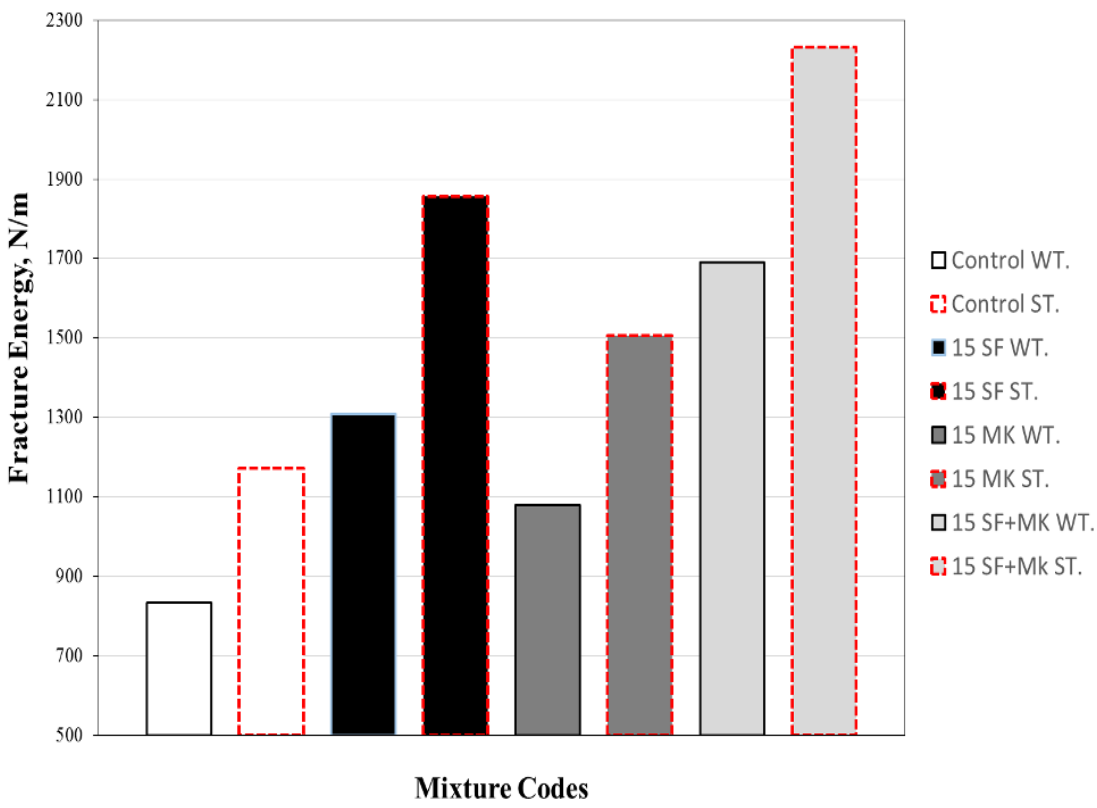

a)

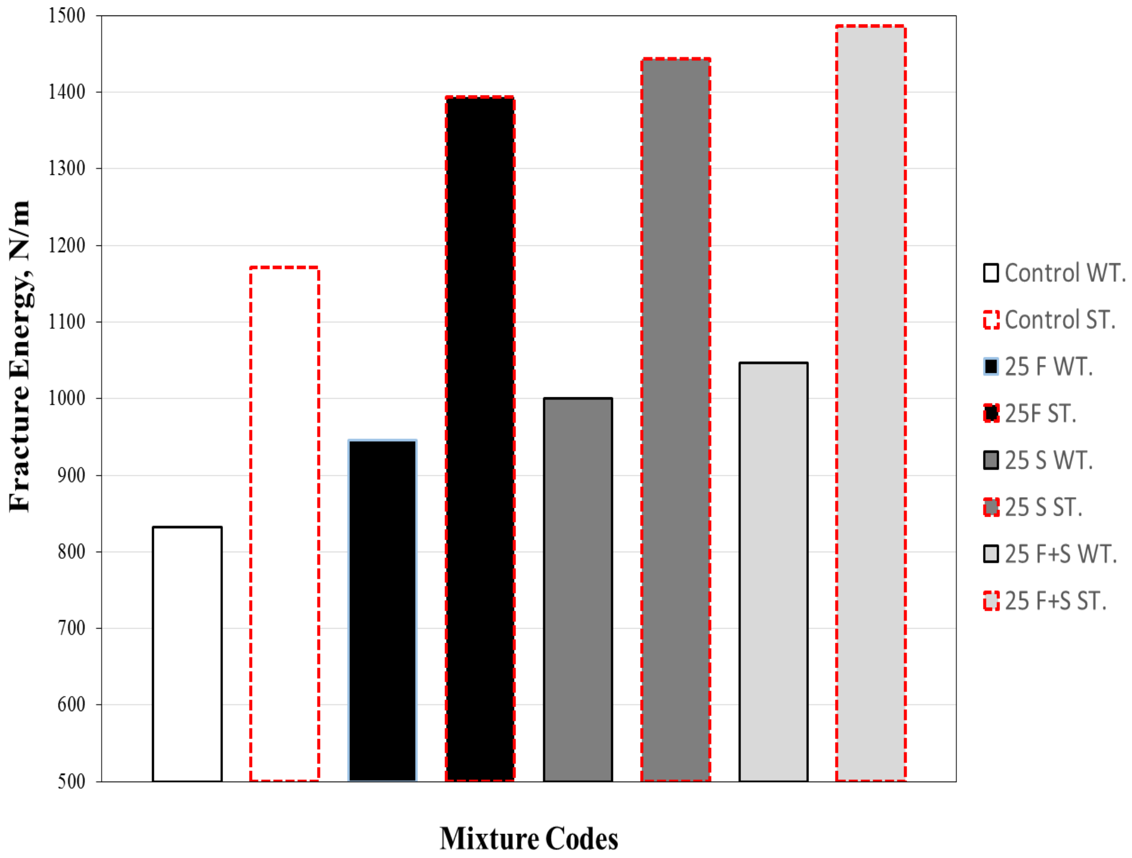
1500
1400
1300
1200
1100
1000
900
800
700
600
500
Fracture Energy, N/m
Mixture Codes
Control WT.
Control ST.
25 F WT.
25F ST.
25 S WT.
25 S ST.
25 F+S WT.
25 F+S ST.

b)

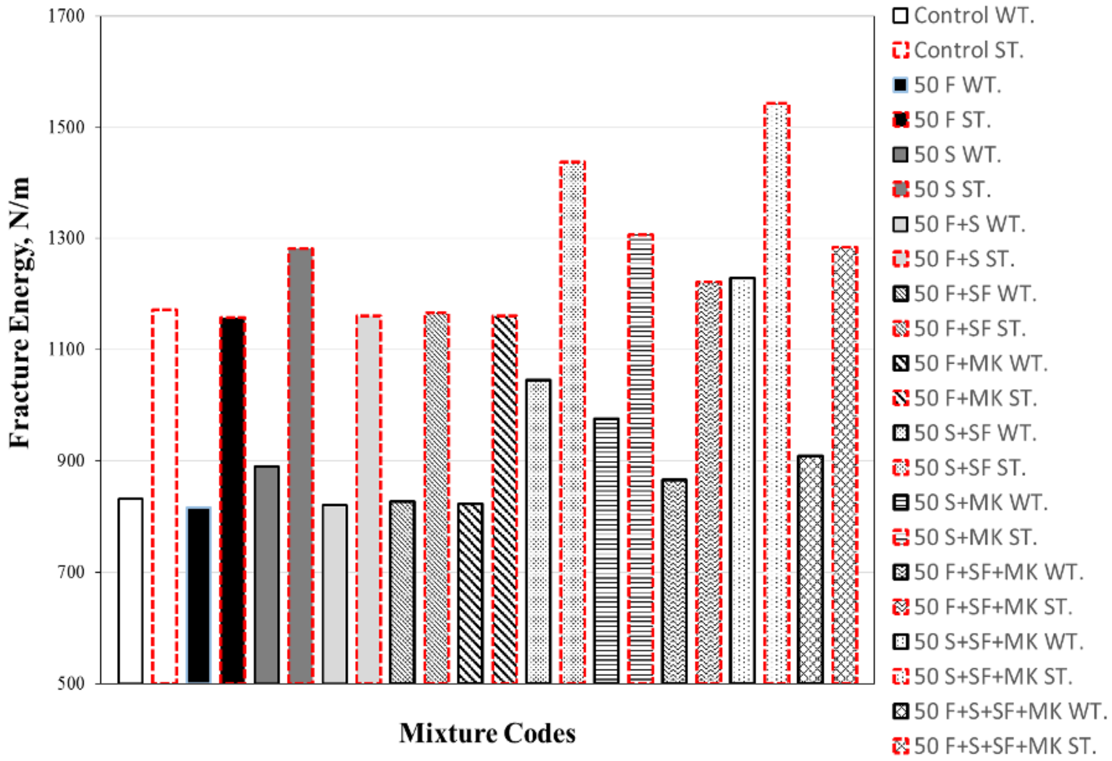
1700
1500
1300
1100
900
700
500
Fracture Energy, N/m
Mixture Codes
Control WT.
Control ST.
50 F WT.
50 F ST.
50 S WT.
50 S ST.
50 F+S WT.
50 F+S ST.
50 F+SF WT.
50 F+SF ST.
50 F+MK WT.
50 F+MK ST.
50 S+SF WT.
50 S+SF ST.
50 S+MK WT.
50 S+MK ST.
50 F+SF+MK WT.
50 F+SF+MK ST.
50 S+SF+MK WT.
50 S+SF+MK ST.
50 F+S+SF+MK WT.
50 F+S+SF+MK ST.

c)

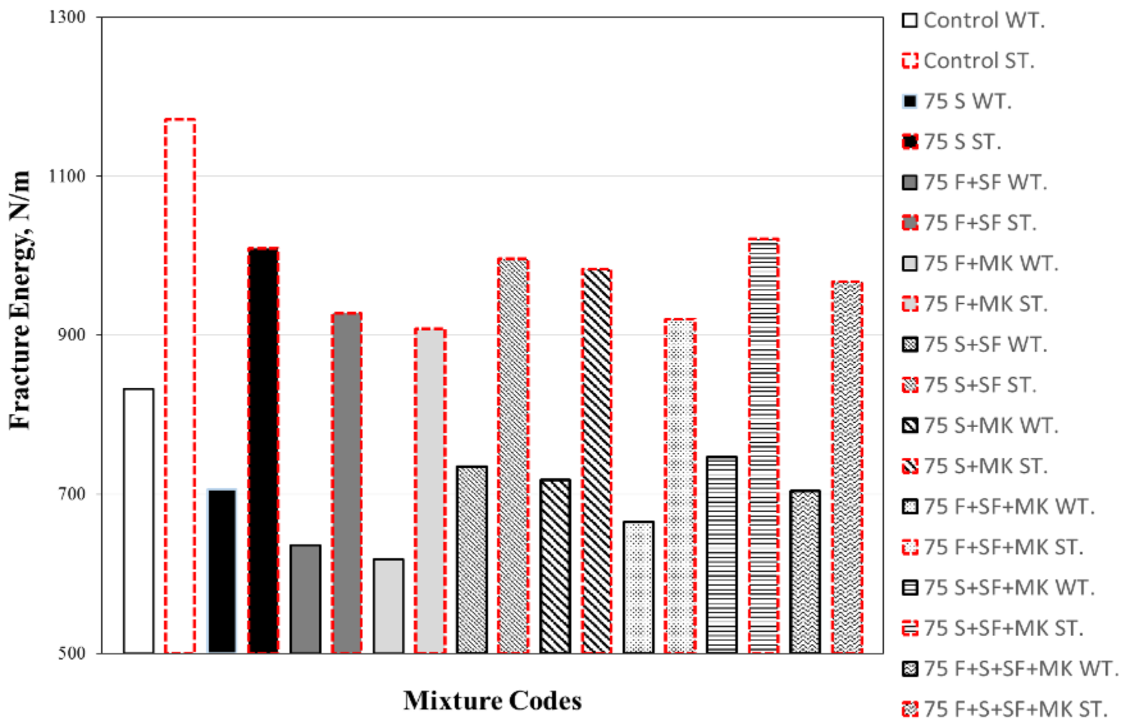

d)

Figure 4.7. Fracture energy of water and steam cured UHPC

4.7 Characteristic Length

As depended on the important concrete parameters like modulus of elasticity, fracture energy, and splitting tensile strength, the characteristic length (l_{ch}) is used for measuring important parameters like ductility and brittleness of concrete. The variation in the characteristic length of UHPCs replaced by various types and amounts of mineral admixtures is presented in Figures 4.8 a, b, c and d. The highest and lowest values of l_{ch} resumed to the mixtures of MK(WC)& MK(SC), S (WC)& FA+S(SC), Control(WC)& S+SF+MK(WC), Control(WC)& FA+S+SF+MK(SC) for the groups of 15, 25, 50, 75% replacement, respectively. Overall, the most ductile and brittleness mixtures were 15%MK (WC) and 50%S+SF+MK (WC) with the values of l_{ch} of 876.5 and 568.5 mm, correspondingly. Thus, according to the test results, the quaternary effect of mineral admixtures, i.e. cement+S+SF+MK, provided the most brittleness concrete despite of better results of the ternary effects, i.e. cement+SF+MK, in the most mechanical properties. This may be attributed to the complexity combined effect of the high cementitious materials of silica fume, metakaolin, slag, and cement.

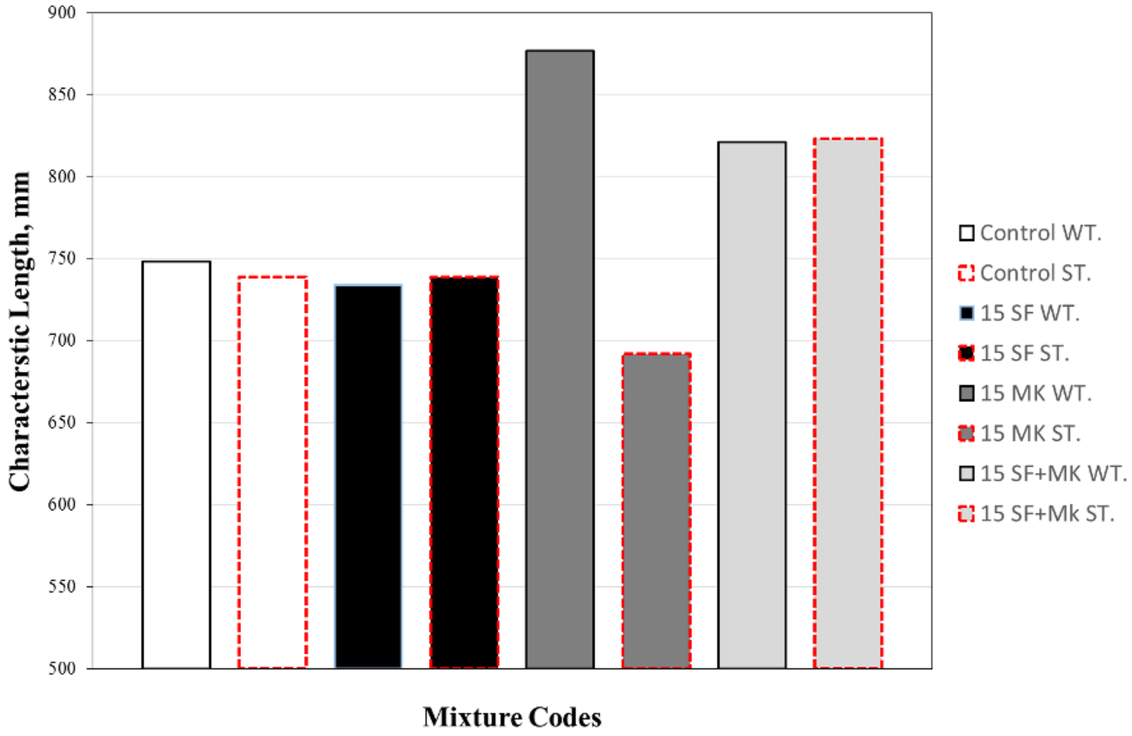
900
850
800
750
700
650
600
550
500
Characterstic Length, mm
Mixture Codes
Control WT.
Control ST.
15 SF WT.
15 SF ST.
15 MK WT.
15 MK ST.
15 SF+MK WT.
15 SF+Mk ST.

a)

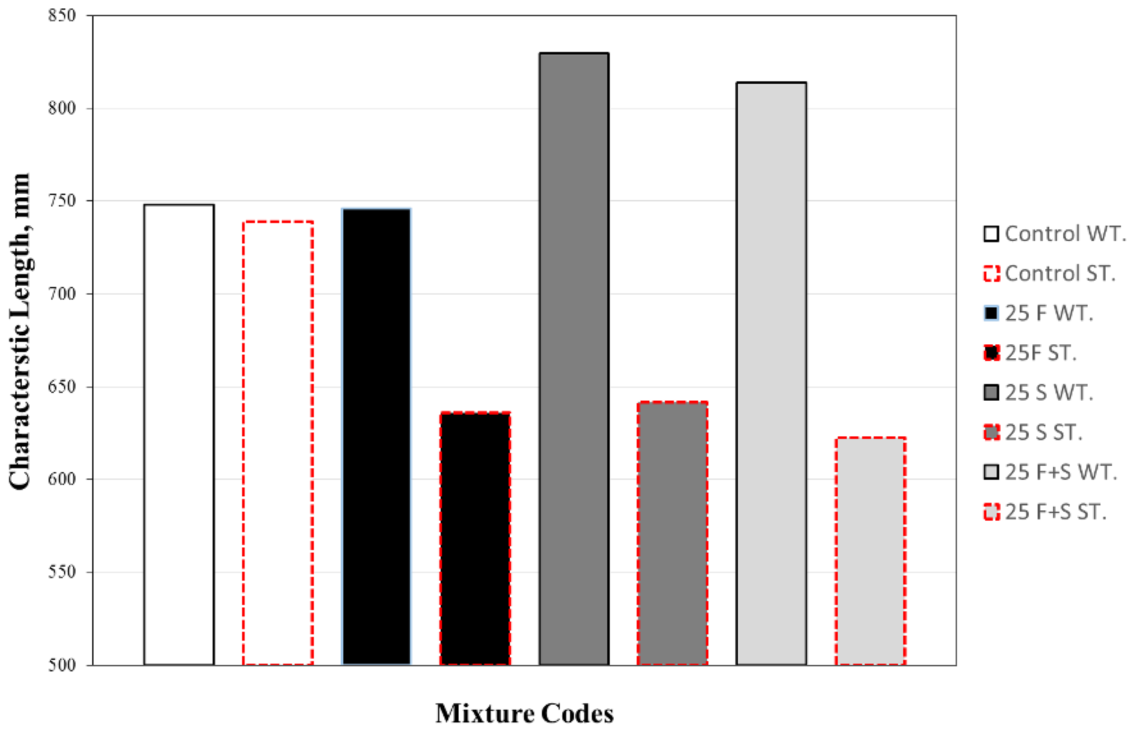
850
800
750
700
650
600
550
500
Characterstic Length, mm
Mixture Codes
Control WT.
Control ST.
25 F WT.
25F ST.
25 S WT.
25 S ST.
25 F+S WT.
25 F+S ST.

b)

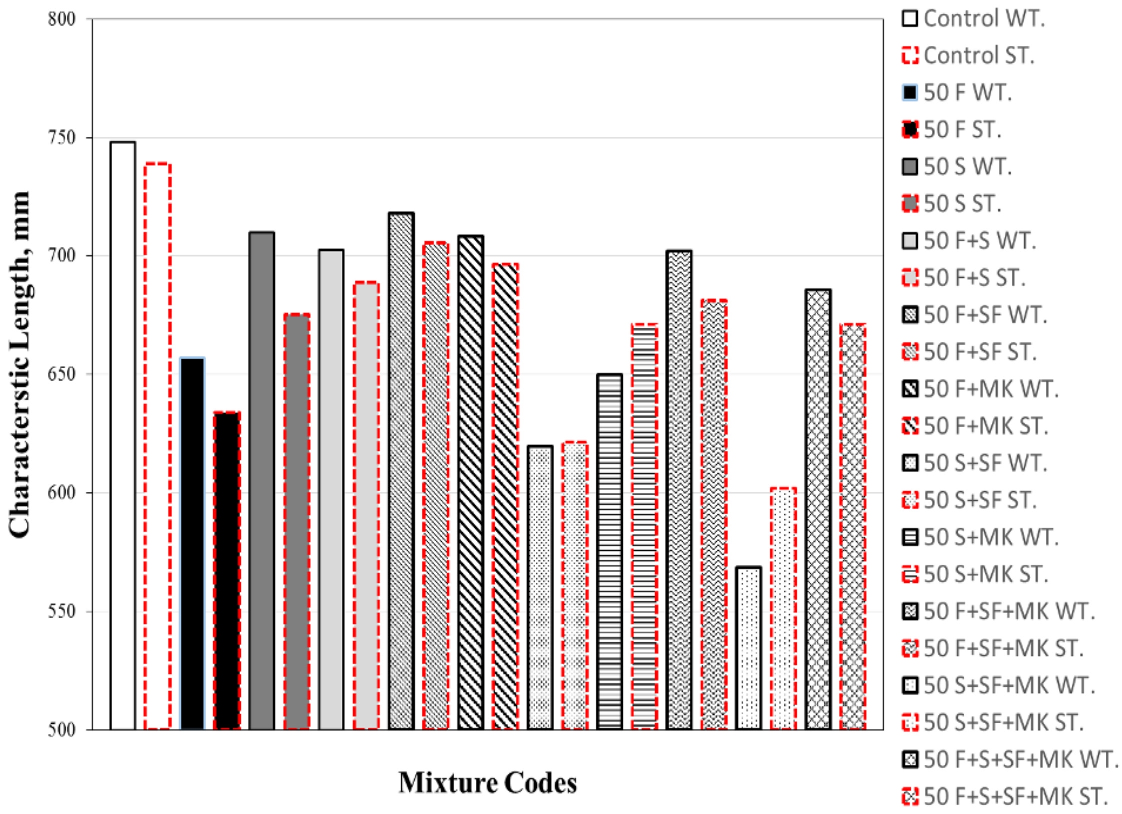

c)

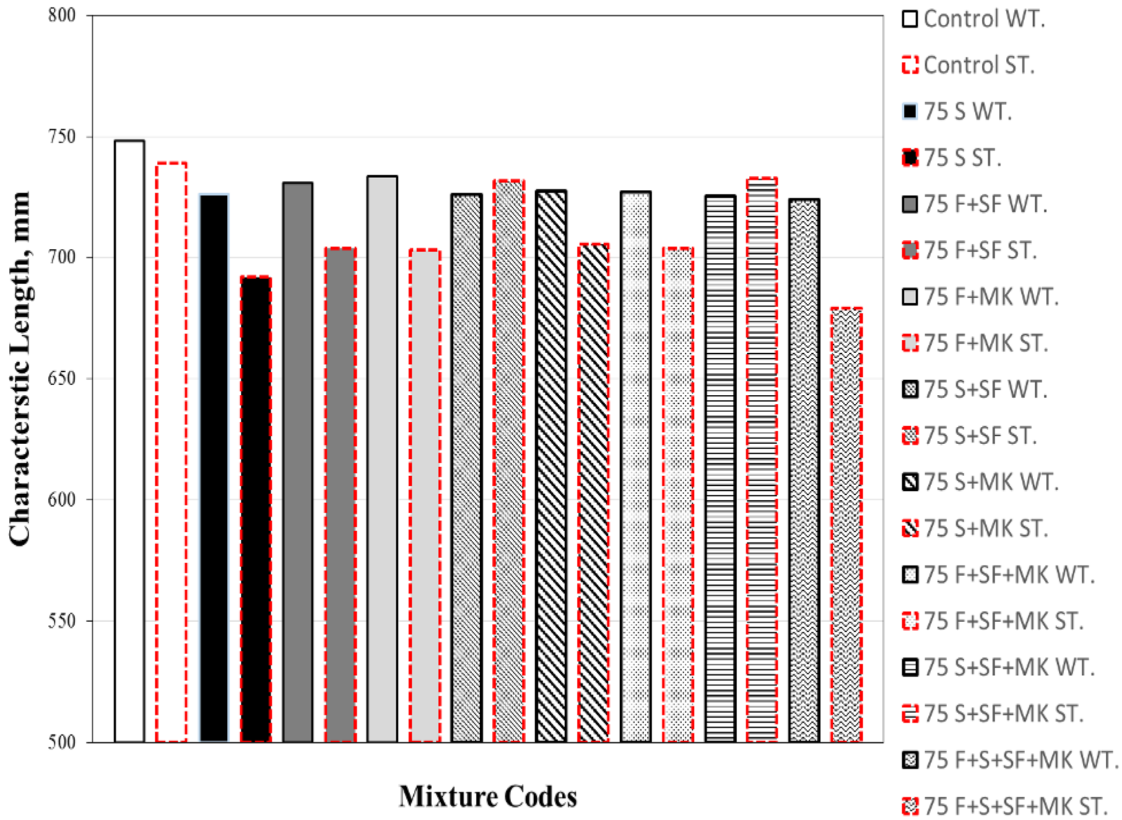

d)

Figure 4.8. Characteristic length of water and steam cured UHPC

CHAPTER 5

RESULTS AND DISCUSSION ON NUMERICAL STUDY

5.1 Axial Capacity of CFST Columns According to Design Codes

The figures of all designed codes are categorized depending on three D/t values of 35, 65 and 95 as the main head figures. Each D/t value met with three fy values of 300, 450, and 650 MPa. Consequently, depending on the different D/t and fy values 18 figures were drawn in addition to sub-figures of a, b, c and d that represented 15, 25, 50 and 75%, respectively.

5.1.1 Eurocode 4

Effects of binary, ternary, quaternary, and quinary of different types of FA, S, SF, and MK with amounts of 15, 25, 50 and 75% of the axial load carrying capacity (N_u) of CFST made with water cured UHPC is illustrated in Figures 5.1-5.3, 5.4-5.6, and 5.7-5.9. Irrespective of mineral admixture types, amounts and status, it was observed that the ultimate axial load of concretes continuously increased with growing ages of UHPC from 7 to 90 days. However, the growth of the results after 28 up to 90 days seemed to be quite limited for mineral replacement of 50% (c) and 75% (d) when there were more enhancements at 15% (a) and 25% (b) were observed, regardless of fy and D/t. Indeed, at 90 days' age among different status of binary, ternary quaternary, and quinary of UHPCs incorporated with 15% SF+MK, 25% S, 50% S+SF and 75% S+SF gives the highest axial load capacity which each value donated as the maximum of the groups of 15, 25, 50, and 75% replacements, respectively. On the other hand, the axial load capacity of the columns infilled with UHPC directly improved with all increases in yield strength and diameter of the steel tube. Subsequently, according to the equations given by EC 4, the mixture containing 50% of S+SF, at 90 cured days, D/t = 95 and fy= 600 Mpa gave the best results overall 26 designed mixtures.

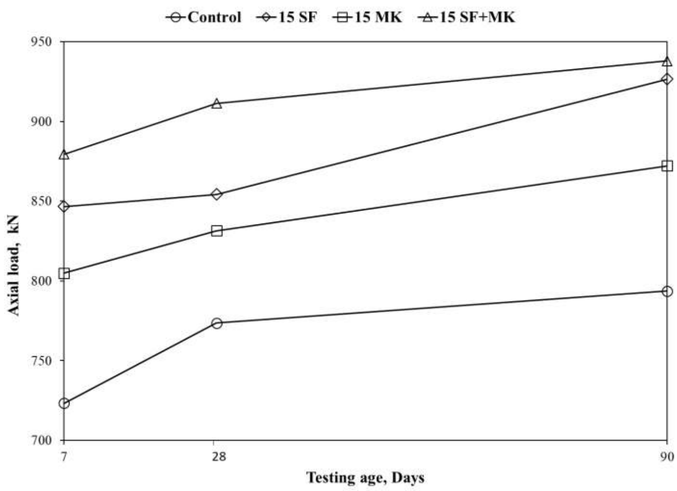

Control
15 SF
15 MK
15 SF+MK
Axial load, kN
Testing age, Days

(a)

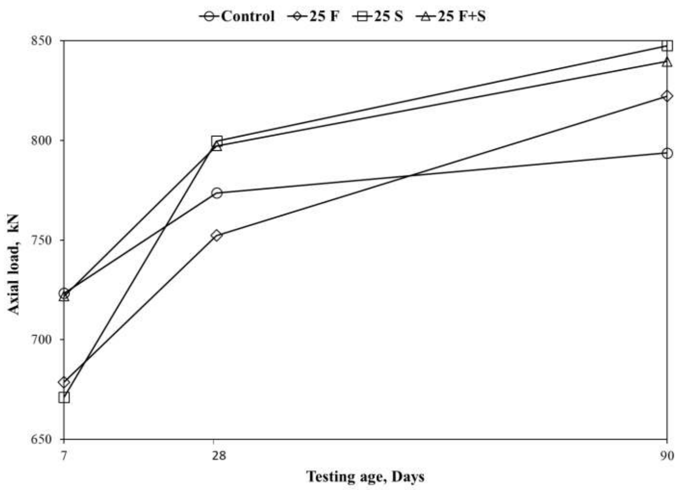

Control
25 F
25 S
25 F+S
Axial load, kN
Testing age, Days

(b)

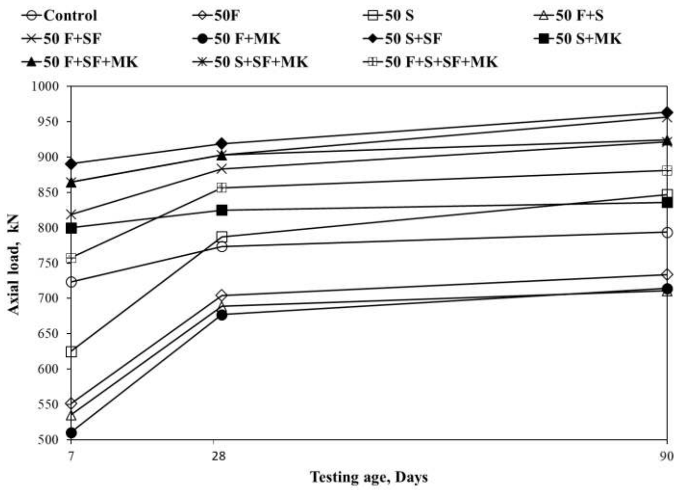

Control
50F
50 S
50 F+S
50 F+SF
50 F+MK
50 S+SF
50 S+MK
50 F+SF+MK
50 S+SF+MK
50 F+S+SF+MK
Axial load, kN
Testing age, Days

(c)

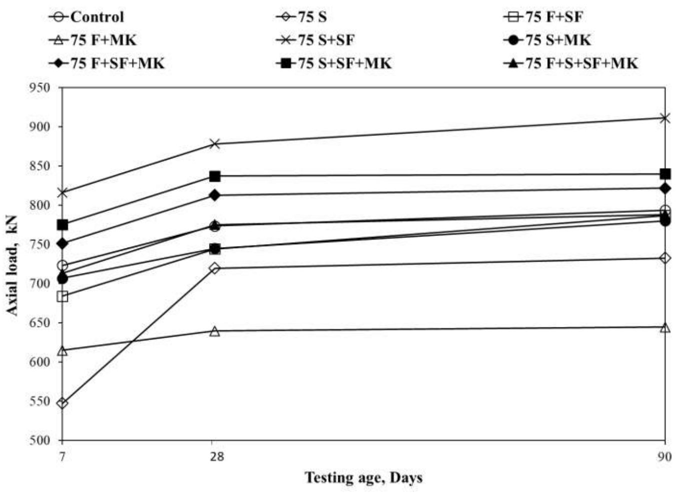

(d)

Figure 5.1. Ultimate axial load of the CFST column having UHPC based on Eurocode 4 for the case of D/t=35 and fy=300 MPa; a) 15, b) 25, c)50, and d) 75% replacement

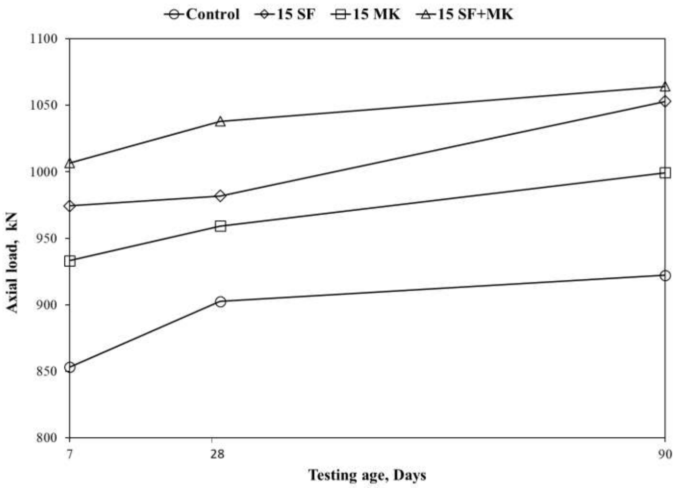

(a)

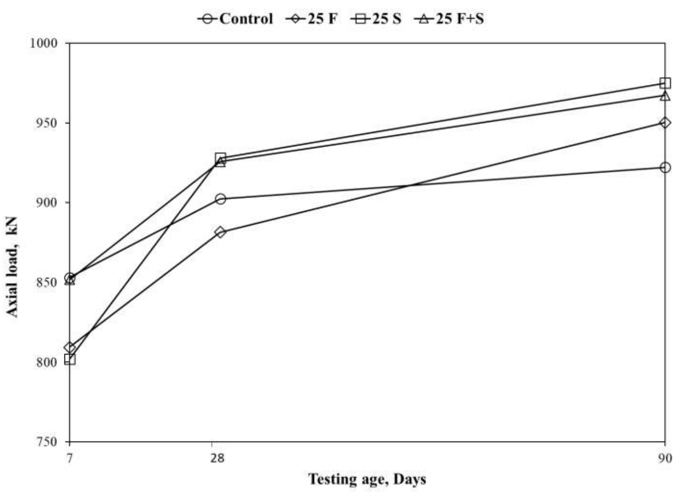

(b)

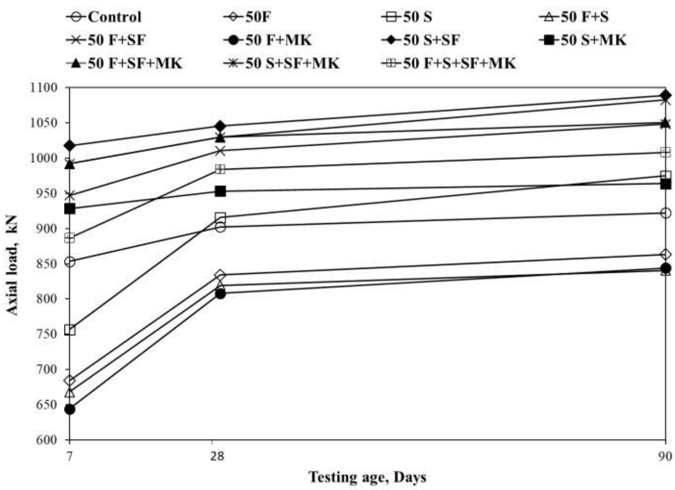

(c)

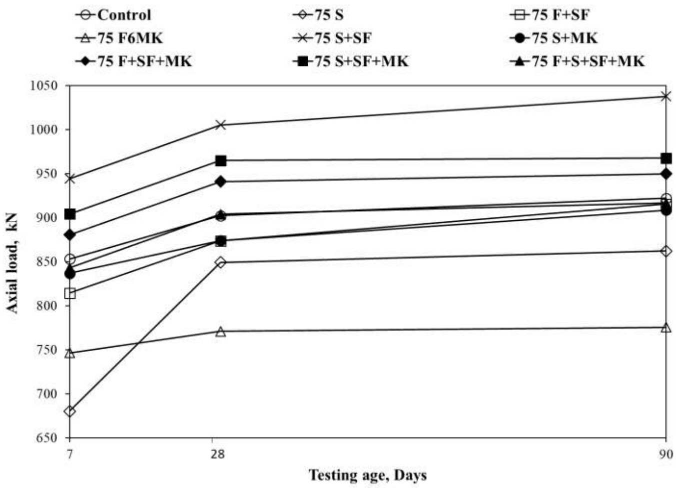

(d)

Figure 5.2. Ultimate axial load of the CFST column having UHPC based on Eurocode 4 for the case of D/t=35 and fy=450 MPa; a) 15, b) 25, c)50, and d) 75% replacement

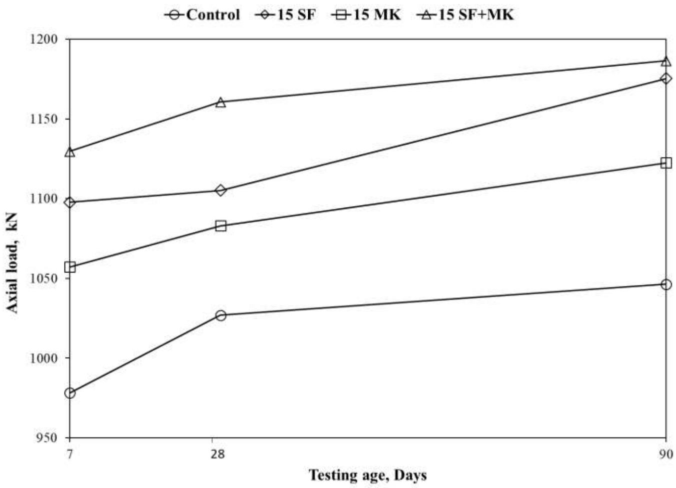

(a)

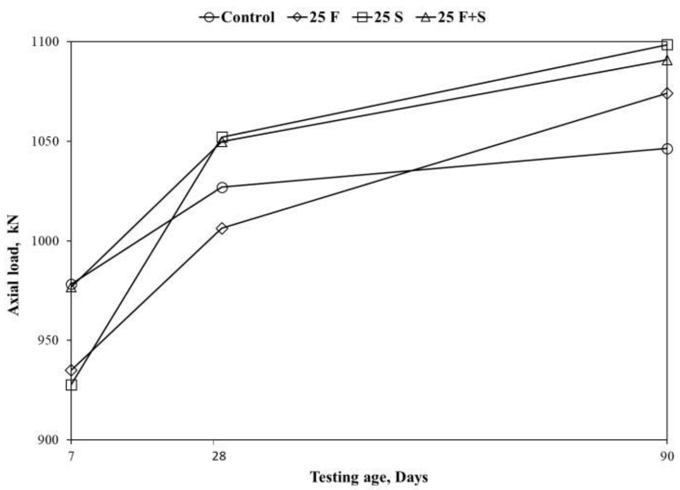

(b)

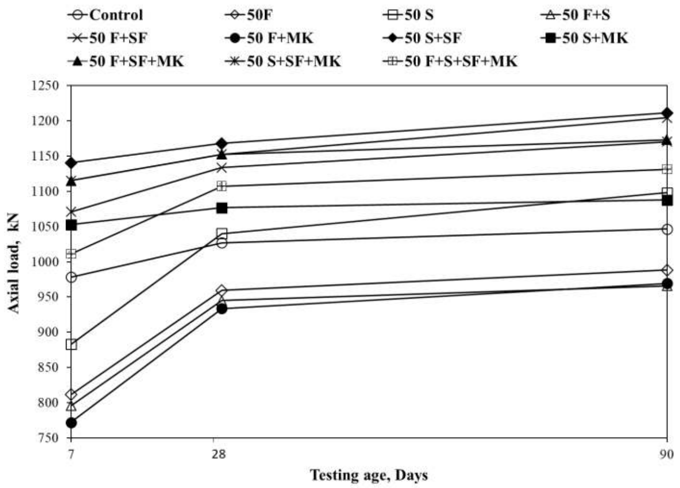

(c)

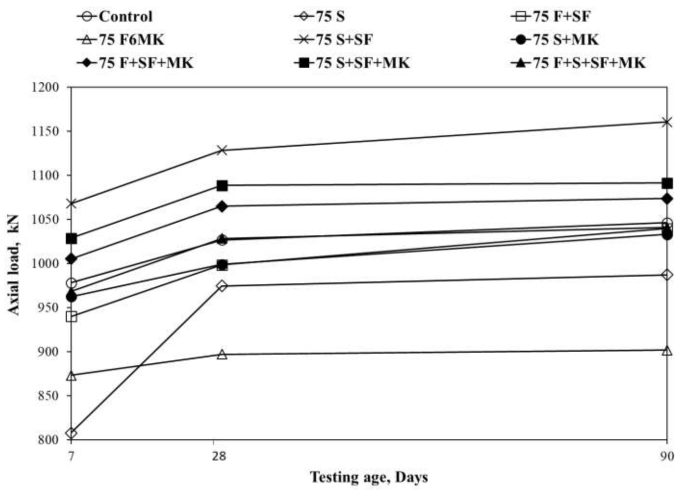

(d)

Figure 5.3. Ultimate axial load of the CFST column having UHPC based on Eurocode 4 for the case of D/t=35 and fy=600 MPa; a) 15, b) 25, c)50, and d) 75% replacement

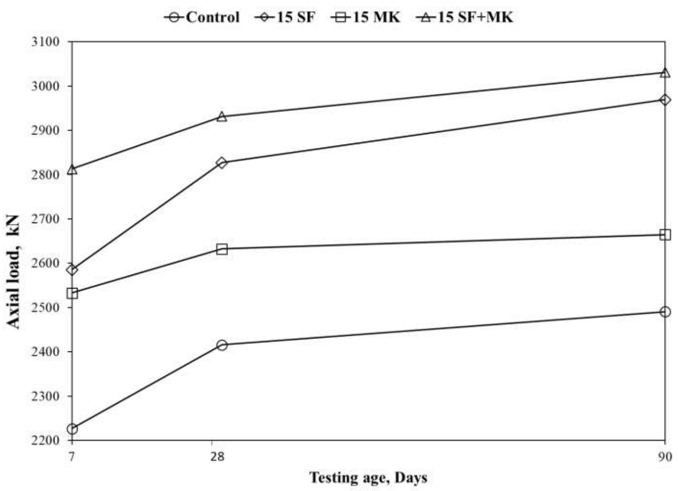
Control
15 SF
15 MK
15 SF+MK
Axial load, kN
Testing age, Days
3100
3000
2900
2800
2700
2600
2500
2400
2300
2200
7
28
90

(a)

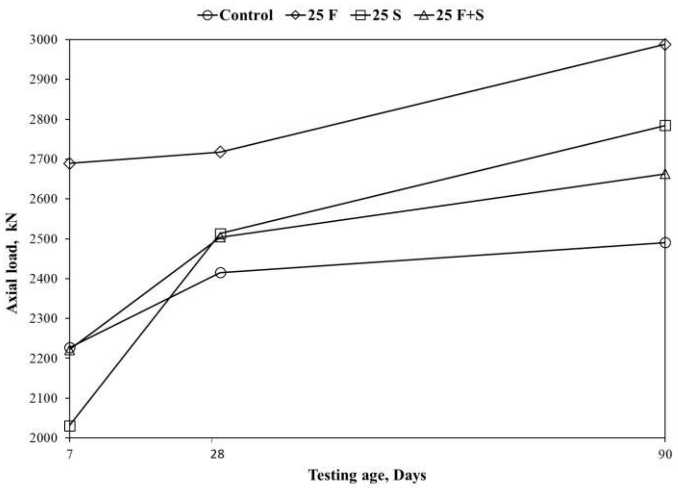
Control
25 F
25 S
25 F+S
Axial load, kN
Testing age, Days
3000
2900
2800
2700
2600
2500
2400
2300
2200
2100
2000
7
28
90

(b)

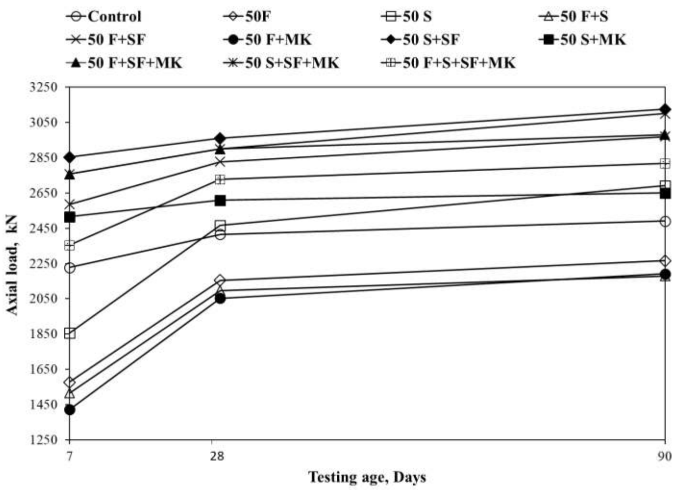
Control
50F
50 S
50 F+S
50 F+SF
50 F+MK
50 S+SF
50 S+MK
50 F+SF+MK
50 S+SF+MK
50 F+S+SF+MK
Axial load, kN
Testing age, Days
3250
3050
2850
2650
2450
2250
2050
1850
1650
1450
1250
7
28
90

(c)

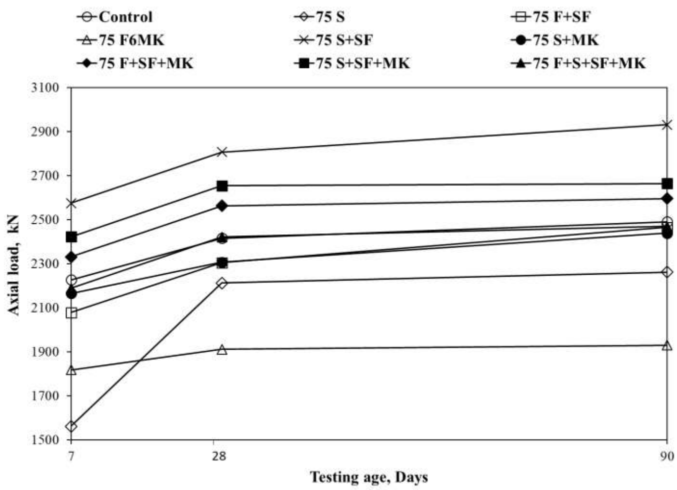

(d)

Figure 5.4. Ultimate axial load of the CFST column having UHPC based on Eurocode 4 for the case of D/t=65 and fy=300 MPa; a) 15, b) 25, c)50, and d) 75% replacement

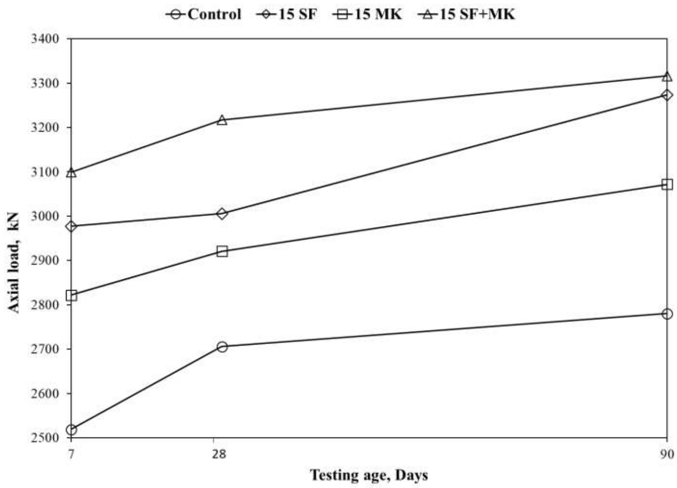

(a)

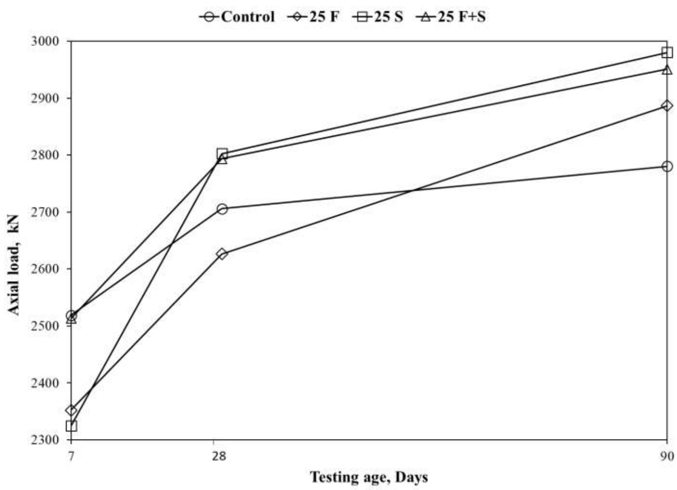

(b)

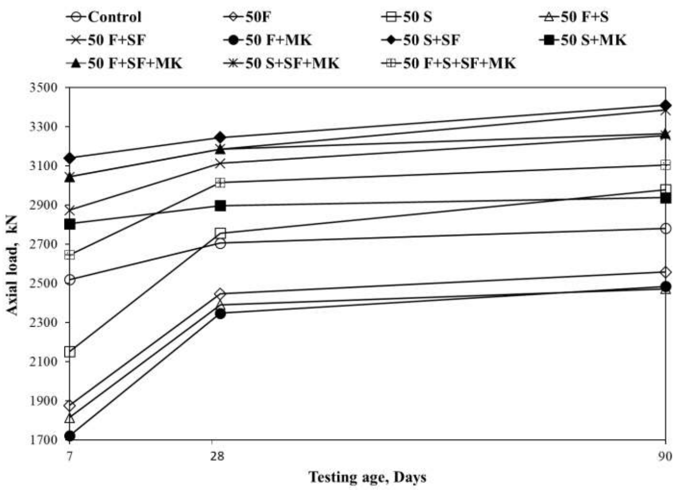

(c)

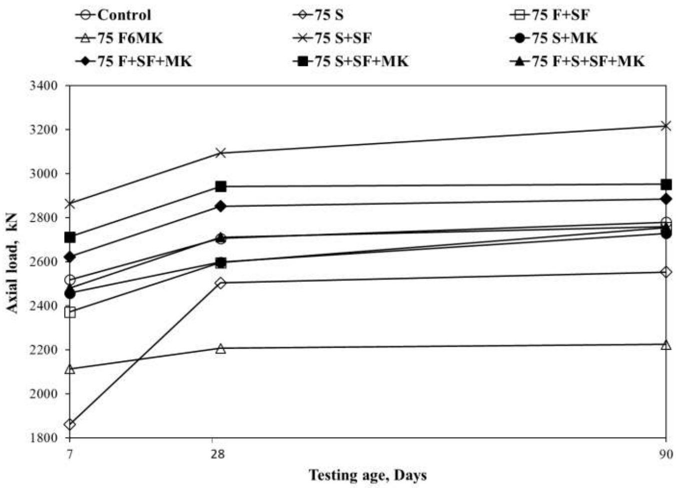

(d)

Figure 5.5. Ultimate axial load of the CFST column having UHPC based on Eurocode 4 for the case of D/t=65 and fy=450 MPa; a) 15, b) 25, c)50, and d) 75% replacement

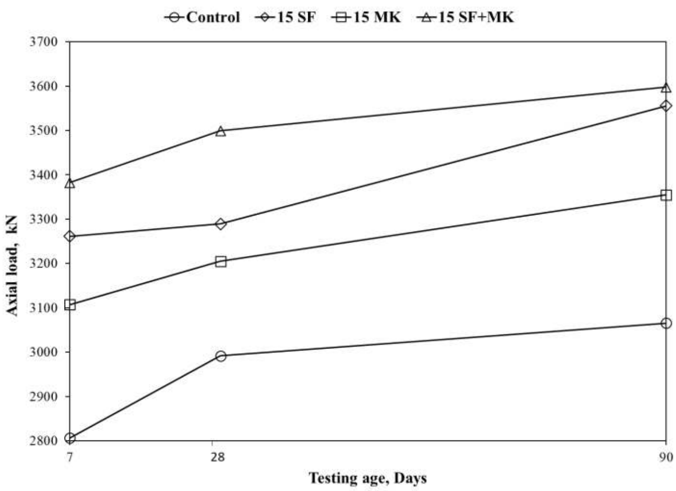

(a)

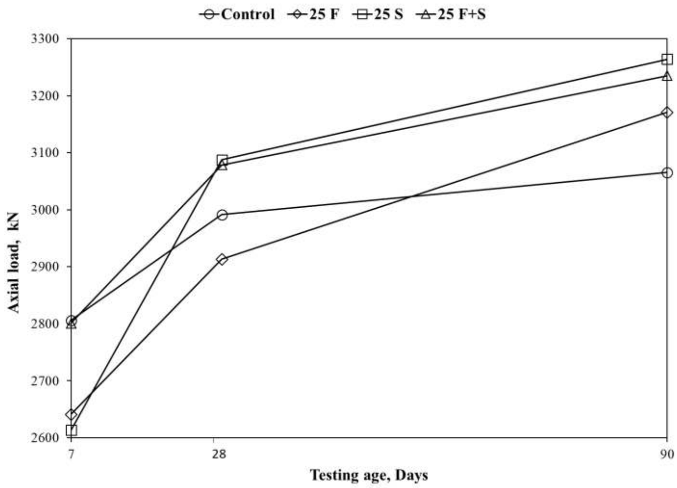

(b)

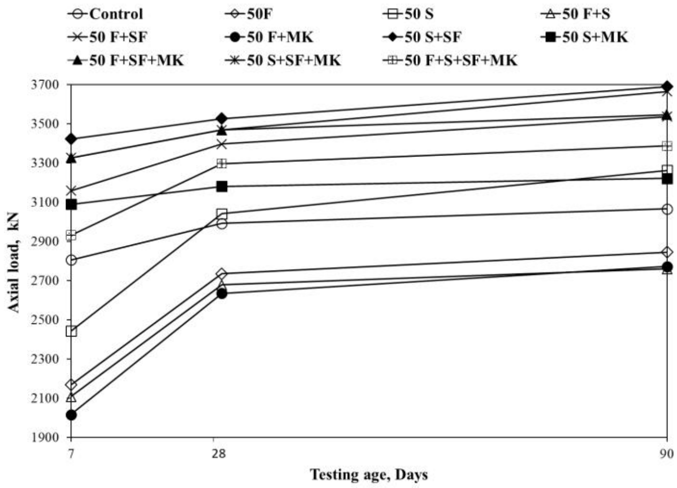

(c)

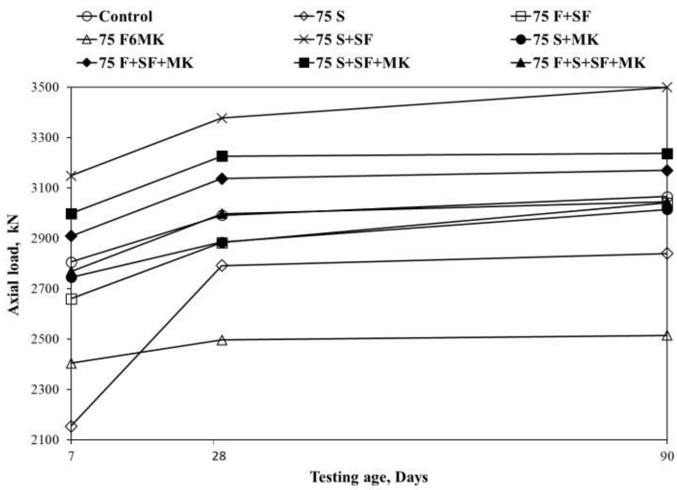

(d)

Figure 5.6. Ultimate axial load of the CFST column having UHPC based on Eurocode 4 for the case of D/t=65 and fy=600 MPa; a) 15, b) 25, c)50, and d) 75% replacement

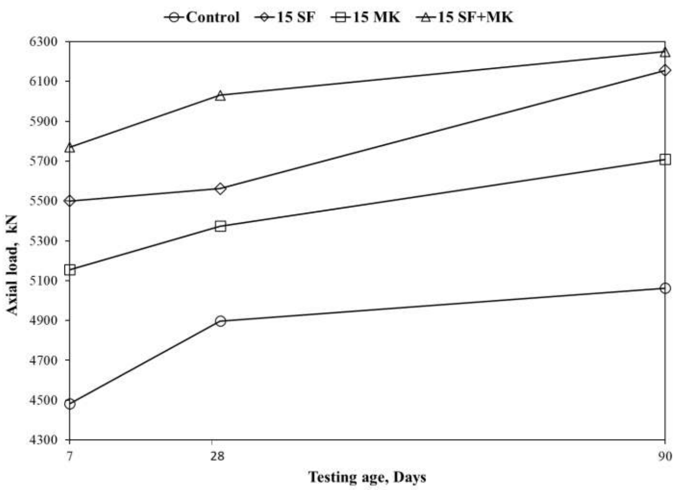
Control
15 SF
15 MK
15 SF+MK
Axial load, kN
Testing age, Days
6300
6100
5900
5700
5500
5300
5100
4900
4700
4500
4300
7
28
90

(a)

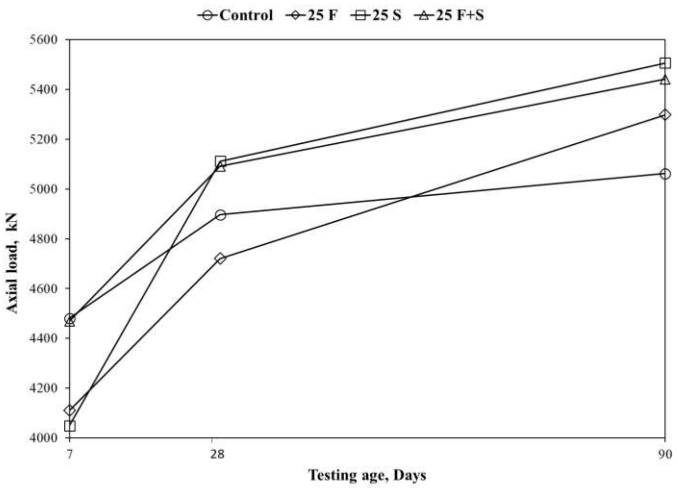
Control
25 F
25 S
25 F+S
Axial load, kN
Testing age, Days
5600
5400
5200
5000
4800
4600
4400
4200
4000
7
28
90

(b)

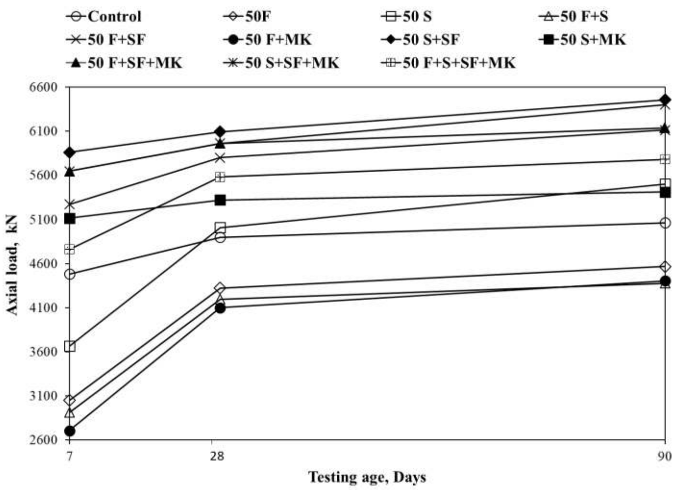
Control
50F
50 S
50 F+S
50 F+SF
50 F+MK
50 S+SF
50 S+MK
50 F+SF+MK
50 S+SF+MK
50 F+S+SF+MK
Axial load, kN
Testing age, Days
6600
6100
5600
5100
4600
4100
3600
3100
2600
7
28
90

(c)

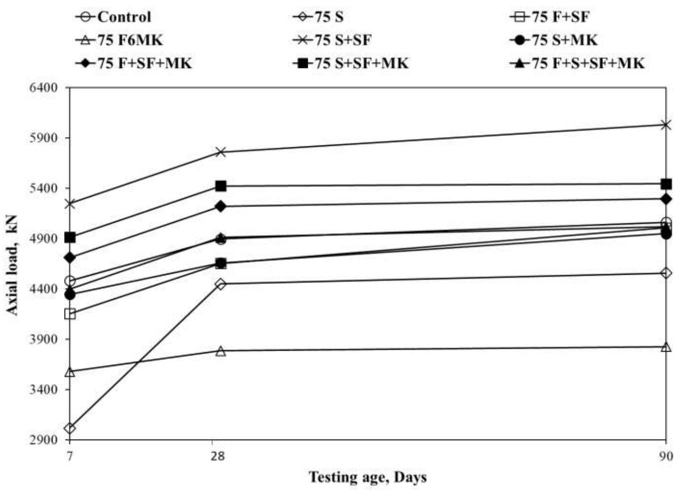

(d)

Figure 5.7. Ultimate axial load of the CFST column having UHPC based on Eurocode 4 for the case of D/t=95 and fy=300 MPa; a) 15, b) 25, c)50, and d) 75% replacement

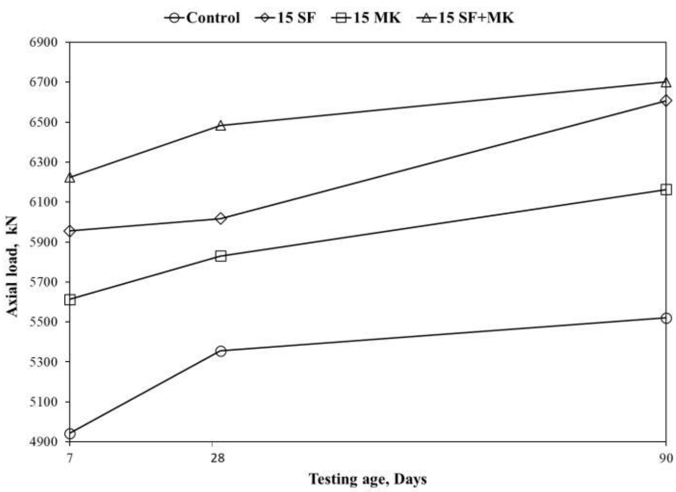

(a)

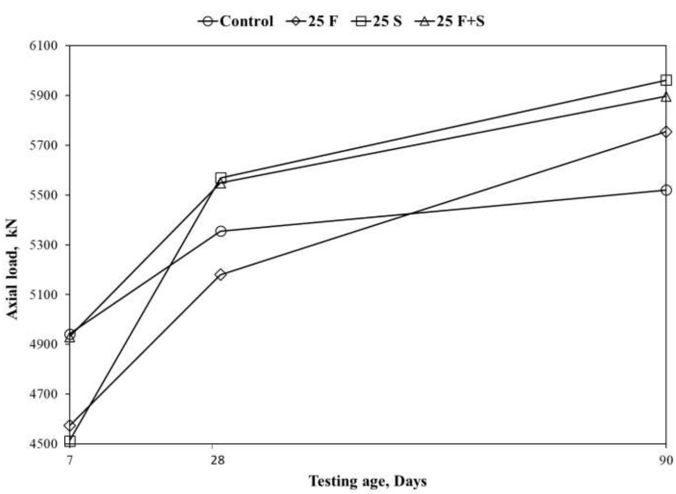

(b)

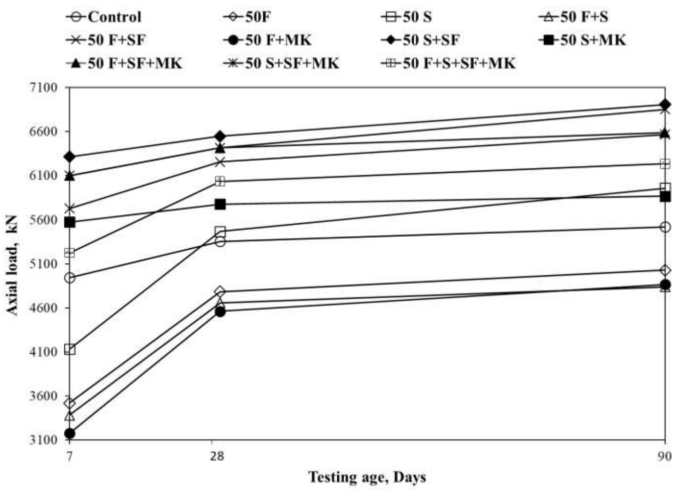

(c)

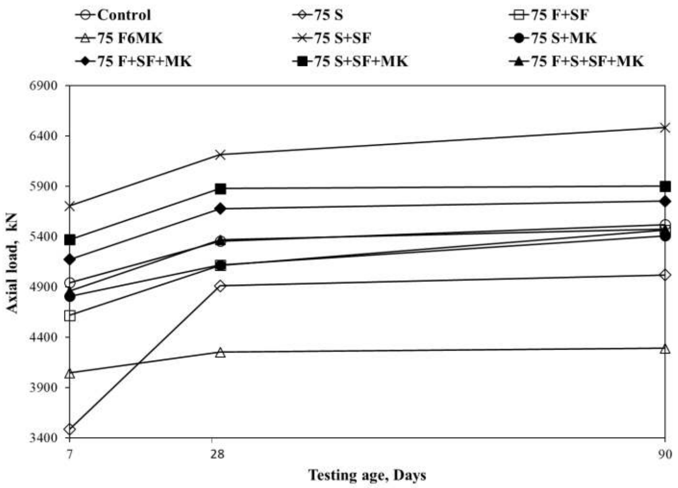

(d)

Figure 5.8. Ultimate axial load of the CFST column having UHPC based on Eurocode 4 for the case of D/t=95 and fy=450 MPa; a) 15, b) 25, c)50, and d) 75% replacement

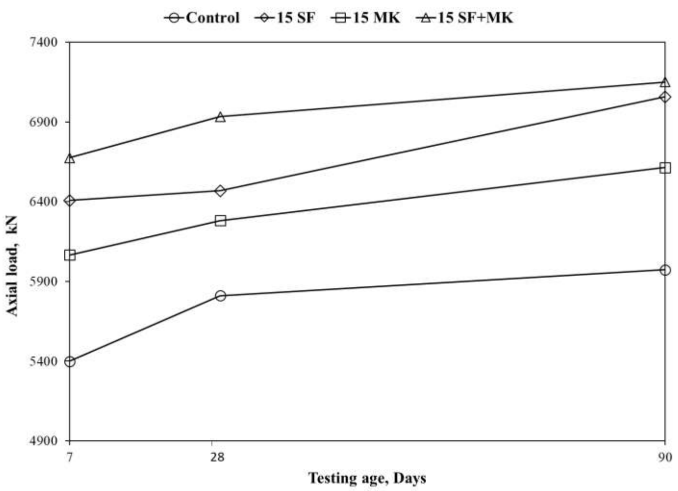

(a)

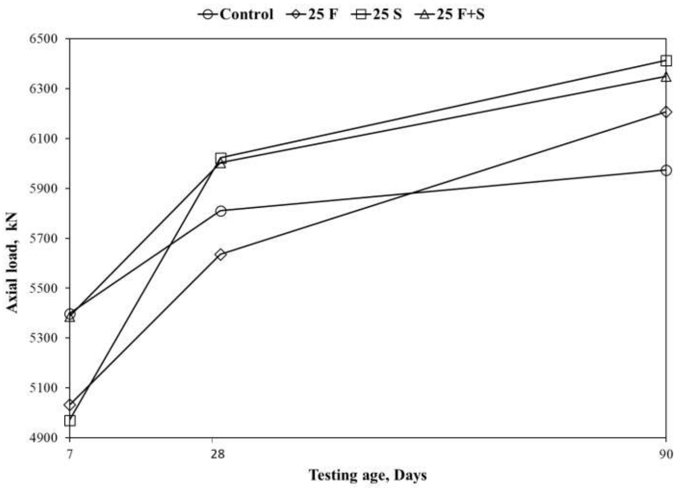

(b)

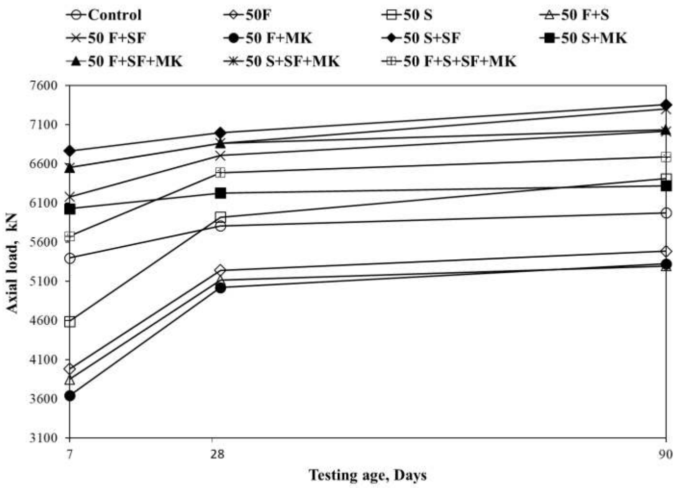

(c)

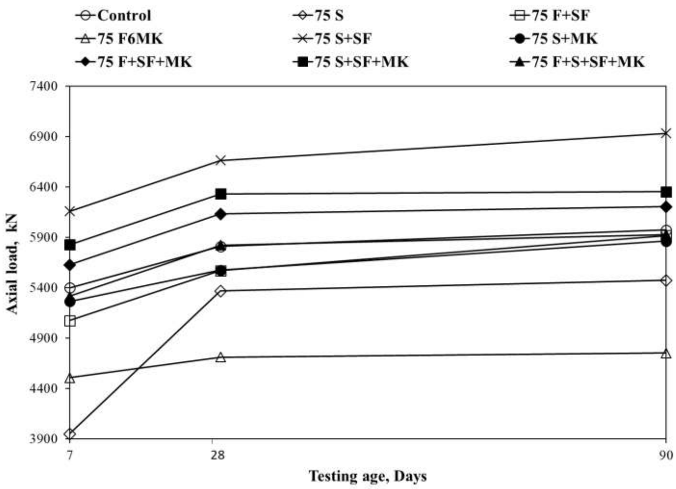

(d)

Figure 5.9. Ultimate axial load of the CFST column having UHPC based on Eurocode 4 for the case of D/t=95 and fy=600 MPa; a) 15, b) 25, c)50, and d) 75% replacement

5.1.2 ACI Code

Effects of different mineral admixture types, diameters and the yield strengths of steel column on the axial load capacity of CFST filled with UHPCs are illustrated in Figures 5.10-5.12, 5.13-5.15, and 5.16-5.18. It was observed that as the D/t increased from 35 to 95 mm and fy from 300 to 600 MPa, all series showed growing trend in the capacity of CFST section in all ages, irrespective to pozzolanic types and amounts. According to the results drawn in above-mentioned figures, replacing of mineral admixtures to UHPC is some complex and sensitive depending on their amount and whether binary or ternary or, etc. Therefore, the best results can be linked to the mixes that included 15% SF, 7.5% SF+ 7.5% MK, 35%S+7.5%SF+7.5%MK and 17.5%FA+17.5%S+7.5%SF+7.5%MK as binary, ternary, quaternary, and quinary, respectively. However, between 26 mixture proportions the highest and lowest axial load capacity of CFST filled with UHPC associated to 35%S+7.5%SF+7.5%MK and 60%FA+15%MK, correspondingly. The lower axial load capacity results of 75% replacement of some mineral admixtures comparing to control mixtures gave a recommendation of up to 50% using pozzolanic materials.

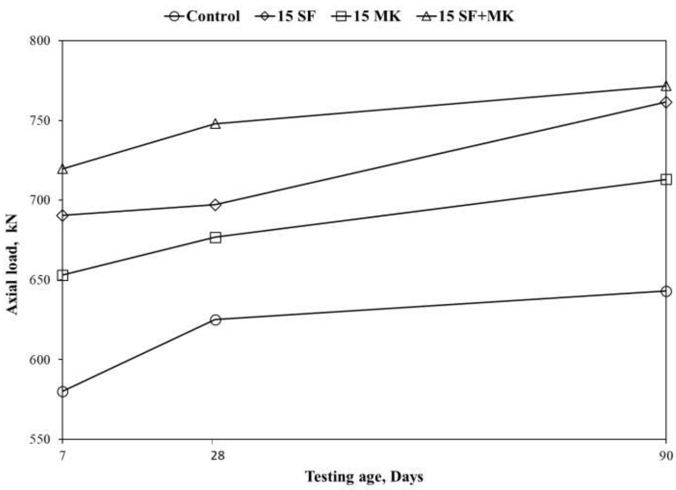

(a)

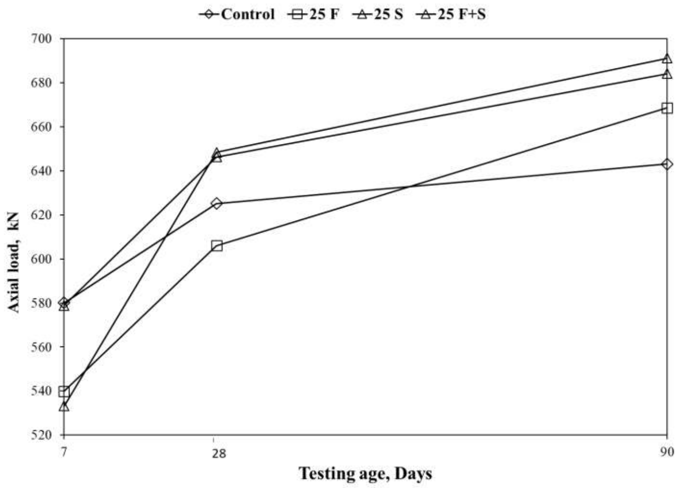

(b)

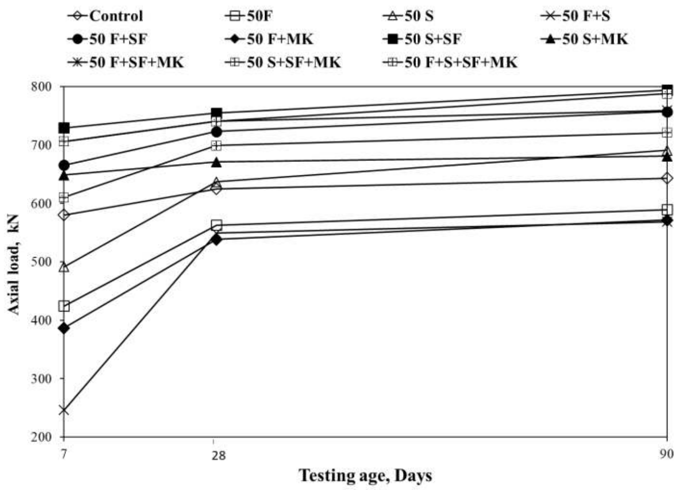

(c)

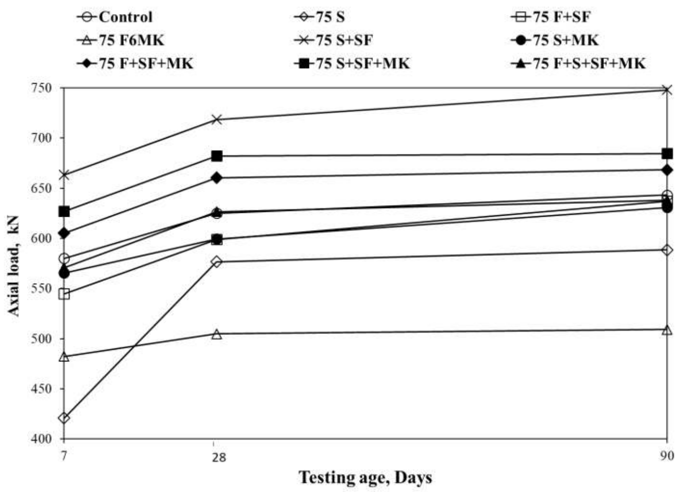

(d)

Figure 5.10. Ultimate axial load of the CFST column having UHPC based on ACI for the case of D/t=35 and fy=300 MPa; a) 15, b) 25, c)50, and d) 75% replacement

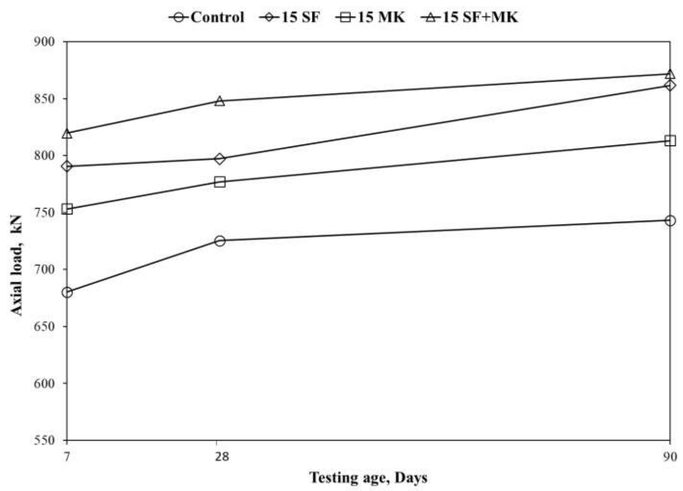

Control
15 SF
15 MK
15 SF+MK
Axial load, kN
Testing age, Days

(a)

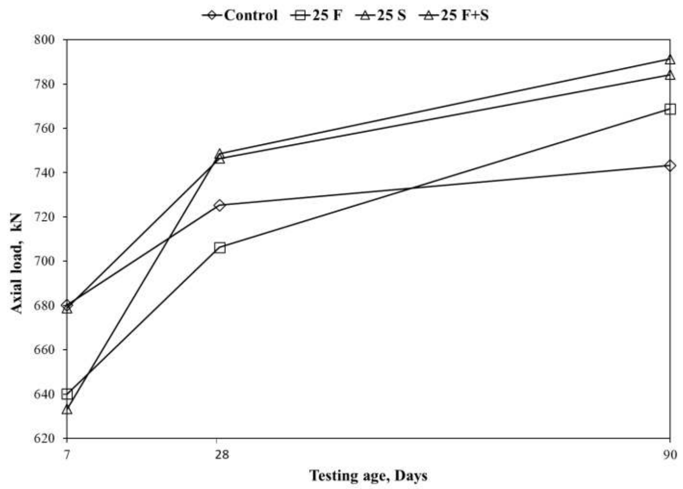

Control
25 F
25 S
25 F+S
Axial load, kN
Testing age, Days

(b)

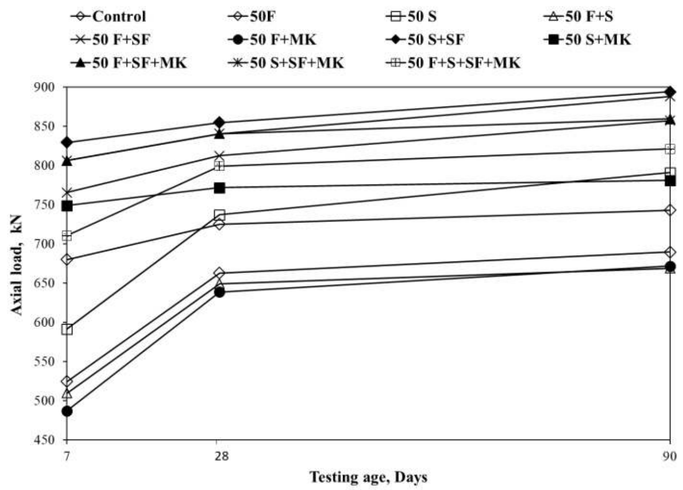

Control
50F
50 S
50 F+S
50 F+SF
50 F+MK
50 S+SF
50 S+MK
50 F+SF+MK
50 S+SF+MK
50 F+S+SF+MK
Axial load, kN
Testing age, Days

(c)

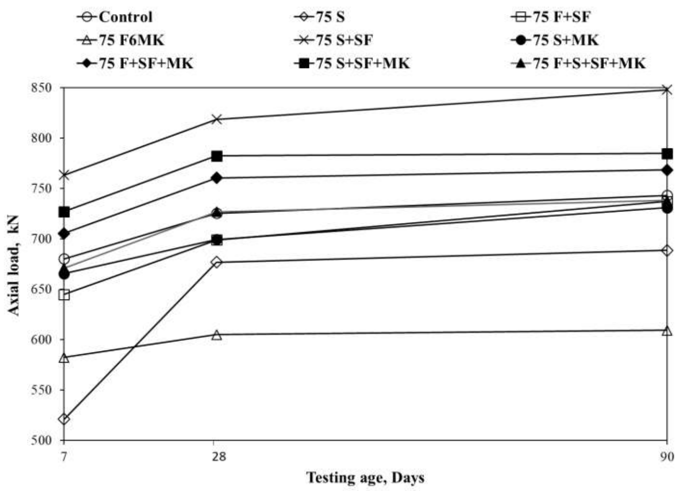

(d)

Figure 5.11. Ultimate axial load of the CFST column having UHPC based on ACI code for the case of D/t=35 and fy=450 MPa; a) 15, b) 25, c)50, and d) 75% replacement

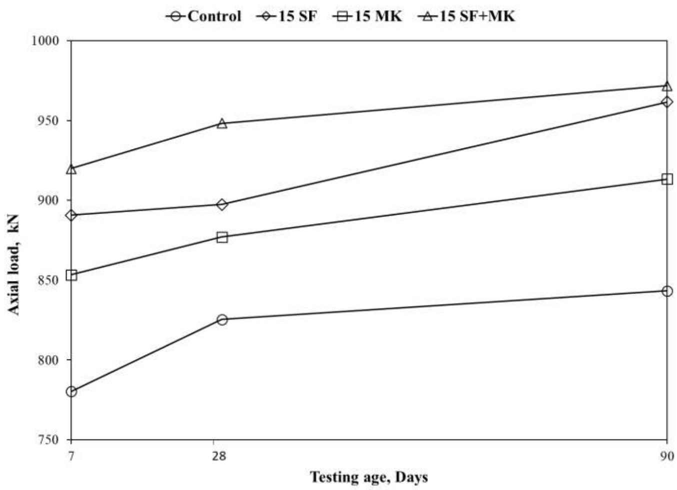

(a)

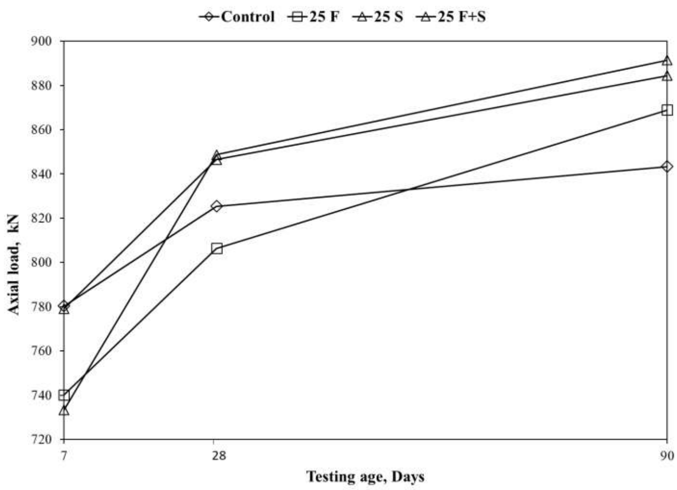

(b)

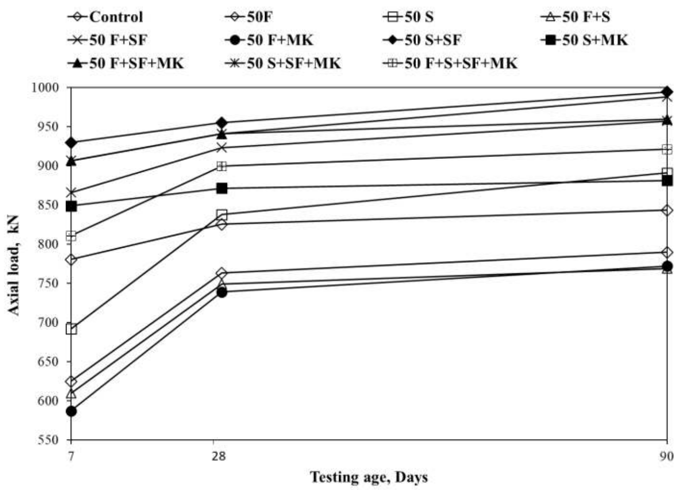

(c)

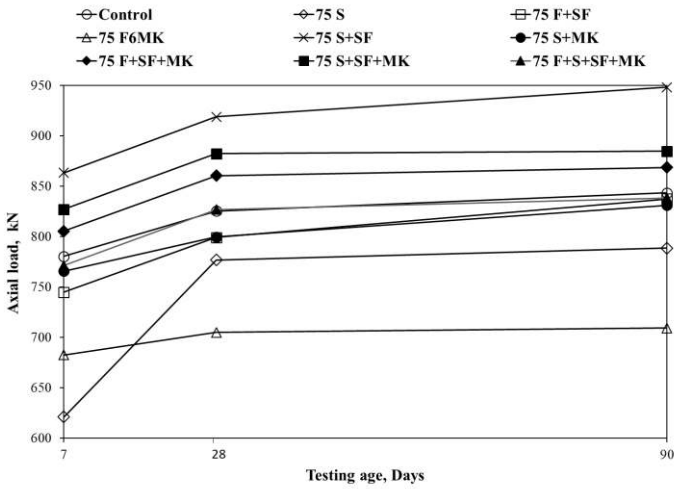

(d)

Figure 5.12. Ultimate axial load of the CFST column having UHPC based on ACI code for the case of D/t=35 and fy=600 MPa; a) 15, b) 25, c)50, and d) 75% replacement

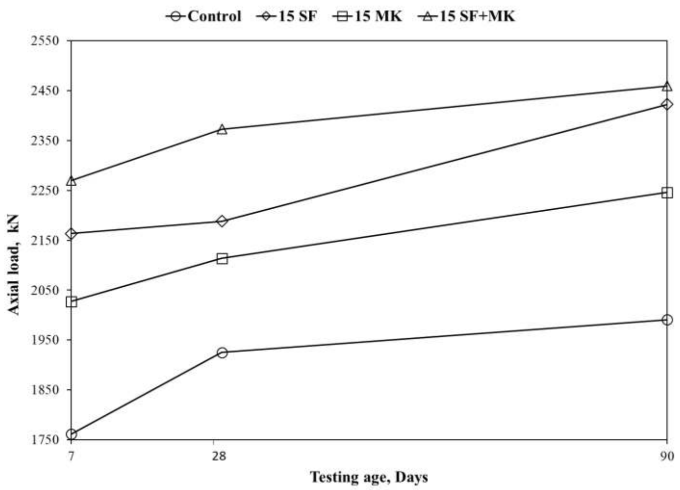

(a)

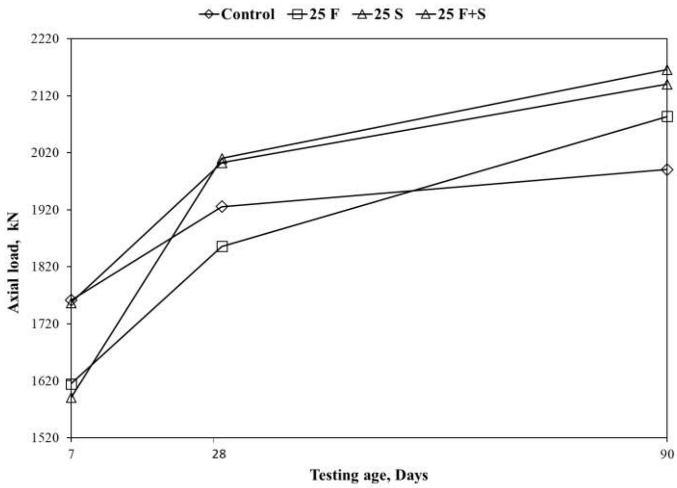

(b)

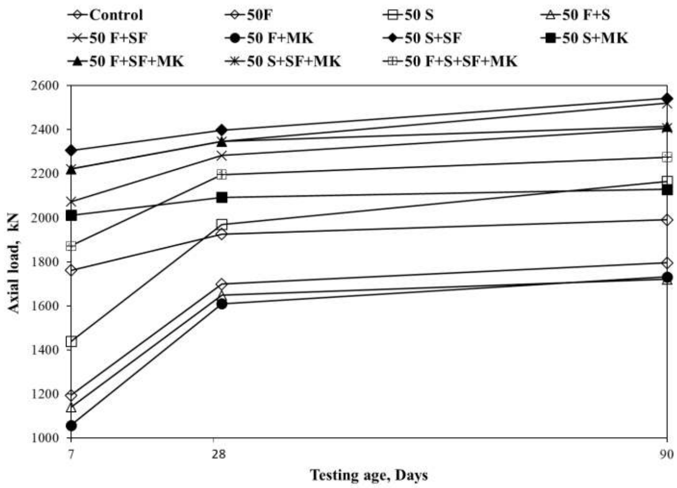

(c)

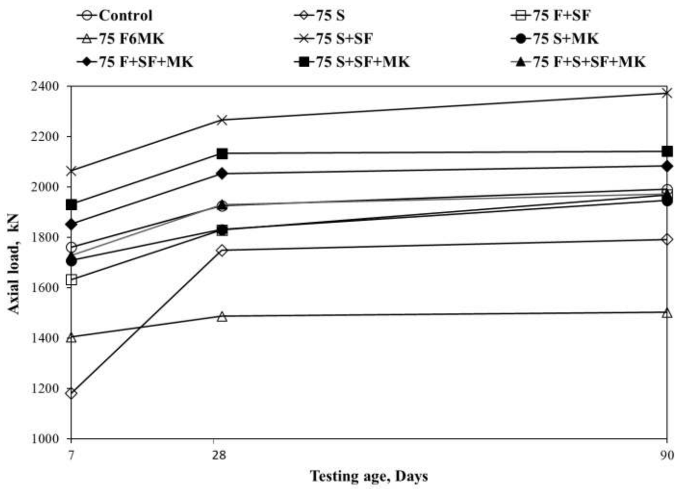

(d)

Figure 5.13. Ultimate axial load of the CFST column having UHPC based on ACI code for the case of D/t=65 and fy=300 MPa; a) 15, b) 25, c)50, and d) 75% replacement

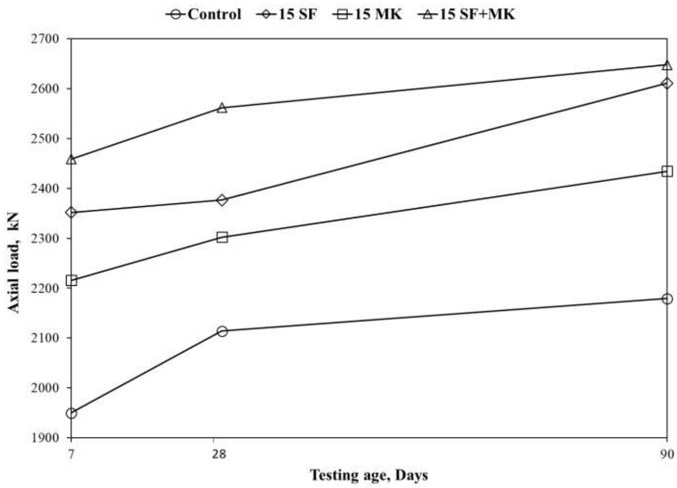
Control
15 SF
15 MK
15 SF+MK
Axial load, kN
Testing age, Days
2700
2600
2500
2400
2300
2200
2100
2000
1900
7
28
90

(a)

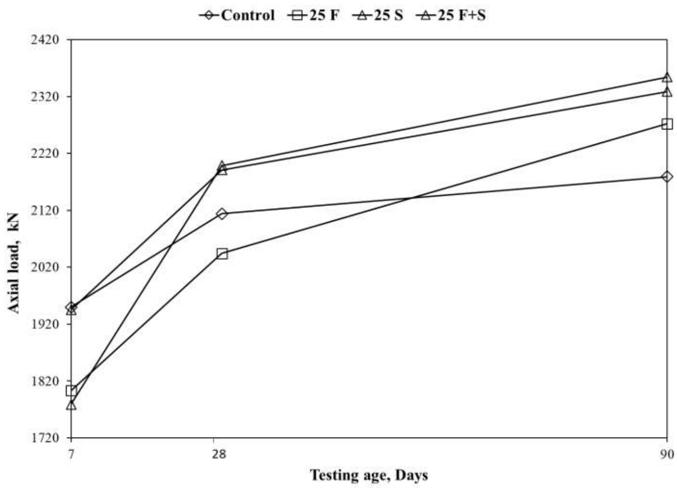
Control
25 F
25 S
25 F+S
Axial load, kN
Testing age, Days
2420
2320
2220
2120
2020
1920
1820
1720
7
28
90

(b)

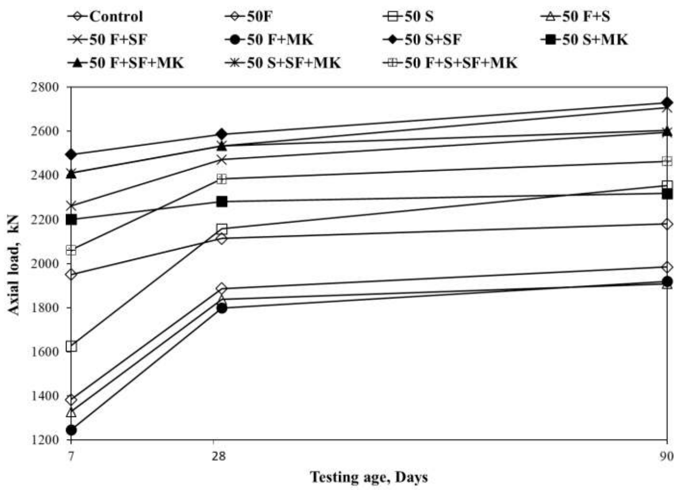
Control
50F
50 S
50 F+S
50 F+SF
50 F+MK
50 S+SF
50 S+MK
50 F+SF+MK
50 S+SF+MK
50 F+S+SF+MK
Axial load, kN
Testing age, Days
2800
2600
2400
2200
2000
1800
1600
1400
1200
7
28
90

(c)

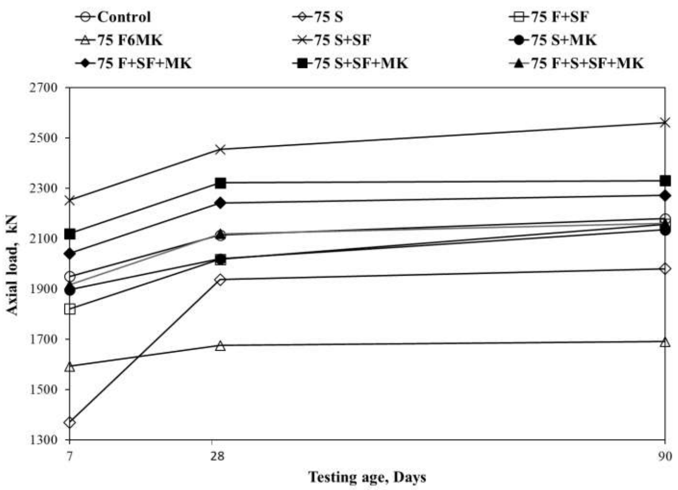

(d)

Figure 5.14. Ultimate axial load of the CFST column having UHPC based on ACI code for the case of D/t=65 and fy=450 MPa; a) 15, b) 25, c)50, and d) 75% replacement

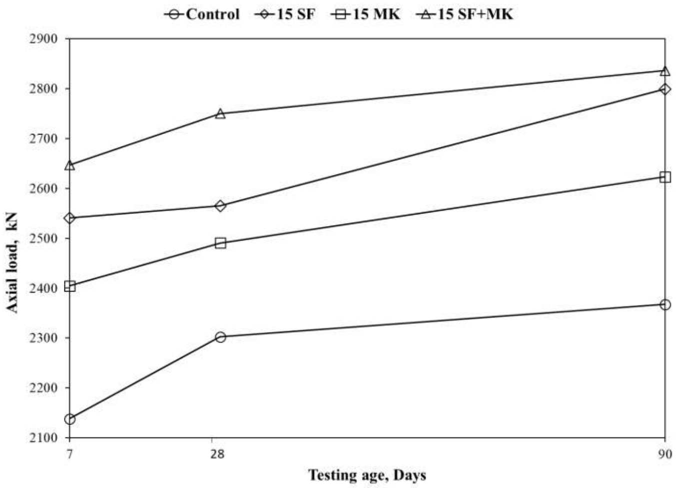

(a)

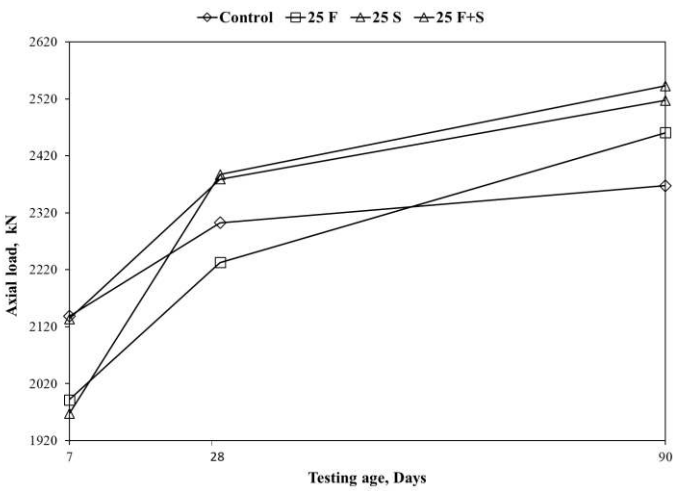

(b)

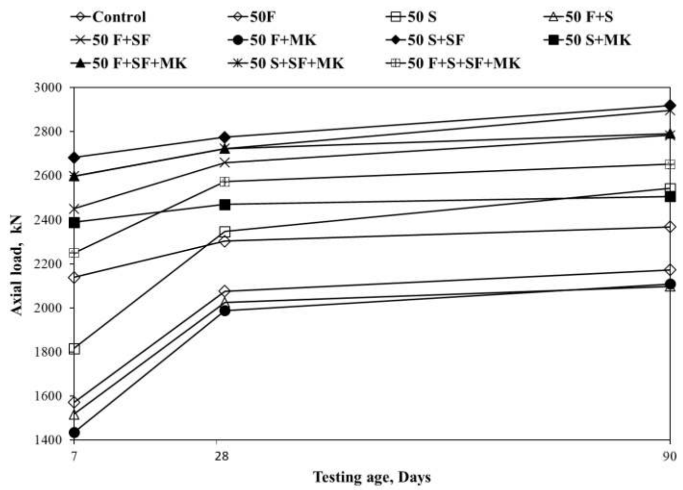

(c)

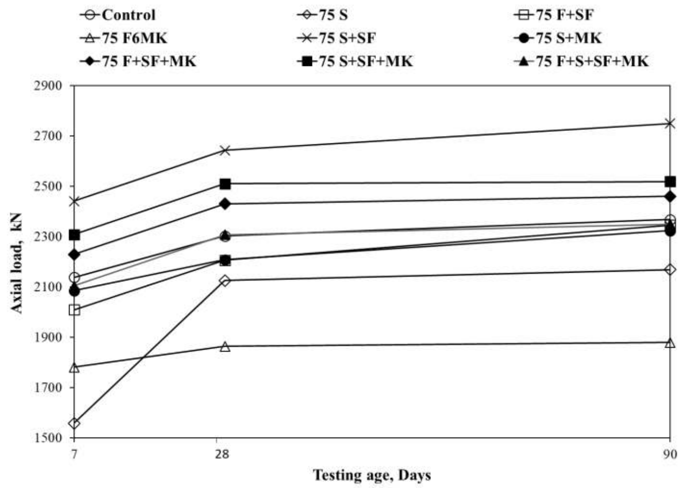

(d)

Figure 5.15. Ultimate axial load of the CFST column having UHPC based on ACI code for the case of D/t=65 and fy=600 MPa; a) 15, b) 25, c)50, and d) 75% replacement

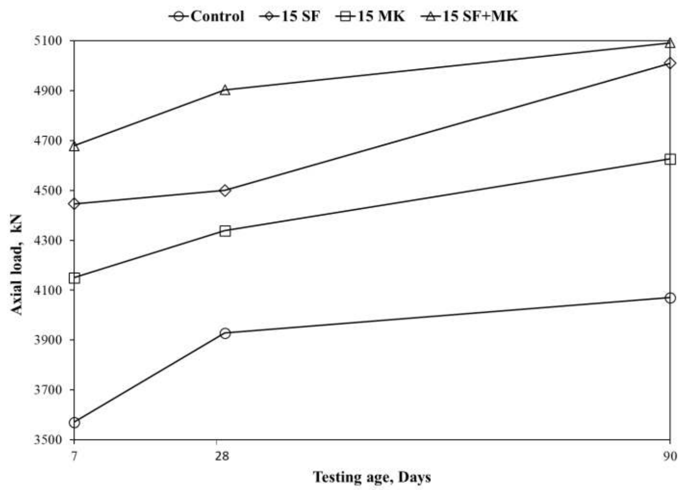

(a)

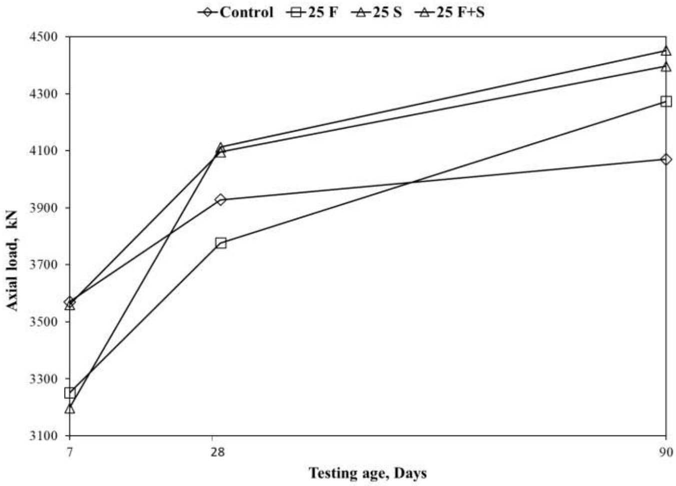

(b)

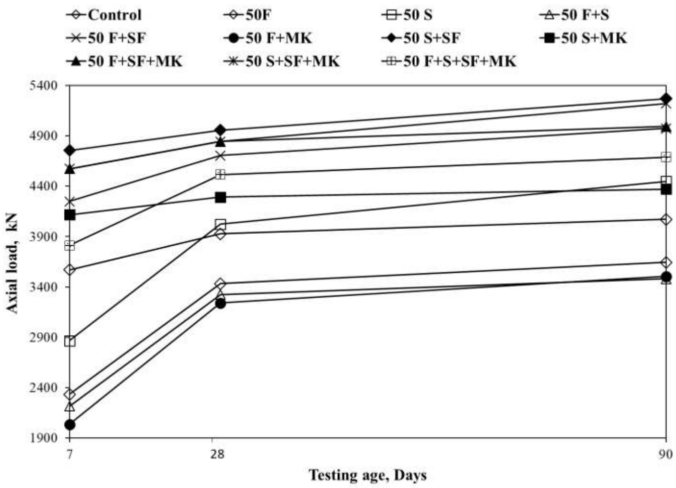

(c)

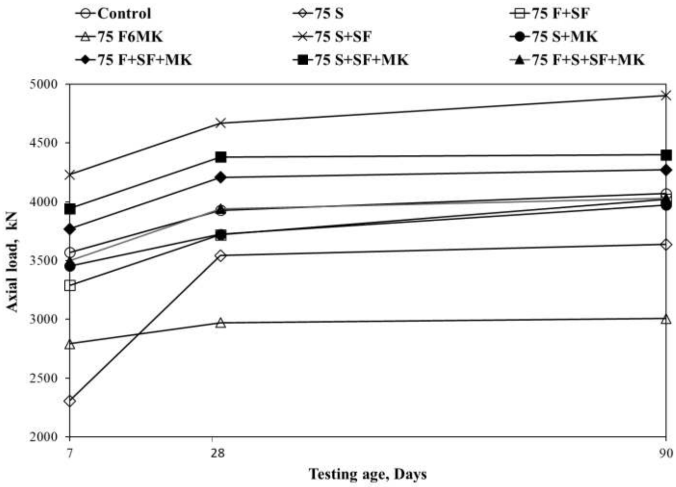

(d)

Figure 5.16. Ultimate axial load of the CFST column having UHPC based on ACI code for the case of D/t=95 and fy=300 MPa; a) 15, b) 25, c)50, and d) 75% replacement

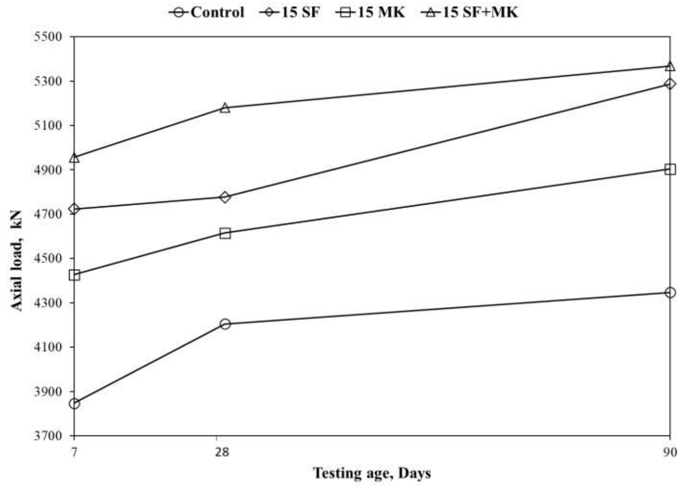
Control
15 SF
15 MK
15 SF+MK
Axial load, kN
Testing age, Days

(a)

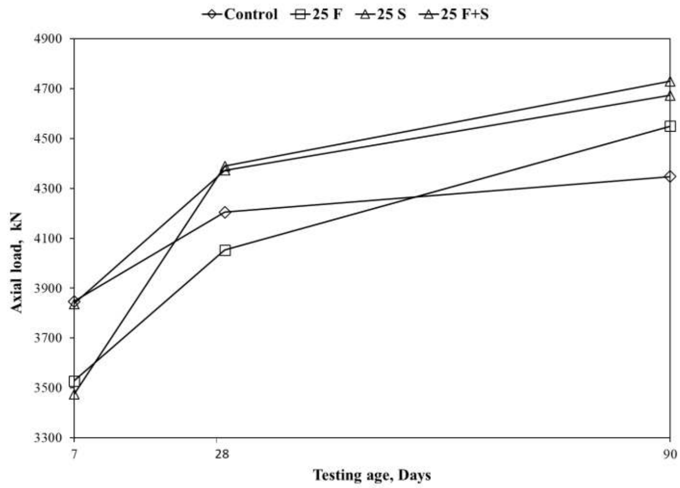
Control
25 F
25 S
25 F+S
Axial load, kN
Testing age, Days

(b)

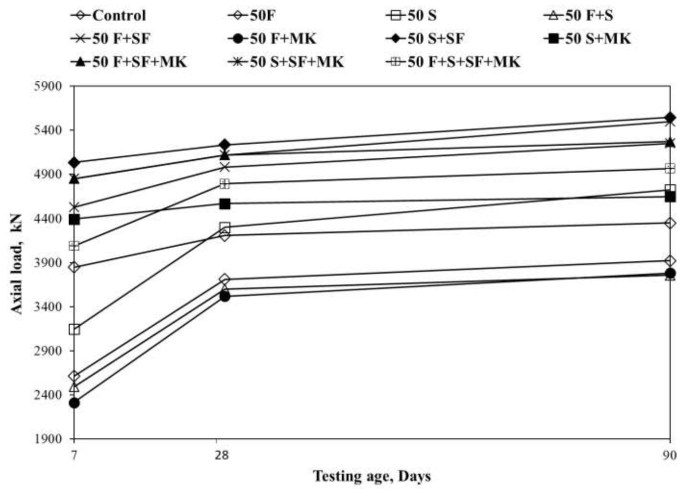
Control
50F
50 S
50 F+S
50 F+SF
50 F+MK
50 S+SF
50 S+MK
50 F+SF+MK
50 S+SF+MK
50 F+S+SF+MK
Axial load, kN
Testing age, Days

(c)

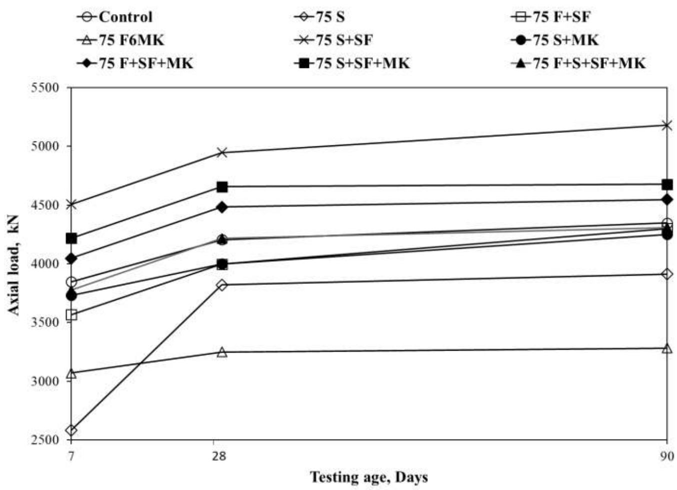

(d)

Figure 5.17. Ultimate axial load of the CFST column having UHPC based on ACI for the case of D/t=95 and fy=450 MPa; a) 15, b) 25, c)50, and d) 75% replacement

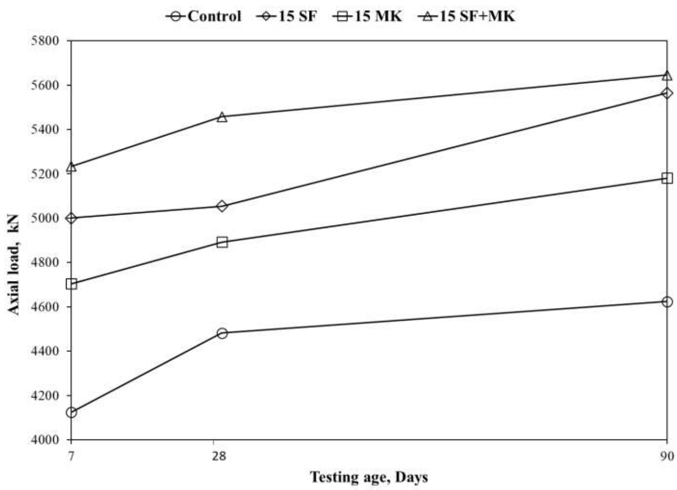

(a)

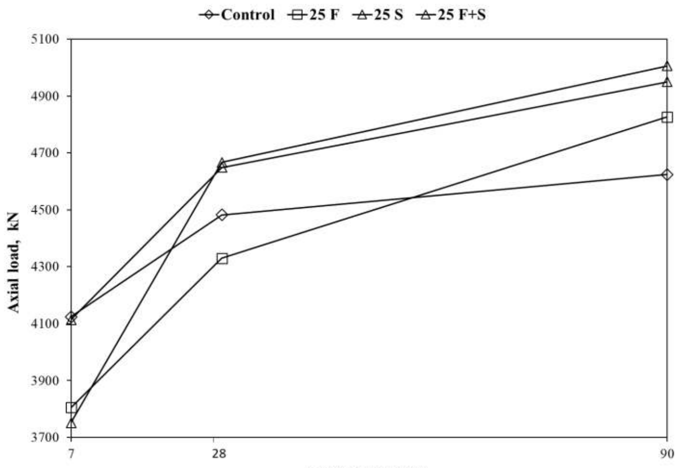

(b)

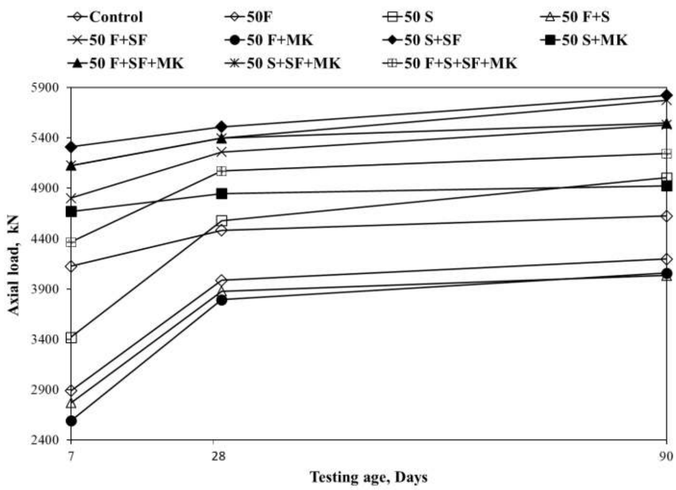

(c)

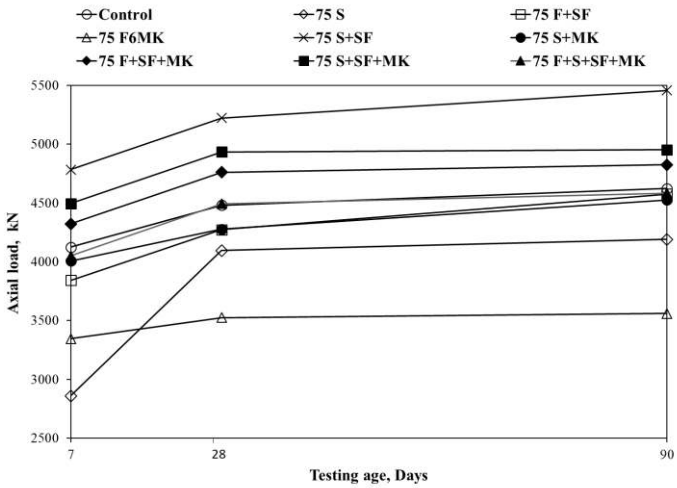

(d)

Figure 5.18. Ultimate axial load of the CFST column having UHPC based on ACI code for the case of D/t=95 and fy=600 MPa; a) 15, b) 25, c)50, and d) 75% replacement

5.1.3 DL/T Code

The theoretical ultimate load carrying capacity of CFST filled with UHPCs with different D/t ratios, and yield strength incorporated with 15%, 25%, 50% and 75% volume replacements of FA, S, SF and MK mineral admixture types are demonstrated in Figures of 5.19-5.21, 5.22-5.24, and 5.25-5.27, respectively. The behavior herein was considered similar to that seen in the previous codes. The minimum ultimate load carrying capacity was observed in Figure 5.15d that for 7 days of testing age when D/t ratio is set as 35 and yield stress is 300 MPa, specifically for the concrete contained 75% pozzolanic materials. The test results recommended using mineral admixture replacement like SF, MK, and S more than FA as a binary replacement, respectively.

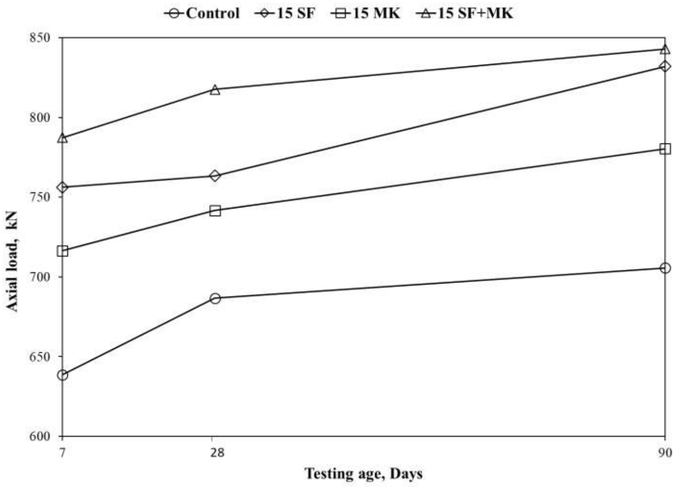

(a)

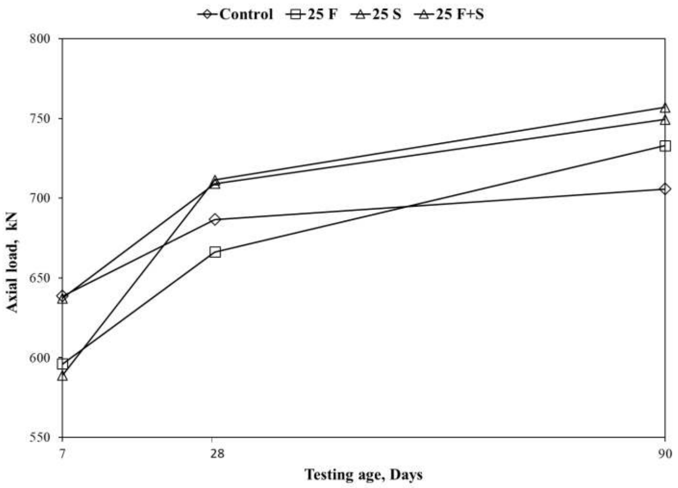

(b)

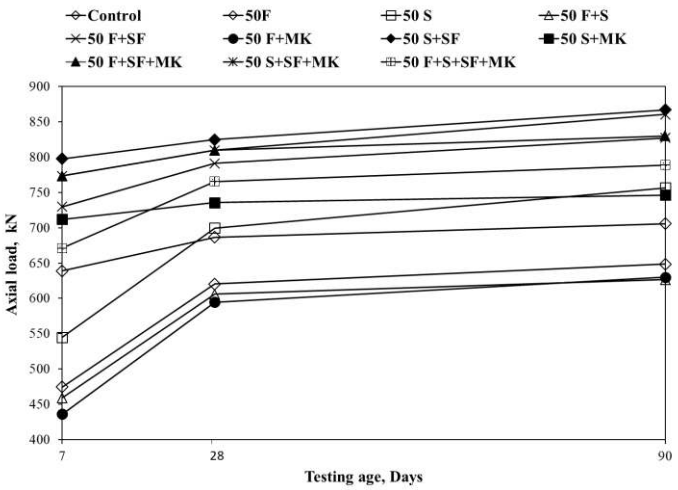

(c)

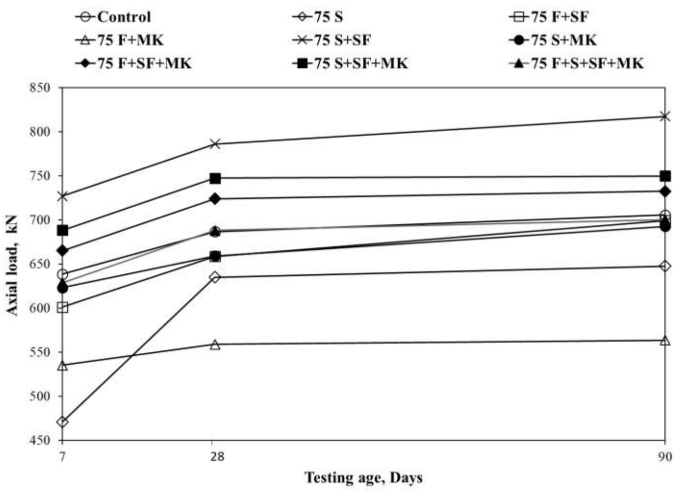

(d)

Figure 5.19. Ultimate axial load of the CFST column having UHPC based on DL/T code for the case of D/t=35 and fy=300 MPa; a) 15, b) 25, c)50, and d) 75% replacement

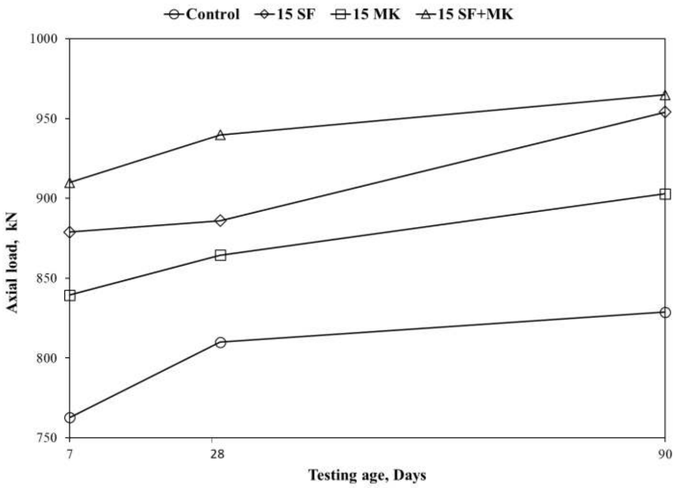

(a)

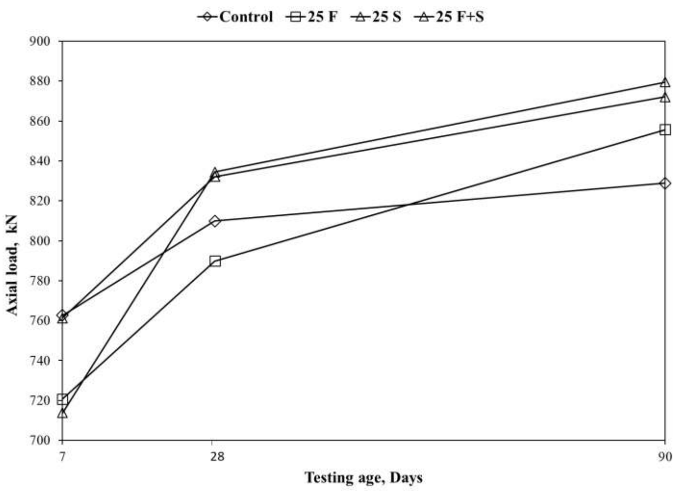

(b)

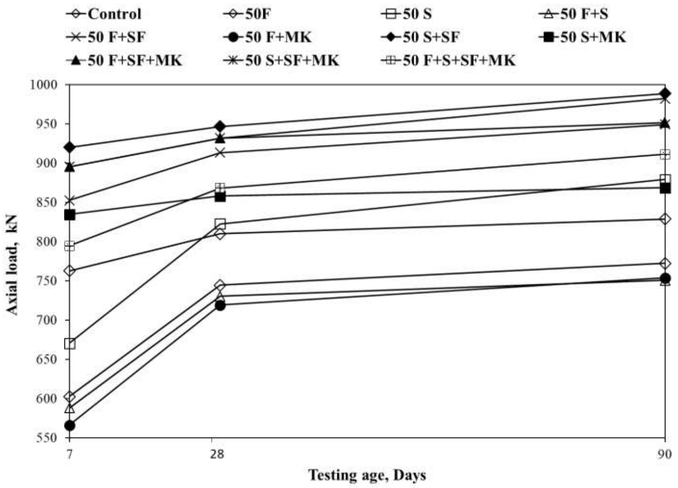

(c)

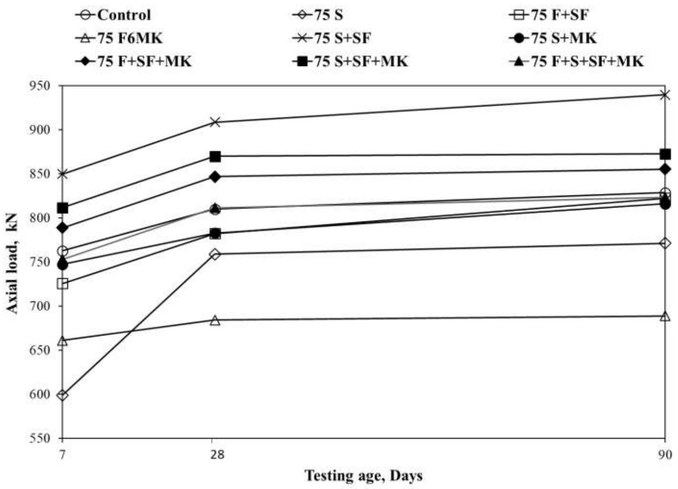

(d)

Figure 5.20. Ultimate axial load of the CFST column having UHPC based on DL/T code for the case of D/t=35 and fy=450 MPa; a) 15, b) 25, c)50, and d) 75% replacement

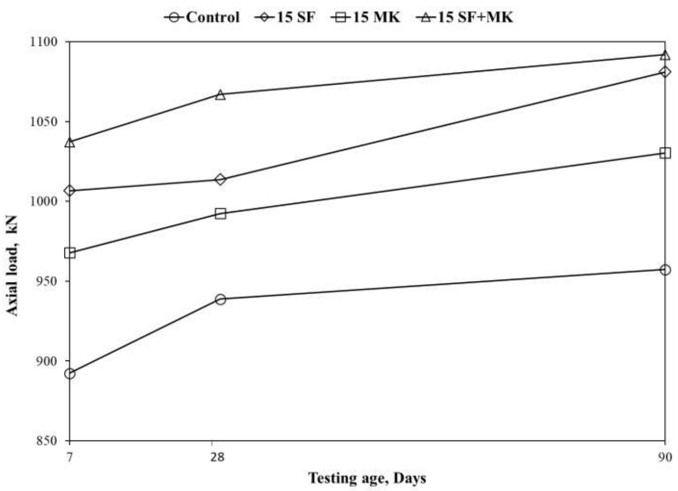

(a)

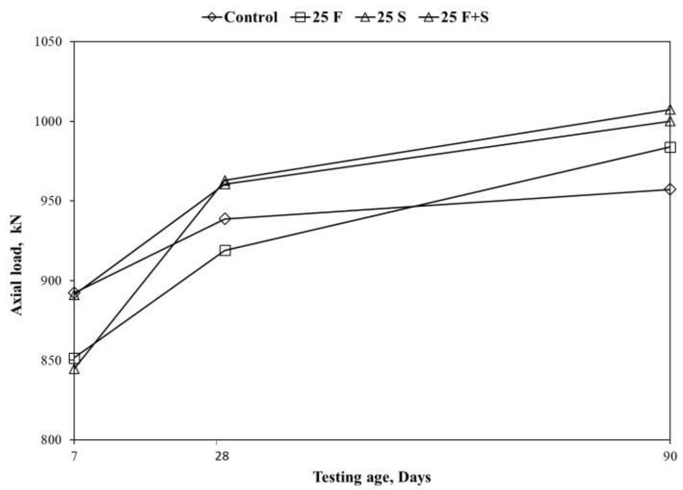

(b)

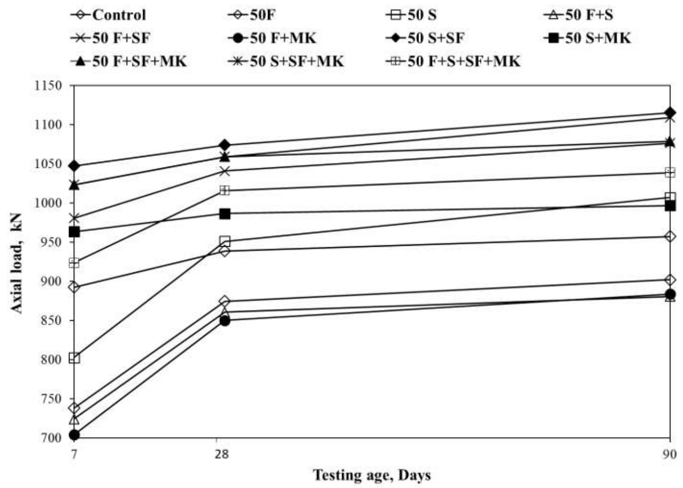

(c)

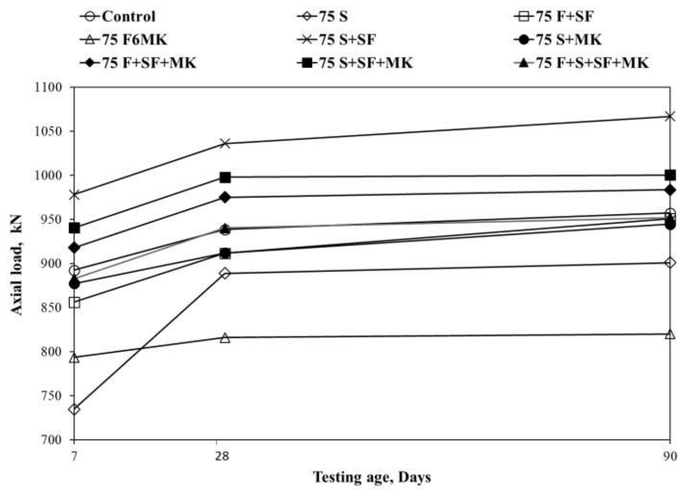

(d)

Figure 5.21. Ultimate axial load of the CFST column having UHPC based on DL/T code at different testing ages for the case of D/t=35 and fy=600 MPa; a) 15, b) 25, c)50, and d) 75% replacement

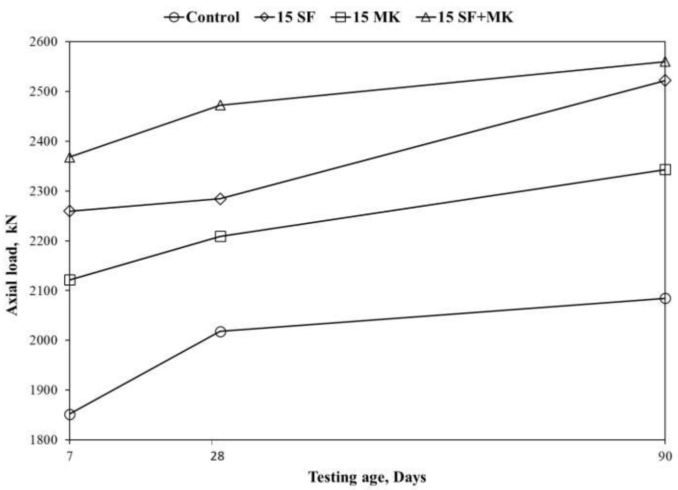

Control
15 SF
15 MK
15 SF+MK
Axial load, kN
Testing age, Days

(a)

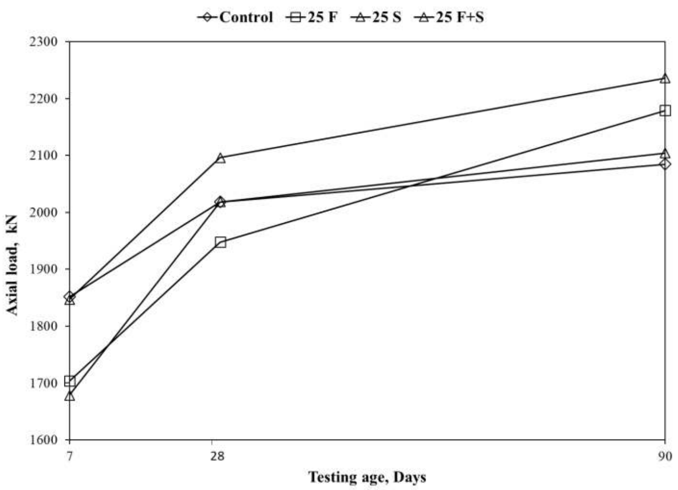

Control
25 F
25 S
25 F+S
Axial load, kN
Testing age, Days

(b)

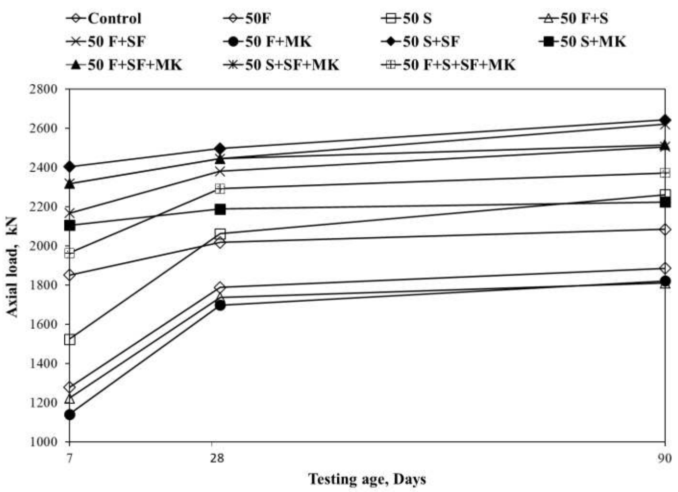

Control
50F
50 S
50 F+S
50 F+SF
50 F+MK
50 S+SF
50 S+MK
50 F+SF+MK
50 S+SF+MK
50 F+S+SF+MK
Axial load, kN
Testing age, Days

(c)

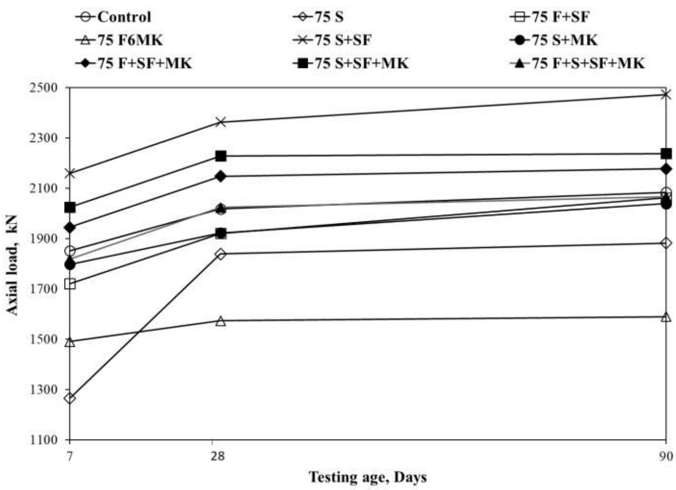

(d)

Figure 5.22. Ultimate axial load of the CFST column having UHPC based on DL/T code for the case of D/t=65 and fy=300 MPa; a) 15, b) 25, c)50, and d) 75% replacement

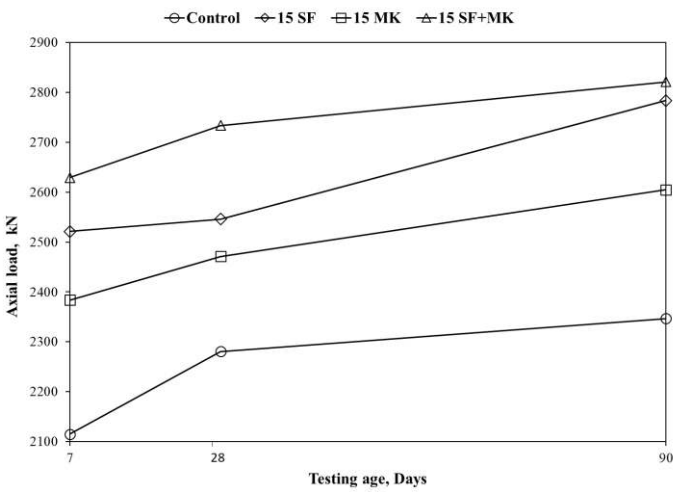

(a)

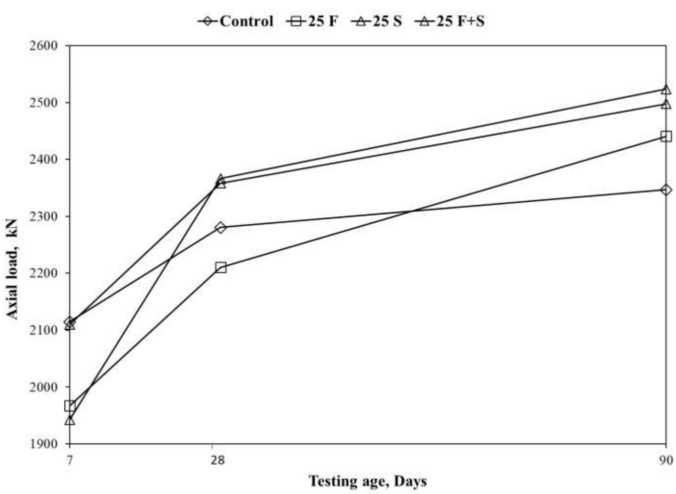

(b)

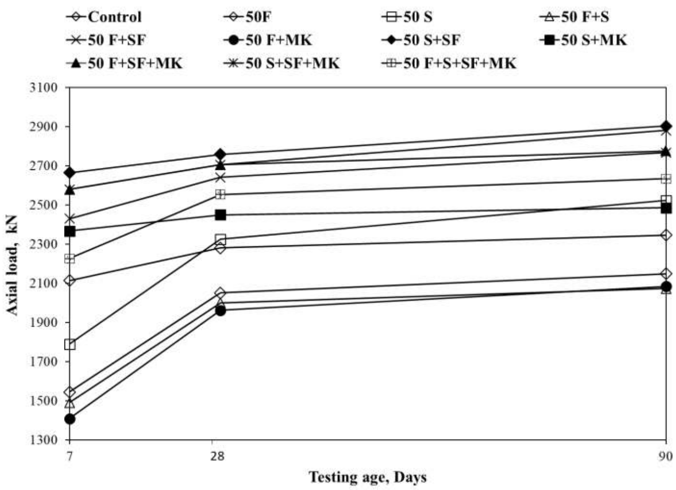

(c)

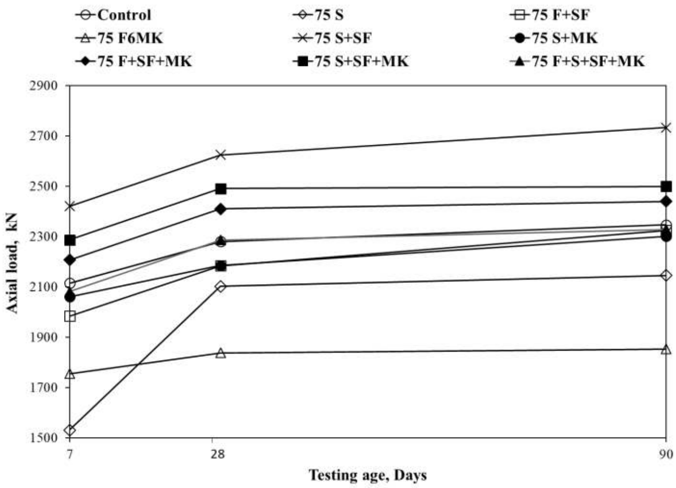

(d)

Figure 5.23. Ultimate axial load of the CFST column having UHPC based on DL/T code for the case of D/t=65 and fy=450 MPa; a) 15, b) 25, c)50, and d) 75% replacement

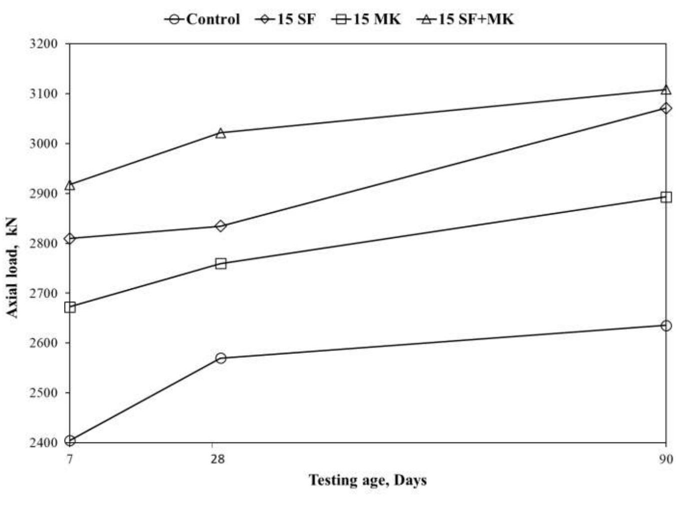

(a)

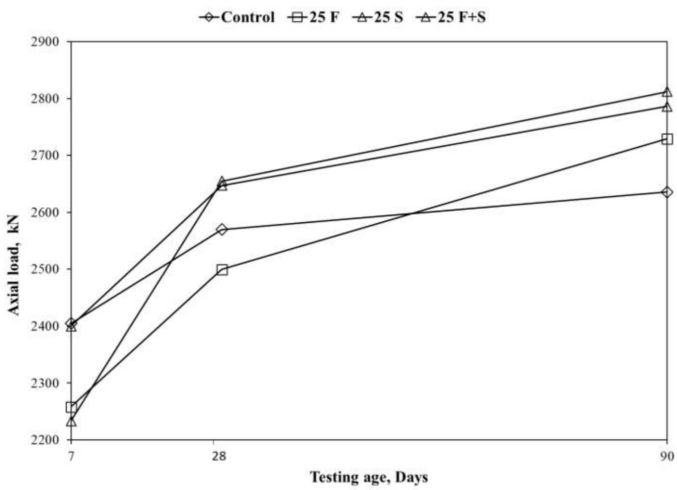

(b)

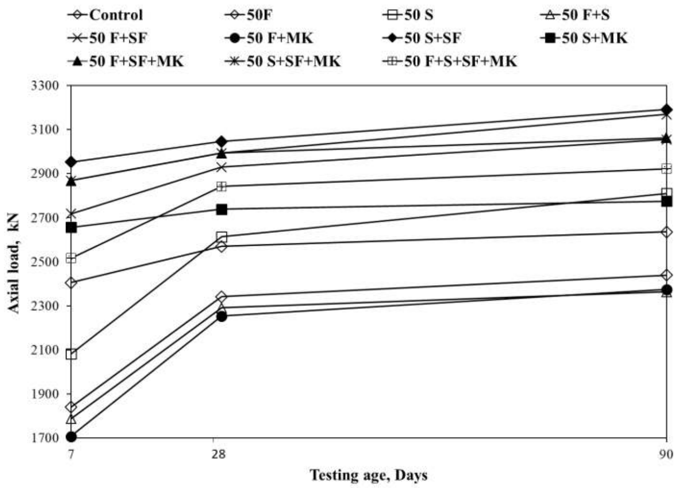

(c)

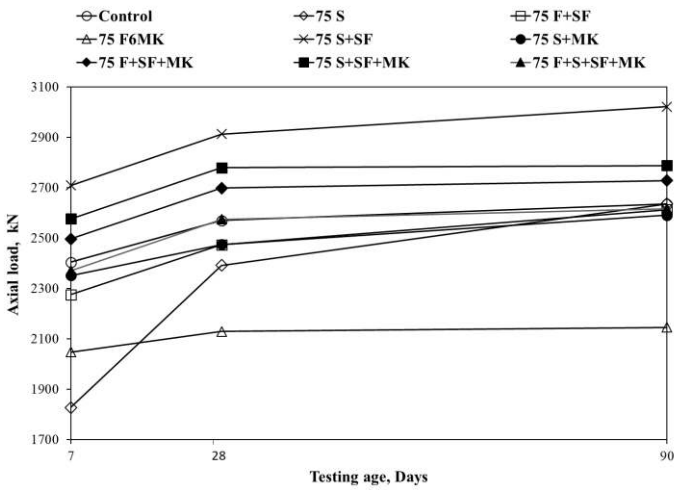

(d)

Figure 5.24. Ultimate axial load of the CFST column having UHPC based on DL/T code for the case of D/t=65 and fy=600 MPa; a) 15, b) 25, c)50, and d) 75% replacement

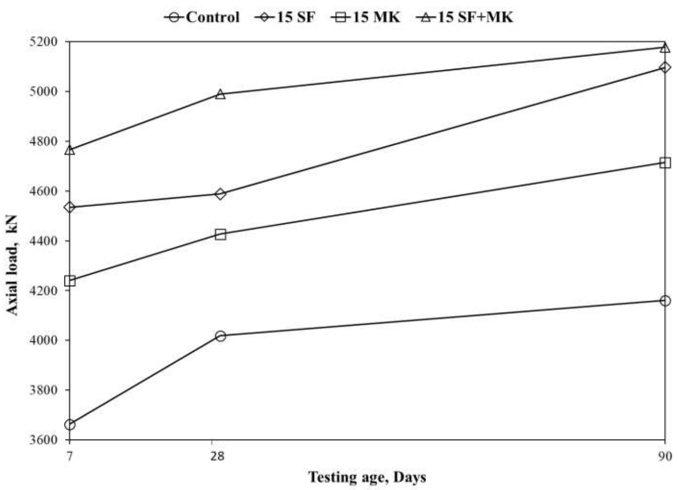
Control
15 SF
15 MK
15 SF+MK
Axial load, kN
Testing age, Days
5200
5000
4800
4600
4400
4200
4000
3800
3600
7
28
90

(a)

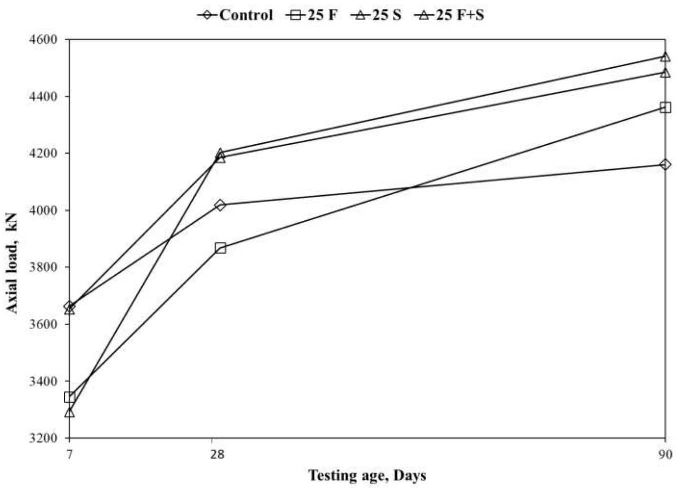
Control
25 F
25 S
25 F+S
Axial load, kN
Testing age, Days
4600
4400
4200
4000
3800
3600
3400
3200
7
28
90

(b)

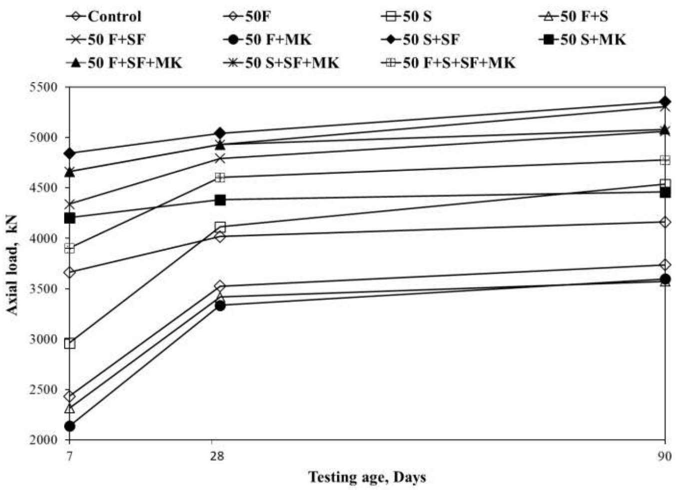
Control
50F
50 S
50 F+S
50 F+SF
50 F+MK
50 S+SF
50 S+MK
50 F+SF+MK
50 S+SF+MK
50 F+S+SF+MK
Axial load, kN
Testing age, Days
5500
5000
4500
4000
3500
3000
2500
2000
7
28
90

(c)

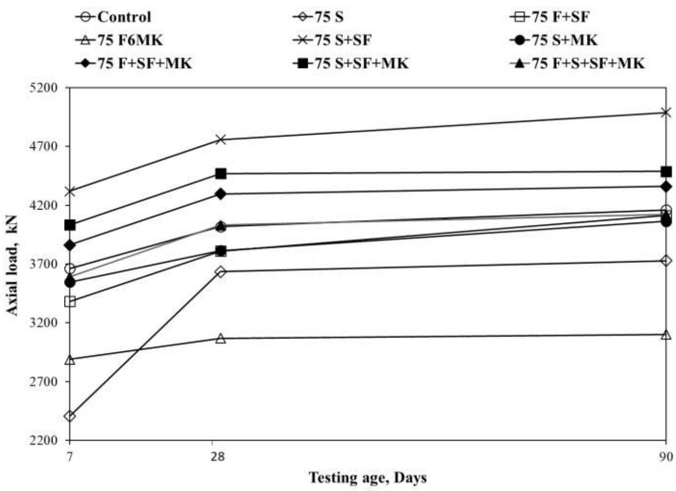

(d)

Figure 5.25. Ultimate axial load of the CFST column having UHPC based on DL/T code for the case of D/t=95 and fy=300 MPa; a) 15, b) 25, c)50, and d) 75% replacement

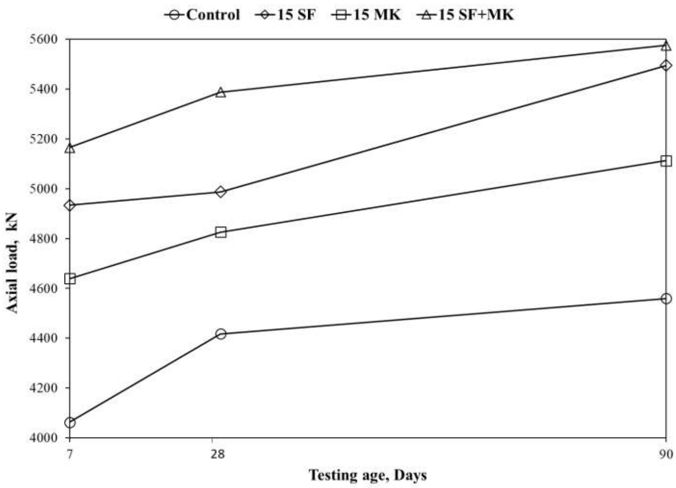

(a)

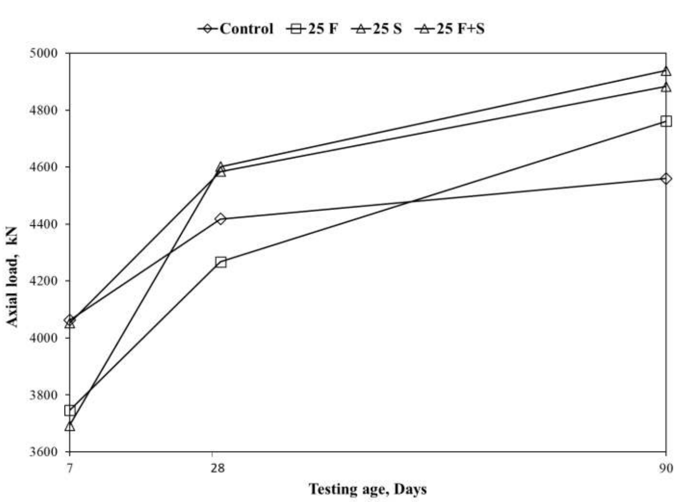

(b)

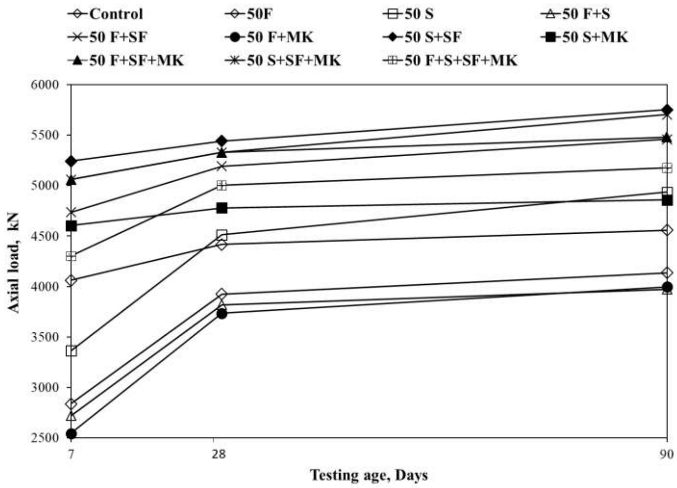

(c)

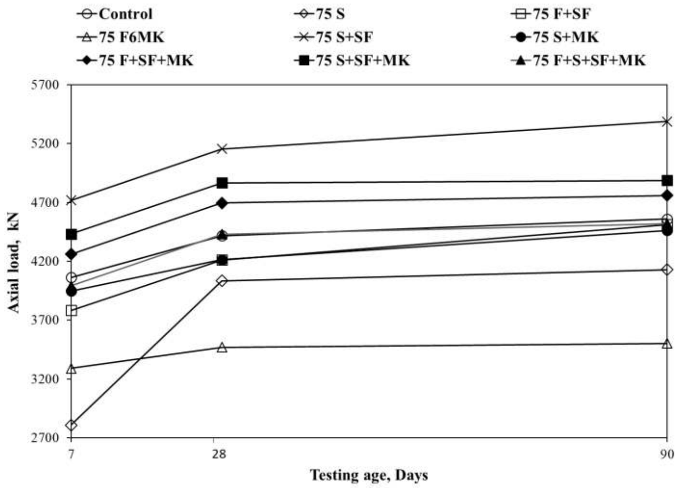

(d)

Figure 5.26. Ultimate axial load of the CFST column having UHPC based on DL/T code for the case of D/t=95 and fy=450 MPa; a) 15, b) 25, c)50, and d) 75% replacement

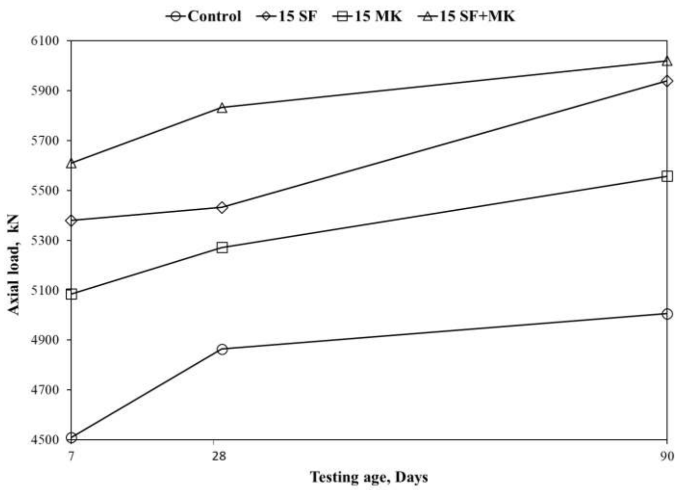

(a)

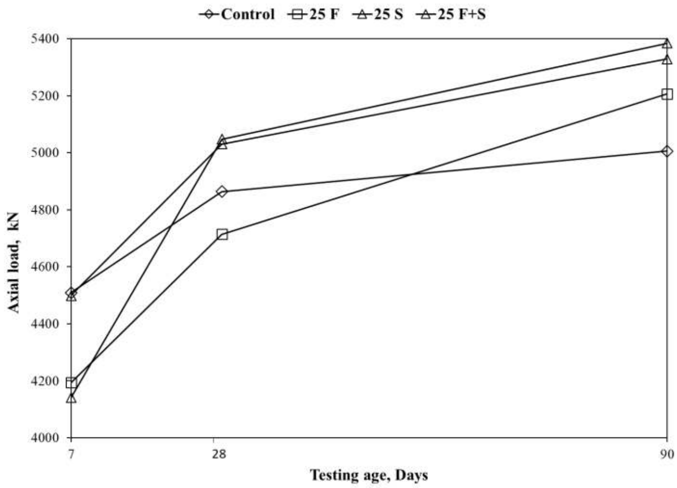

(b)

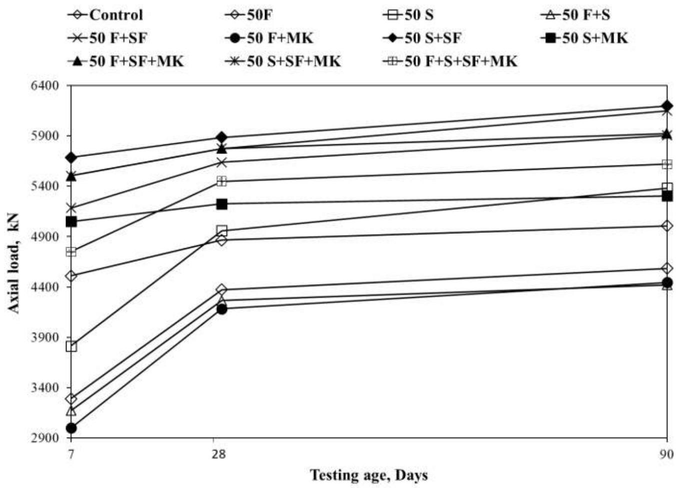

(c)

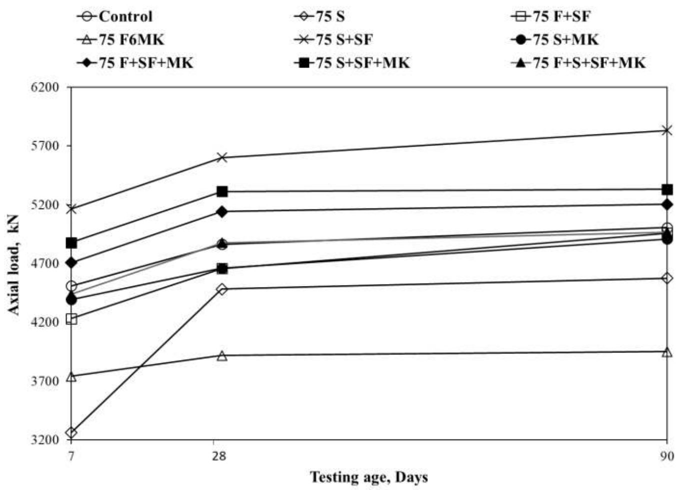

(d)

Figure 5.27. Ultimate axial load of the CFST column having UHPC based on DL/T code for the case of D/t=95 and fy=600 MPa; a) 15, b) 25, c)50, and d) 75% replacement

5.2 Effect of D/t Ratio on Capacity of CFST Columns

Effects of water cured at the ages of 7, 28 and 90 days on the axial load capacity of CSFT circular columns filled with HPFRC are presented in Figures 5.28, 5.29 and 5.30, respectively. Moreover, the subfigures of a, b and c donated the effect of three values of D/t (35, 65, and 95) versus on the results that obtained the equations from EC4, ACI and DL/T codes, correspondingly. From aforementioned figures, with increasing D/t from 35 to 95 the axial load capacity value of EC4 recorded the highest value followed by DL/t then ACI for all concrete ages. Regardless of the ages, the increment ratio of 95 D/t had some disparity of the results while with any decreasing D/t value, the axial load capacity samples approached to each other as obviously seen at 35 of D/t. Furthermore, the growth of the results after 28 days appeared to be quite restricted as there was little improvement observed at 90 days, irrespective of codes. Such phenomenon was perhaps due to the quickening of finishing chemical reactions of replaced mineral admixtures. Consequently, the favorite bigger diameter of CSFT columns is maybe due to that the same amount of axial load distributed over bigger cross section area.

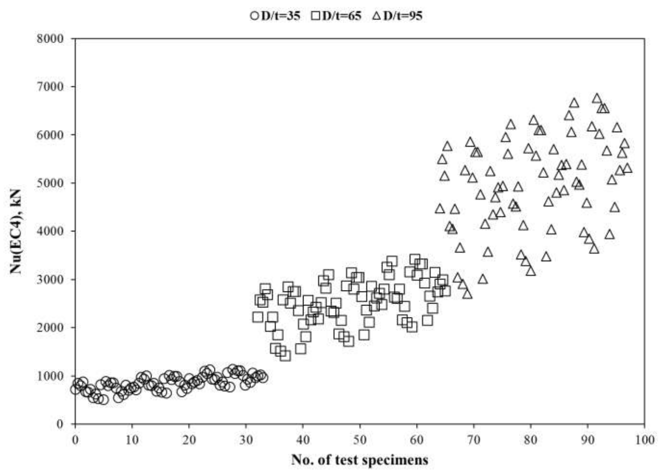

(a)

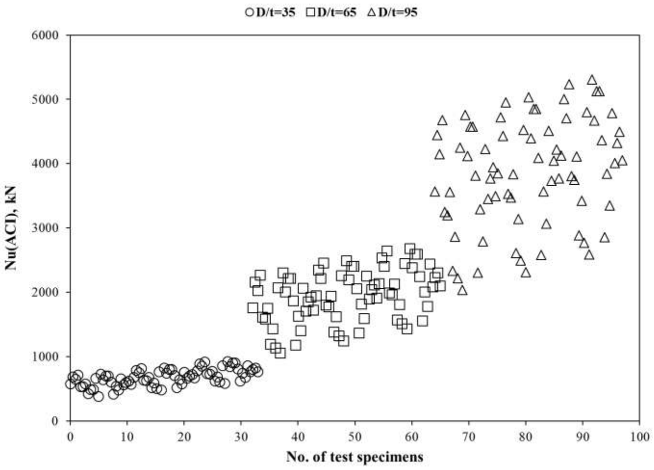

(b)

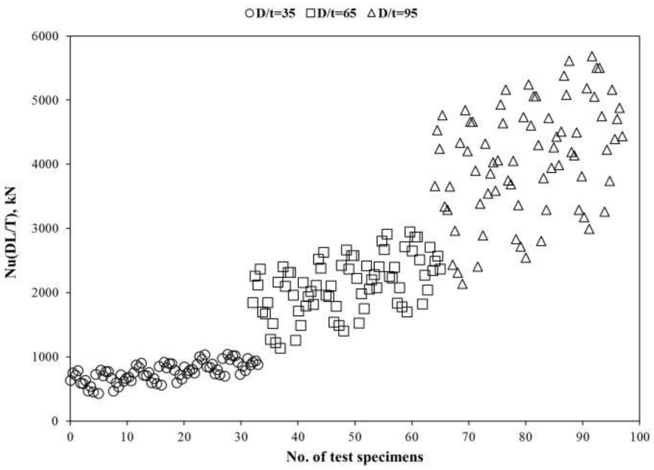

(c)

Figure 5.28. Effect of D/t ratio of the ultimate capacity of the composite columns tested at 7 days for different design codes

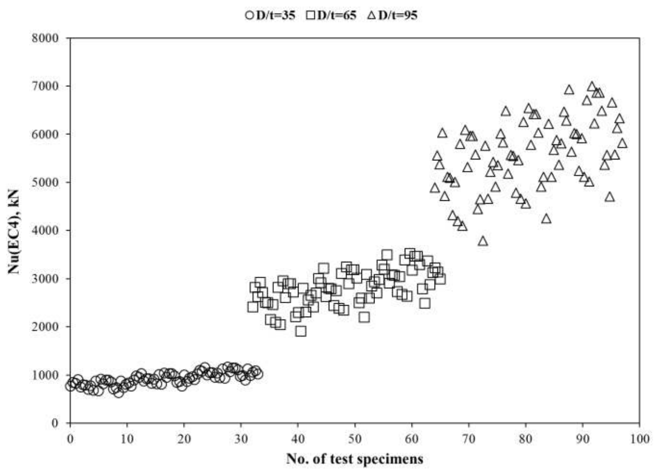

(a)

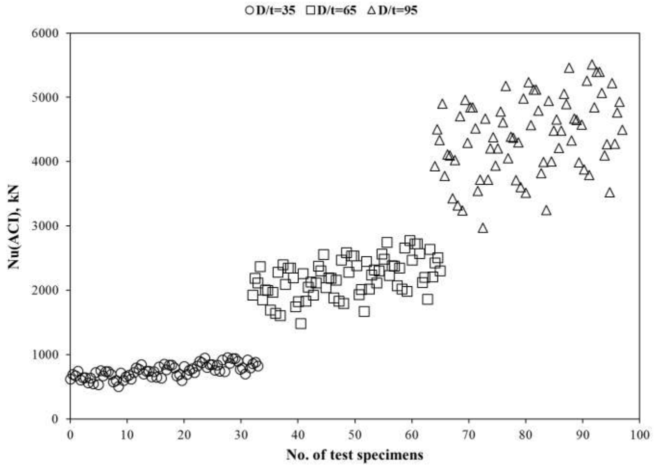

(b)

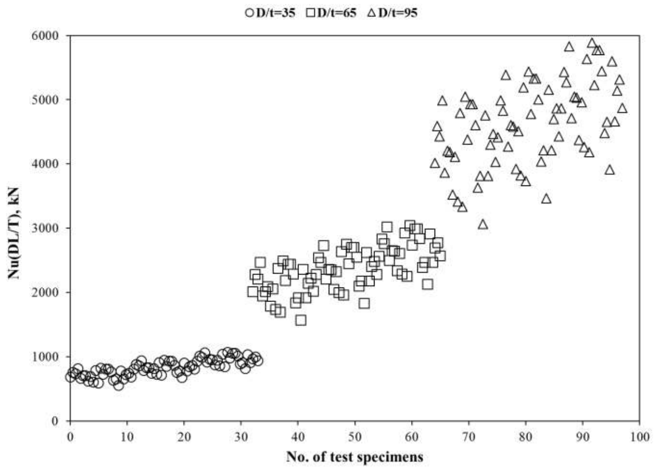

(c)

Figure 5.29. Effect of D/t ratio of the ultimate capacity of the composite columns tested at 28 days for different design codes

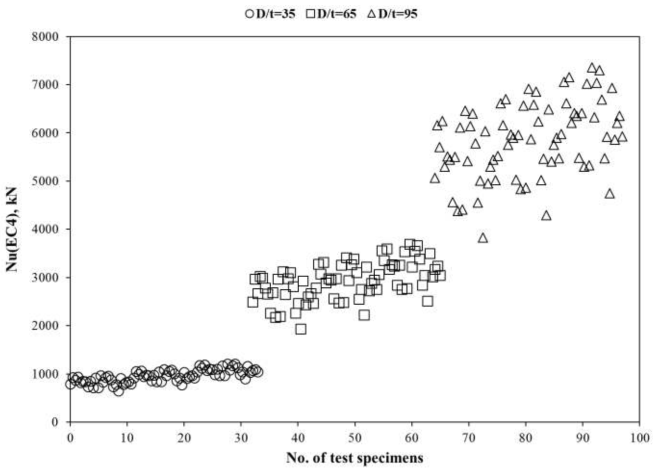

(a)

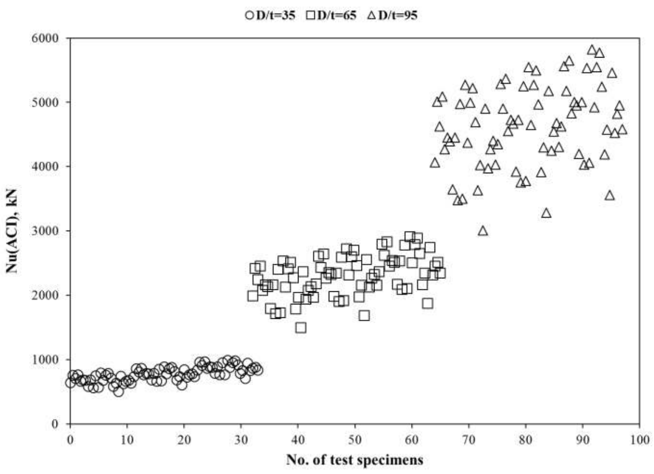

(b)

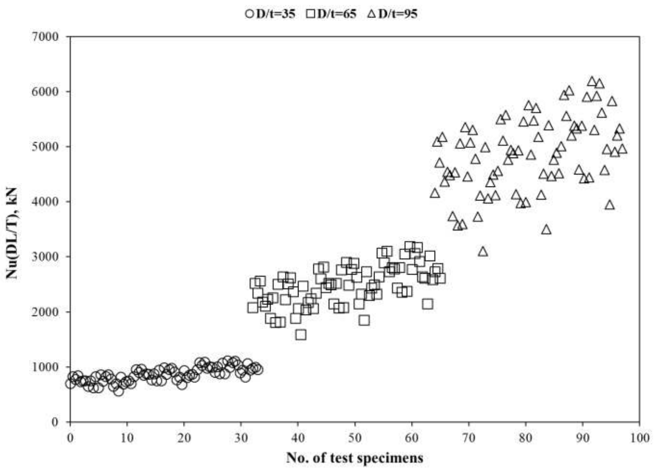

(c)

Figure 5.30. Effect of D/t ratio of the ultimate capacity of the composite columns tested at 90 days for different design codes

5.3 Correlation Between EC4 and Others

In order to examine the effectiveness of the existing formulation codes, Euro Code (EC4) was used as a reference to compare the results of the other codes. Thus, Figures 5.31 and 5.32 have been drawn all data which show the scatter EC4 versus the other codes for 7, 28, and 90 days of water cured, respectively. From aforementioned figures, it's clear that DL/T closer to EC4 than ACI with a bisector line of y=1.26x and y=1.19x, correspondingly, at 90 days. This behavior may have related to numbers of parameters and factors. For example, ACI code depended on four elements on the calculation of axial strength for composite columns, but EC4 and DL/T based on many other factors (see equations in Section 3.3). The trend of findings agreed with plenty of previous literature stressing the trend of CFST columns [94, 128-131].

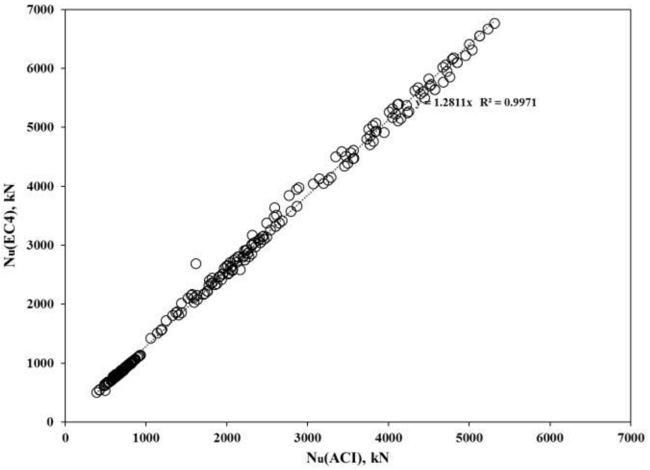

(a)

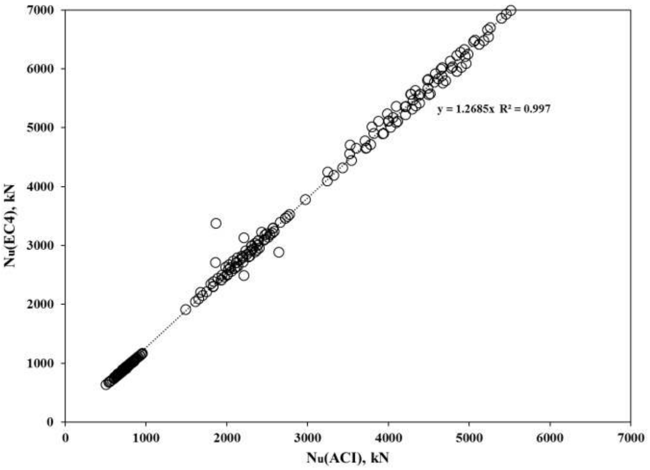

(b)

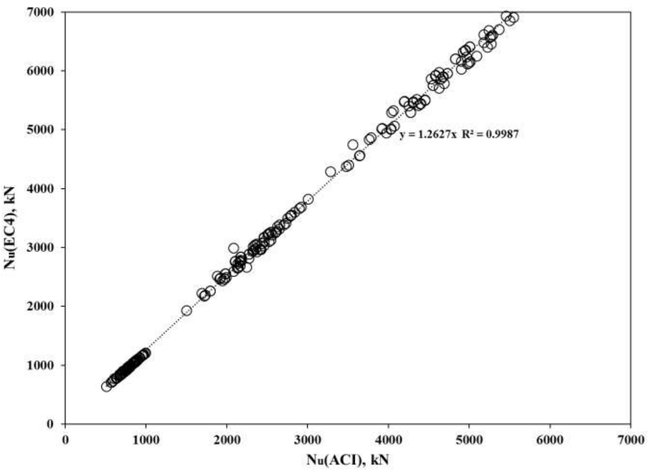

(c)

Figure 5.31. Correlation between EC4 and ACI to predict the capacity of composite columns with UHPC: a) 7 b) 28 and c) 90 days of testing age

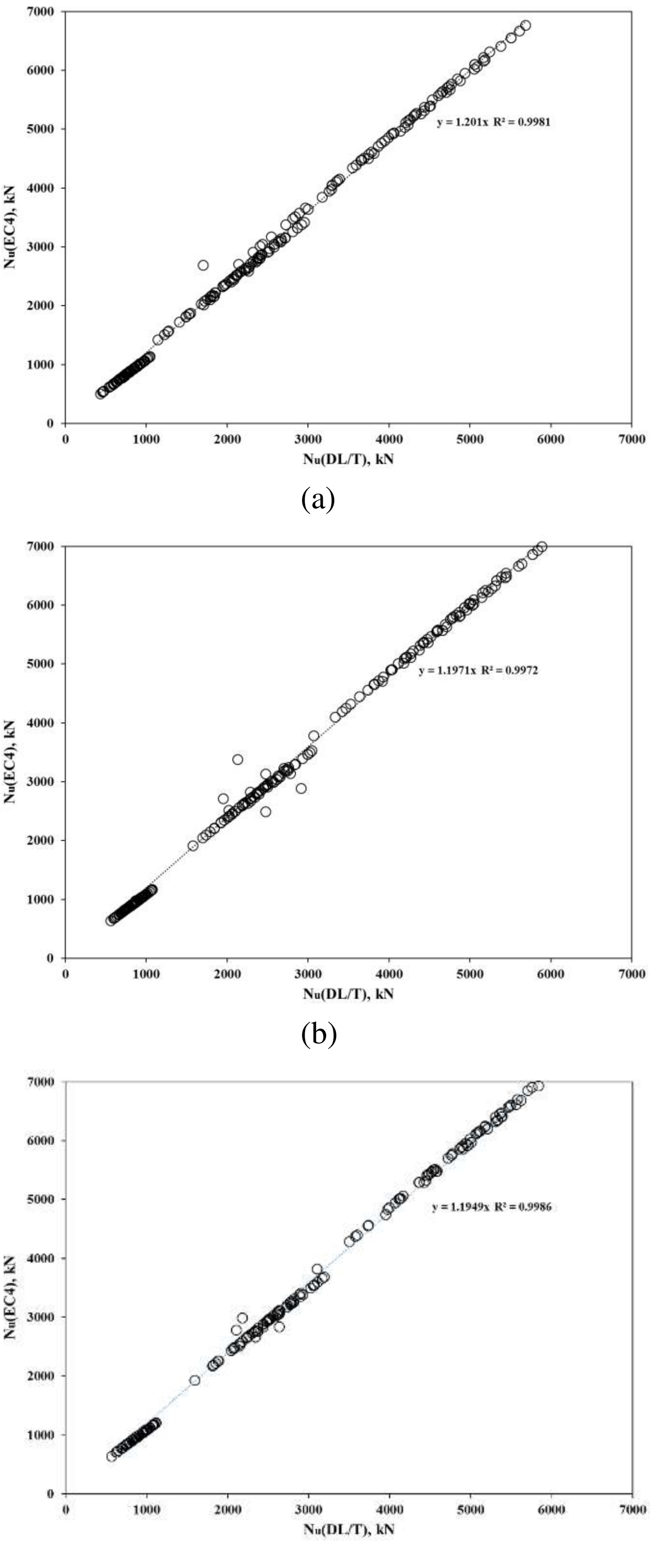

(a)

(b)

(c)

Figure 5.32. Correlation between EC4 and DL/T to predict the capacity of composite columns with UHPC: a) 7 b) 28 and c) 90 days of testing age

CHAPTER 6

SUMMARY AND CONCLUSION

The following conclusions were drawn based on the findings of this study:

1. It is obvious that the results of steam curing were much better than corresponding water curing for all cases of replacing amounts and mixing systems. Thus, it is recommended to cure UHPC by steam method nor standard curing.
2. The test results showed that the mineral admixtures like SF and MK more beneficial than S and then FA on increasing the results. However, despite of their results, using high volumes of S and FA materials served the environmental issues as they listed as disposal materials according to LEED organization. Furthermore, it seems like there is a limit demand point for mineral admixtures inside UHPC, after that any other replacement will be on behalf of cement, which has the most cementitious properties.
3. There is a critical point between using cement and the other mineral admixtures, and it seems look like using more than 50% of mineral admixtures undesirable. Unless designing mixtures for the aim of solving an environmental issue by utilizing high volumes of disposal materials like FA and S is ethical.
4. It can be concluded that mineral admixtures different with each other on effecting on the strength results which the most active is SF then followed respectively by each of MK, S, and FA. The replacement levels undesirable for using mineral admixtures more than 25% for FA, and 50% of S because the results of compressive strength were less than the control mixture. While mixing mineral admixtures in the form of multi-blended systems have the decrease an adverse effect of using high volumes.
5. Comparing to the control concrete, there were slightly decreased in the tensile strength results in a contribution of 50% of FA and somewhat higher values for 50% of S replacement. Furthermore, a binary combination of FA+ S showed better performance than only S or FA replacement. Whereas, the mixtures contain 75% of SF with MK and/or S kept the UHPC general limitations, regardless to lower all results than the control mixture.

6. It was observed that the effect of using 15 and 25% of mineral admixtures resulted of increment of the results, comparing to control mixture. While, despite declining the results at 50 % and 70% but the elastic moduli for the mixtures were near or higher than the control mixture for the former and the most mixture results within the range of UHPC limitations for the latter.
7. At replacement levels of 25, and 50, comparing to their corresponding control mixtures, the maximum enhancements of the flexural strength were belonging to the mixtures of FA+S, and S+SF+MK with 10.7 and 6 % for water curing and 18.3, 7 % for steam curing, correspondingly. On the other hand, related to the 75 % replacements, all mixtures recorded lower results than the control mixtures, but the mixture of 30%FA+30%S+7.5%SF+7.5%MK had the highest results than the others.
8. The load-displacement curves for the beam incorporating with SF and MK demonstrated a steady drop in load carrying capacity after the peak load, compared to the steeper drop in the mixtures with FA and S. On the other hand, it was observed that the UHPC with SF provided the highest fracture energy followed by MK, S, and FA, respectively.
9. According to the test results, the quaternary effect of mineral admixtures, i.e. cement+S+SF+NK, provided the most brittleness concrete despite of better results of the ternary effects, i.e. cement+SF+MK, in the most mechanical properties.
10. It was observed that the ultimate axial load of concretes continuously increased with growing ages of HPFRC from 7 to 90 days. However, the growth of the results after 28 up to 90 days seemed to be quite limited for mineral replacement of 50% and 75% then there were more enhancements at 15% and 25%. On the other hand, the axial load capacity of the columns infilled with HPFRC directly improved with all increases in yield strength and diameter of the steel tube.
11. The lower axial load capacity results of 75% replacement of some mineral admixtures comparing to control mixtures gave a recommendation of up to 50% using pozzolanic materials. According to the results, replacing of mineral admixtures to UHPC is some complex and sensitive depending on their amount and whether binary or ternary or, etc.
12. According to equations, at 90 days' age among different status of binary, ternary quaternary, and quinary of UHPCs incorporated with 15% SF+MK, 25% S, 50% S+SF and 75% S+F provides the highest axial load capacity which each value

donated as the maximum of the groups of 15, 25, 50, and 75% replacements, respectively. However, the minimum ultimate load carrying capacity was observed for 7 days of testing age when D/t ratio is set as 35 and yield stress is 300 Mpa, specifically for the concrete contained 75% pozzolanic materials.

13. With increasing D/t from 35 to 95, the axial load capacity value of EC4 recorded the highest value followed by DL/t then ACI for all concrete ages. Regardless of the ages, the increment ratio of 95 D/t had some disparity of the results while with any decreasing D/t value the axial load capacity samples approached to each other as obviously seen at 35 of D/t. furthermore, the growth of the results after 28 days appeared to be quite restricted as there was little improvement observed at 90 days, irrespective of codes.

14. From the test results, it's clear that DL/T closer to EC4 than ACI with a bisector line of y=1.26x and y=1.19x, correspondingly, at 90 days. This behavior may have related to numbers of parameters and factors. For example, ACI code depended on four elements on the calculation of axial strength for composite columns, but EC4 and DL/T based on many other factors.

REFERENCES

[1]. Gohil Gaurav, P. and Raval, A. (2016). Experimental Study used of SCMs on Engineering Properties of Reactive Powder Concrete. *Journal of Civil Engineering and Environmental Technology*. **3**: p. 75-77

[2]. Mahmoud, K. (2009), Mechanical Properties of Ultra High Performance Concrete Produced in Gaza Strip. *The Islamic University of Gaza, High Studies Deanery, Faculty of Engineering Civil Engineering Department Design and Rehabilitation of Structures*.p. 20-22.

[3]. Ahlborn, T.M., Peuse, E.J., and Misson, D.L. (2008), high-performance-concrete for michigan bridges material performance–phase I. *Michigan Tech Transportation Institute*. p. 931-1295.

[4]. Yunsheng, Z. (2008). Preparation of C200 green reactive powder concrete and its static–dynamic behaviors. *Cement and Concrete Composites*. **30**(9): p. 831-838.

[5]. Ambika, D. and Sivaraja, M. (2016). A study on mechanical properties of various mineral admixtures used in reactive powder concrete. *Int J Adv Engg Tech/Vol. VII/Issue II/April-June*. **567**: p. 570.

[6]. Buitelaar, P. (2000), Heavy reinforced ultra high performance concrete. in *Proceedings of the Int. Symp. on UHPC, Kassel, Germany*.p. 40-42.

[7]. Hajar, Z. (1999), Design and construction of the world first high performance concrete road bridges. in *Proceedings of the Int. Symp. on UHPC, Kassel, Germany*.p.15-16.

[8]. Acker, P. and Behloul, M. (2001), Ductal® technology: A large spectrum of properties, a wide range of applications. in *Proc. of the Int. Symp. on UHPC Kassel, Germany*.p. 30-32.

[9]. Korpa, A., Kowald, T., and Trettin, R. (2014). Principles of Development, Phase Composition and Nanostructural Features of Multiscale Ultra High Performance Concrete Modified with Pyrogenic Nanoparticles–A Review Article. *American Journal of Materials Science and Application*. **2**(2): p. 17.

[10]. Darshika Shah, M.N.P.,.Vakil, M.D (June 2014). Parametric study of concrete filled steel tube column. *International Journal of Engineering Development and Research (IJEDR)*. **Volume.2**(Issue 2): p. pp.1678-1682.

[11]. Fam, A., Qie, F.S., and Rizkalla, S. (2004). Concrete-filled steel tubes subjected to axial compression and lateral cyclic loads. *Journal of Structural Engineering*. **130**(4): p. 631-640.

[12]. Lim, J. and Nethercot, D. (2004). Stiffness prediction for bolted moment-connections between cold-formed steel members. *Journal of Constructional Steel Research*. **60**(1): p. 85-107.

[13]. Schneider, S.P., Kramer, D.R., and Sarkkinen, D.L. (2002), The design and construction of concrete-filled steel tube column frames. in *13th World Conference on Earthquake Engineering, Vancouver, BC, Canada*.p. 50-52.

[14]. Taranath, B. (1998), Steel, concrete, and composite design of tall buildings. 1998: *McGraw-Hill Professional*.p. 12-13.

[15]. Denarié, E., Bruhwiler, E., and Znidaric, A. (2005). Full scale application of UHPFRC for the rehabilitation of bridges-from the lab to the field. *5th FWP/SAMARISSustainable and Advanced Material for Road Infrastructures*. P. 50-52.

[16]. Richard, P. and Cheyrezy, M. (1995). Composition of reactive powder concretes. *Cement and concrete research*. **25**(7): p. 1501-1511.

[17]. Evirgen, B., Tuncan, A., and Taskin, K. (2014). Structural behavior of concrete filled steel tubular sections (CFT/CFSt) under axial compression. *Thin-Walled Structures*. **80**: p. 46-56.

[18]. Gardner, N.J. and Jacobson, E.R. (2015), Structural behavior of concrete filled steel tubes. in *Journal Proceedings*. P.12.

[19]. Shakir-Khalil, H. and Zeghiche, J. (1989). Experimental behaviour of concrete-filled rolled rectangular hollow-section columns. *Structural Engineer*. **67**: p. 346-53.

[20]. de Oliveira, W.L.A. (2009). Influence of concrete strength and length/diameter on the axial capacity of CFT columns. *Journal of Constructional Steel Research*. **65**(12): p. 2103-2110.

[21]. Bukovsk, P. and Karmazínov, M. (2012). Behaviour of the tubular columns filled by concrete subjected to buckling compression. *Procedia Engineering*. **40**: p. 68-73.

[22]. Uy, B. (2008). Stability and ductility of high performance steel sections with concrete infill. *Journal of Constructional Steel Research*. **64**(7): p. 748-754.

[23]. Liew, J.R., Xiong, M., and Xiong, D. (2015), Design of Concrete Filled Tubular Beam-columns with High Strength Steel and Concrete. in *Structures*. Elsevier.p.35-36.

[24]. Schmidt, M. and Fehling, E. (2016), high-performance concrete: research, development and application in Europe. in *7th International Symposium on the Utilization of High-Strength and High-Performance-Concrete, ACI Washington*. p.45-47.

[25]. Dattatreya, J., Harish, K., and Neelamegam, M. (2007). Use of particle packing theory for the development of reactive powder concrete. *The Indian Concrete Journal*. **81**(1): p. 31-45.

[26]. Plawsky, J. (2003). Exploring the effect of dry premixing of sand and cement on the mechanical properties of mortar. *Cement and Concrete Research*. **33**(2): p. 255-264.

[27]. Staquet, S. and Espion, B. (2015), Influence of cement and silica fume type on compressive strength of reactive powder concrete. in *6thInt. Symp. on High Strength/High Performance Concrete*.p. 55-56.

[28]. Blais, P.Y. and Couture, M. (1999). Precast, prestressed pedestrian bridge: World's first Reactive Powder Concrete structure. *PCI journal*. **44**(5): p. 60-71.

[29]. Mindess, S., Young, J.F., and Darwin, D. (2003), Concrete 2nd Edition. *Upper Saddle River, NJ: Pearson Education, Inc*.p. 15-16.

[30]. Monteiro, P. (2006), Concrete: Microstructure, Properties, and Materials. 2006: *McGraw-Hill Publishing*.p. 45-46.

[31]. Kowald, T. and Trettin, R. (2015), Influence of surface-modified carbon nanotubes on ultrahigh performance concrete. in *Proceedings of International Symposium on Ultra High Performance Concrete*.p. 23-24.

[32]. Almansour, H. and Lounus, Z. (2000), Structural Performance of Precast Pre-stressed Bridge Girders Built with Ultra High Performance Concrete. in *Institute for Research in Construction. The Second International Symposium on Ultra High Performance Concrete*.p. 45-46.

[33]. Hoang, K. (2015), Influence of types of steel fiber on properties of ultra high performance concrete. in *The 3rd AFC International Conference ACG/VCA*.p. 23-24.

[34]. Orgass, M. and Klug, Y. (2014), Fibre-reinforced high strength concretes. in *International Symposium on Ultra High Performance Concrete, Kessel Germany*.p. 23-24.

[35]. Jungwirth, J. and Muttoni, A. (2013), Structural behavior of tension members in Ultra High Performance Concrete. in *International symposium on ultra high performance concrete*. International Symposium on Ultra High Performance Concrete.p. 30-31.

[36]. Rossi, P. (2001). High Performance Fiber-Reinforced Concretes. *Concrete international*. **23**(12): p. 46-52.

[37]. Bonneau, O. (1997). Mechanical properties and durability of two industrial reactive powder concretes. *ACI Materials journal*. **94**(4): p. 286-290.

[38]. Rong, Z., Sun, W., and Zhang, Y. (2010). Dynamic compression behavior of high performance cement based composites. *International Journal of Impact Engineering*. **37**(5): p. 515-520.

[39]. Habel, K., Denarié, E., and Brühwiler, E. (2006). Structural response of elements combining ultrahigh-performance fiber-reinforced concretes and reinforced concrete. *Journal of Structural Engineering*. **132**(11): p. 1793-1800.

[40]. Redaelli, D. (2013), Testing of reinforced high performance fibre concrete members in tension. in *Proceedings of the 6th Int. Ph. D. Symposium in Civil Engineering, Zurich 2006*. Proceedings of the 6th Int. Ph. D. Symposium in Civil Engineering, Zurich 2006.p.23-24.

[41]. Jungwirth, J. and Muttoni, A. (2012), Structural use of high performance fiber reinforced concrete. in *FRC in Switzerland: research, applications and perspectives, Conference: FRC-from theory to practice*. FRC in Switzerland: research, applications and perspectives, Conference: FRC-from theory to practice.p. 33-34.

[42]. Reineck, K.-H. and Greiner, S. (2014), Tests on high performance fibre reinforced concrete designing hot-water tanks and UHPFRC-shells. in *Proceedings of the International Symposium on High Performance Concrete, Kassel, Germany*.p. 12-13.

[43]. Teutsch, M. and Grunert, J. (2015), Bending design of steel-fibre-strengthened UHPC. in *Schmidt, M.; Fehling, E.; Geisenhanslüke, C.(Hg.): Proceedings of the International Symposium on Ultra High Performance Concrete (UHPC)*.p. 23-24.

[44]. Dubey, A. and Banthia, N. (1998). Influence of high-reactivity metakaolin and silica fume on the flexural toughness of high-performance steel fiber-reinforced concrete. *ACI Materials Journal*. **95**: p. 284-292.

[45]. LEE, N.P.a.C., D.H. (2005). Reactive. Powder Concrete, Study Report No. 146. *Building Research Levy, New Zealand*: p. pp. 1-29.

[46]. Yaakoub, S.P. (2010). Behavior of Reactive Powder Concrete Beam in Bending. *Ph.D. thesis, University of Technology,Baghdad*.p. 36-37.

[47]. Plank, J. (2009). Effectiveness of polycarboxylate superplasticizers in high strength concrete: the importance of PCE compatibility with silica fume. *Journal of Advanced Concrete Technology*. **7**(1): p. 5-12.

[48]. Collepardi, S. (1997). Mechanical properties of modified reactive powder concrete. *ACI Special Publications*. **173**: p. 1-22.

[49]. Rougeau, P. and Borys, B. (2012), Ultra high performance concrete with ultrafine particles other than silica fume. in *Ultra high performance concrete (UHPC). International symposium on ultra high performance concrete*.p. 40-41.

[50]. Yazici, H. (2007). The effect of curing conditions on compressive strength of ultra high strength concrete with high volume mineral admixtures. *Building and environment*. **42**(5): p. 2083-2089.

[51]. Li, Z. and Ding, Z. (2003). Property improvement of Portland cement by incorporating with metakaolin and slag. *Cement and Concrete Research*. **33**(4): p. 579-584.

[52]. Thomas, M. (1999). Use of ternary cementitious systems containing silica fume and fly ash in concrete. *Cement and concrete research*. **29**(8): p. 1207-1214.

[53]. Popovics, S. (1993). Portland cement-fly ash-silica fume systems in concrete. *Advanced Cement Based Materials*. **1**(2): p. 83-91.

[54]. Lam, L., Wong, Y., and Poon, C.-S. (1998). Effect of fly ash and silica fume on compressive and fracture behaviors of concrete. *Cement and Concrete Research*. **28**(2): p. 271-283.

[55]. Gonen, T. and Yazicioglu, S. (2007). The influence of mineral admixtures on the short and long-term performance of concrete. *Building and Environment*. **42**(8): p. 3080-3085.

[56]. Qian, X. and Li, Z. (2001). The relationships between stress and strain for high-performance concrete with metakaolin. *Cement and Concrete Research*. **31**(11): p. 1607-1611.

[57]. Schachinger, I. (2014), Effect of curing temperature at an early age on the long-term strength development of UHPC. in *2nd International Symposium on Ultra High Performance Concrete*.p. 20-21.

[58]. Khadiranaikar, R. and Muranal, S. (2012). TECHNOLOGY (IJCIET). *Journal Impact Factor*. **3**(2): p. 455-464.

[59]. Lin, W.T. (2008). Effect of steel fiber on the mechanical properties of cement-based composites containing silica fume. *Journal of Marine Science and Technology*. **16**(3): p. 214-221.

[60]. Liu, C.-T. and Huang, J.-S. (2008). Highly flowable reactive powder mortar as a repair material. *Construction and Building Materials*. **22**(6): p. 1043-1050.

[61]. Uzawa, M., Shimoyama, Y., and Koshikawa, S. (2005), Fresh and strength properties of new cementitious composite material using reactive powder. 2005: *Nihon University*.p. 31-32.

[62]. Lee, M.-G., Wang, Y.-C., and Chiu, C.-T. (2007). A preliminary study of reactive powder concrete as a new repair material. *Construction and building materials*. **21**(1): p. 182-189.

[63]. Ma J. (2012), Comparative investigations on high performance concrete with and without coarse aggregates. in *Proceedings of international symposium on ultra high performance concrete, Germany*.p. 22-23.

[64]. Donnaes, and Phillippenes (1998). Reactive Powder Concrete. Strengthens Structural Design Concrete products.**101 Issue 8**: p 66.

[65]. Graybeal, B.A. (2005), Characterization of the behavior of high performance concrete.p.11-12.

[66]. Voo, J.Y.L., Foster, D.S.J., and Gilbert, R. (2003), Shear strength of fibre reinforced reactive powder concrete girders without stirrups. 2003: *University of New South Wales, School of Civil and Environmental Engineering*.p. 15-16.

[67]. Kim, S. (2008). Development of ultra high performance concrete for hybrid stayed cable bridge. *Korea Institute of Construction Technology*.p. 23-24.

[68]. Fehling, E. (2005), Entwicklung, Dauerhaftigkeit und Berechnung hochfester Betone (UHPC)[Development, durability and design of high strength concrete (UHPC)]. *Research Report, University of Kassel, Structural Materials and Engineering, Kassel, Germany. Series*.p. 24-25.

[69]. Behloul, M. and Cheyrezy, M. (2002). Ductal reference projects. Presentation at Bouygues Headquarters *Challenger, St Quentin en Yveslines, France*.p.30-31.

[70]. Kollmorgen, G. (2004). Impact of Age and Size on the Mechanical Behavior of an High Performance Concrete. *Michigan Technological University*.p. 33-34.

[71]. Semioli, W.J. (2001). The New Concrete Technology. *Concrete International*. **Vol. 23, No. 11**: p. pp. 75–79.

[72]. Resplendino, J. and Petitjean, J. (2014), high-performance concrete: First recommendations and examples of application. in *Proceedings of the Third International Symposium on High Performance Concrete*.p. 12.
[73]. Brouwer, G. (2001). Bridge to the future. *Civil Engineering*. **71**(11): p. 50.
[74]. Searls, L.i. (2007). Wapello Bridge. *Lafarge North America*.p. 23.
[75]. Rebentrost, M. and Cavill, B. (2012), Reactive powder concrete bridges. in *austroads bridge conference, 6th, 2006, perth, western australia*.p. 15.
[76]. Knowles, R.B. and Park, R. (1969). Strength of concrete filled steel tubular columns. *Journal of the Structural Division, ASCE*. **12**: p. 2565–2587.
[77]. Knowles, R.B. and Park, R. (1970). Axial load design for concrete filled steel tubes. *Journal of the Structural Division*. **96**(10): p. 2125-2153.
[78]. O'Shea, M.D. and Bridge, R.Q. (1994). Tests of thin-walled concrete-filled steel tubes.p. 11.
[79]. Tomii, M., Yoshimura, K., and Morishita, Y. (2000), Experimental studies on concrete-filled steel tubular stub columns under concentric loading. in *Stability of Structures Under Static and Dynamic Loads:*. ASCE.p. 14.
[80]. Zhang, W. and Shahrooz, B.M. (1999). Comparison between ACI and AISC for concrete-filled tubular columns. *Journal of Structural Engineering*. **125**(11): p. 1213-1223.
[81]. Roeder, C.W., Cameron, B., and Brown, C.B. (1999). Composite action in concrete filled tubes. *Journal of structural engineering*. **125**(5): p. 477-484.
[82]. Sakino, K. (2004). Behavior of centrally loaded concrete-filled steel-tube short columns. *Journal of Structural Engineering*. **130**(2): p. 180-188.
[83]. Han, L.-H. and Yao, G.-H. (2003). Influence of concrete compaction on the strength of concrete-filled steel RHS columns. *Journal of Constructional Steel Research*. **59**(6): p. 751-767.
[84]. Johansson, M. (2002). The efficiency of passive confinement in CFT columns. *Steel and Composite Structures*. **2**(5): p. 379-396.
[85]. Dundu, M. (2012). Compressive strength of circular concrete filled steel tube columns. *Thin-Walled Structures*. **56**: p. 62-70.
[86]. Giakoumelis, G. and Lam, D. (2004). Axial capacity of circular concrete-filled tube columns. *Journal of Constructional Steel Research*. **60**(7): p. 1049-1068.
[87]. Vrcelj, Z. and Uy, B. (2002). Strength of slender concrete-filled steel box columns incorporating local buckling. *Journal of Constructional Steel Research*. **58**(2): p. 275-300.

[88]. Zeghiche, J. and Chaoui, K. (2005). An experimental behaviour of concrete-filled steel tubular columns. *Journal of Constructional Steel Research*. **61**(1): p. 53-66.

[89]. Hossain, K.M.A. (2003). Axial load behaviour of thin walled composite columns. *Composites Part B: Engineering*. **34**(8): p. 715-725.

[90]. Gupta, P., Sarda, S., and Kumar, M. (2007). Experimental and computational study of concrete filled steel tubular columns under axial loads. *Journal of Constructional Steel Research*. **63**(2): p. 182-193.

[91]. Lachemi, M., Hossain, K.M., and Lambros, V.B. (2006). Axial load behavior of self-consolidating concrete-filled steel tube columns in construction and service stages. *ACI structural journal*. **103**(1): p. 38.

[92]. Fujimoto, T. (2004). Behavior of eccentrically loaded concrete-filled steel tubular columns. *Journal of Structural Engineering*. **130**(2): p. 203-212.

[93]. Han, L.-H. and Yang, Y.-F. (2001). Influence of concrete compaction on the behavior of concrete filled steel tubes with rectangular sections. *Advances in Structural Engineering*. **4**(2): p. 93-100.

[94]. Han, L.-H. and Yao, G.-H. (2004). Experimental behaviour of thin-walled hollow structural steel (HSS) columns filled with self-consolidating concrete (SCC). *Thin-Walled Structures*. **42**(9): p. 1357-1377.

[95]. Yu, Q., Tao, Z., and Wu, Y.-X. (2008). Experimental behaviour of high performance concrete-filled steel tubular columns. *Thin-Walled Structures*. **46**(4): p. 362-370.

[96]. Schneider, S.P. (1998). Axially loaded concrete-filled steel tubes. *Journal of structural Engineering*. **124**(10): p. 1125-1138.

[97]. Khaloo, A. (2014). Mechanical performance of self-compacting concrete reinforced with steel fibers. *Construction and Building Materials*. **51**: p. 179-186.

[98]. El-Dieb, A.S. (2009). Mechanical, durability and microstructural characteristics of high-strength self-compacting concrete incorporating steel fibers. *Materials & Design*. **30**(10): p. 4286-4292.

[99]. El-Dieb, A. and Taha, M.R. (2012). Flow characteristics and acceptance criteria of fiber-reinforced self-compacted concrete (FR-SCC). *Construction and Building Materials*. **27**(1): p. 585-596.

[100]. Fava, C. (2014), Fracture behaviour of self-compacting concrete. in *Proceedings of the 3rd international RILEM symposium on self-compacting concrete. Reykjavik: RILEM Publications SARL*.p. 25.

[101]. Cattaneo, S., Giussani, F., and Mola, F. (2012). Flexural behaviour of reinforced, prestressed and composite self-consolidating concrete beams. *Construction and Building Materials*. **36**: p. 826-837.

[102]. EFNARC, F. (2002). Specification and guidelines for self-compacting concrete. *European 29 Federation of National Associations Representing producers and applicators of specialist 30 building products for Concrete (EFNARC)*. **32**: p. 31.

[103]. Saenz, L.P. (1964). Equation for the stress-strain curve of concrete. *ACIJour*. **61**(9): p. 1229-235.

[104]. Shanmugam, N. and Lakshmi, B. (2001). State of the art report on steel–concrete composite columns. *Journal of constructional steel research*. **57**(10): p. 1041-1080.

[105]. Yang, Z. (2013). Numerical simulation of strength concrete-filled steel columns. *Engineering Review*. **33**(3): p. 211-217.

[106]. Xiong, M.-X., Xiong, D.-X., and Liew, J.R. (2017). Flexural performance of concrete filled tubes with high tensile steel and high strength concrete. *Journal of Constructional Steel Research*. **132**: p. 191-202.

[107]. Li G., Yang Z., and Lang Y. (2010). Experimental behavior of high strength concrete-filled square steel tube under bi-axial eccentric loading. *Advanced Steel Construction*. **6**(4): p. 963-975.

[108]. Yadav, R. (2016). Comparative Analysis of Reinforced Concrete Buildings and Concrete Filled Steel Tube Buildings in Nepal. *International Conference on Earthquake Engineering and Post Disaster Reconstruction Planning, Nepal*: p. pp. 70-77.

[109]. Chen, B.-C. and Wang, T.-L. (2009). Overview of concrete filled steel tube arch bridges in China. *Practice periodical on structural design and construction*. **14**(2): p. 70-80.

[110]. Operations, E.a.R. (2016). Bridge Design Manual (LRFD). *Washington State Department of Transportation (WSDOT)*.p. 13.

[111]. de Normalisation, C.E. (2015), Eurocode 4: Design of composite steel and concrete structures part 1-1: General rules and rules for buildings. EUROCODE.p. 12-13.

[112]. Liew, J.Y.R. (2015). Design of Concrete Filled Tubular Members with High Strength Materials. *An extension of Eurocode 4 Method to C90/105 Concrete and S550 Steel*.p.23-24.

[113]. Wang, A.J. (2017). Raffles City in Hangzhou China-The Engineering of a 'Vertical City'of Vibrant Waves. *International Journal*. **6**(1): p. 33-47.

[114]. Ravindra, K. and Henderson, N. (1999), Specialist Techniques and Materials for Concrete Production. *Thomas Telford Publishing, Thomas Telford Ltd*.p. 33.

[115]. Akcay, B. (2012). Interpretation of aggregate volume fraction effects on fracture behavior of concrete. *Construction and Building Materials*. **28**(1): p. 437-443.

[116]. Kazemi, S. and Lubell, A.S. (2012). Influence of specimen size and fiber content on mechanical properties of high-performance fiber-reinforced concrete. *ACI Materials Journal-American Concrete Institute*. **109**(6): p. 675.

[117]. Skazlić, M., Serdar, M., and Bjegović, D. (2013), Influence of test specimen geometry on compressive strength of ultra high performance concrete. in *Second International Symposium on Ultra High Performance Concrete*.p. 23.

[118]. Gesoglu, M. (2016). Properties of low binder high performance cementitious composites: Comparison of nanosilica and microsilica. *Construction and Building Materials*. **102**: p. 706-713.

[119]. Neville, A.M. (1995), Properties of concrete. 1995.

[120]. Mehta, P. and Gjørv, O. (1982). Properties of portland cement concrete containing fly ash and condensed silica-fume. *Cement and Concrete Research*. **12**(5): p. 587-595.

[121]. Yazıcı, H. (2008). Utilization of fly ash and ground granulated blast furnace slag as an alternative silica source in reactive powder concrete. *Fuel*. **87**(12): p. 2401-2407.

[122]. Maeder, U. (2015), Ceracem, a new high performance concrete: characterisations and applications. in *First international symposium on ultra high performance concrete, Kassel*.p. 16.

[123]. Yazıcı, H. (2009). Mechanical properties of reactive powder concrete containing mineral admixtures under different curing regimes. *Construction and building materials*. **23**(3): p. 1223-1231.

[124]. Zhang, Y., Sun, W., and Liu, S. (2002). Study on the hydration heat of binder paste in high-performance concrete. *Cement and Concrete Research*. **32**(9): p. 1483-1488.

[125]. Council, U.G.B. (2004). Leadership in energy and environmental design. *Building Design and Construction, version*. **4**.p. 14.

[126]. Yalçınkaya, Ç. and Yazıcı, H. (2017). Effects of ambient temperature and relative humidity on early-age shrinkage of UHPC with high-volume mineral admixtures. *Construction and Building Materials*. **144**: p. 252-259.

[127]. Beygi, M.H. (2013). The effect of water to cement ratio on fracture parameters and brittleness of self-compacting concrete. *Materials & Design*. **50**: p. 267-276.

[128]. Kato, B. (1995). Compressive strength and deformation capacity of concrete-filled tubular stub columns (Strength and rotation capacity of concrete-filled tubular columns, Part 1). *Journal of Structural and Construction Engineering, AIJ*. **468**: p. 183-91.

[129]. Lu, Z.-H. and Zhao, Y.-G. (2010). Suggested empirical models for the axial capacity of circular CFT stub columns. *Journal of Constructional Steel Research*. **66**(6): p. 850-862.

[130]. Luksha, L. and Nesterovich, A. (2013), Strength testing of large-diameter concrete filled steel tubular members. in *Proceedings of the Third International Conference on Steel-Concrete Composite Structures, Wakabayashi, M.(ed.), Fukuoka, Japan, Association for International Cooperation and Research in Steel-Concrete Composite Structures*.p. 14-16.

[131]. Yu, Z., Ding, F., and Lin, S. (2002). Researches on Behavior of High-performance Concrete Filied Tubular Steel Short Columns. *Journal of building structures*. **2**: p.5.

PERSONAL INFORMATION

Name and Surname: Aseel Madallah MOHAMMED

Nationality: Iraqi

Birth place and date: Iraq-Anbar /09-January-1981

Marital status Widow

Phone number: +90 536 067 4802 in Turkey

Email: aseelrawan11@yahoo.com

HIGH EDUCATION Degree	Graduate School	Year
Master Degree	University of anbar/ Anbar	2005
Bachelor of Science	University of anbar/ Anbar	2002

WORK EXPERIENCE

Year	Place	Enrollment
2007-Present	Anbar university	Lecturer

HOBBIES

Studying

FOREIGN LANGUAGE

English

Arabic